



Room 14-0551  
77 Massachusetts Avenue  
Cambridge, MA 02139  
Ph: 617.253.5668 Fax: 617.253.1690  
Email: docs@mit.edu  
<http://libraries.mit.edu/docs>

## **DISCLAIMER OF QUALITY**

Due to the condition of the original material, there are unavoidable flaws in this reproduction. We have made every effort possible to provide you with the best copy available. If you are dissatisfied with this product and find it unusable, please contact Document Services as soon as possible.

Thank you.

**Due to the poor quality of the original document, there is some spotting or background shading in this document.**

A THEORY OF NUCLEATION  
FOR SOLID METALLIC SOLUTIONS

By

MATS HILLERT

Civ. Ing., Chalmers Institute of Technology  
(1947)

S.M., Massachusetts Institute of Technology  
(1954)

Submitted in Partial Fulfillment of the  
Requirements for the Degree of  
DOCTOR OF SCIENCE

at the

Massachusetts Institute of Technology

1956

Signature of Author  
Department of Metallurgy  
May 14, 1956

Signature of Professors  
in Charge of Research

Signature of Chairman  
Department Committee  
on Graduate Research

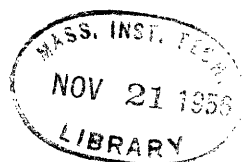
---

---

---

---

Metall  
Thesis  
1956



A THEORY OF NUCLEATION FOR SOLID METALLIC SOLUTIONS

63

By

Mats Hillert

Submitted to the Department of Metallurgy, May, 1956, in partial  
Fulfillment of the Requirements for the Degree of  
Doctor of Science in Metallurgy

ABSTRACT

It is shown that the concept of size of a nucleus can be eliminated in nucleation theories treating transformations wherein the atoms only change places with each other, and where sharp discontinuous boundaries between the phases are not formed. A new nucleation theory is developed which treats compositional changes in one crystalline direction only. Spontaneous nucleation inside the spinodal and a periodic variation of the composition are predicted. The wave length of this periodicity can be measured by X-ray diffraction methods and the phenomenon appears in the form of diffuse side bands to the main reflections in a powder pattern.

Experimental measurements of this wave length as a function of composition, annealing time and annealing temperature were made on Cu-Ni-Fe alloys. A fair agreement with the predictions was found. However, it was not possible to prove experimentally the significance of the spinodal on the nucleation process and several explanations are given.

Different X-ray treatments of periodic structures are brought together in a more general treatment.

A new diffusion equation is derived for cases where the third derivative of the concentration is considerable. It can account for the fact that a concentration gradient does not always cause downhill diffusion outside the spinodal or uphill diffusion inside the spinodal.

The nearest-neighbor interaction model for solutions is discussed and the quasi-chemical equation is derived without the assumption that the interaction energy is independent of temperature and composition. It is shown that the interaction energy should be calculated from the free energy of mixing, not from the heat of mixing.

Thesis Supervisors: Morris Cohen  
Professor of Physical Metallurgy

B. L. Averbach  
Associate Professor of Physical Metallurgy

Handwritten: (Mats Hillert) Nov. 21, 1956

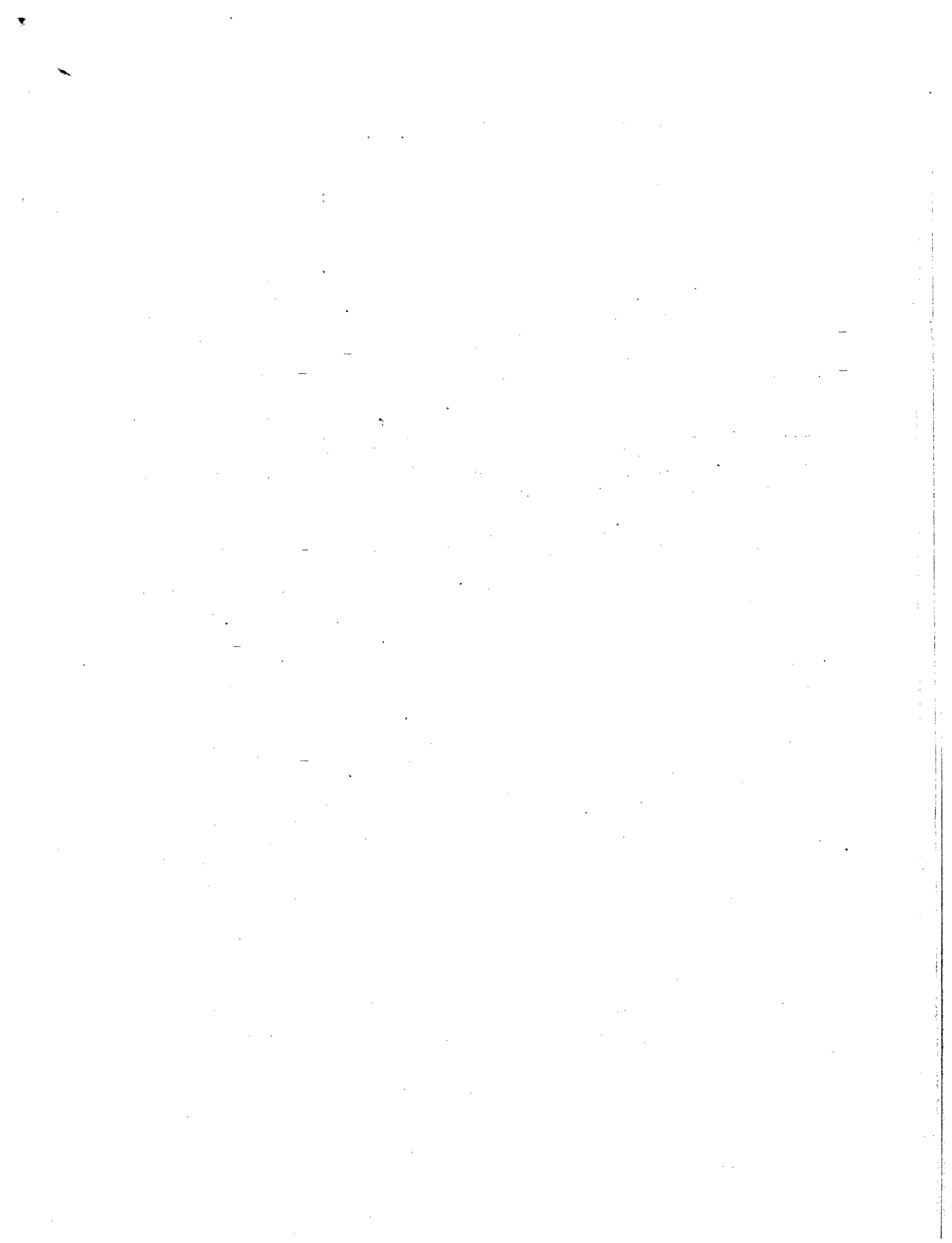


## TABLE OF CONTENTS

<u>Chapter Number</u>		<u>Page Number</u>
	LIST OF FIGURES .....	iv
	LIST OF TABLES .....	vii
	ACKNOWLEDGMENTS .....	viii
I.	INTRODUCTION .....	1
II.	THEORY OF NUCLEATION .....	4
	1. The Concept of the Critical Nucleus .....	4
	2. Review of Nucleation Theories .....	5
	3. Comparison of Borelius', Becker's and Hobstetter's Treatments .....	10
	4. Objections to Becker's and Hobstetter's Treatments .....	11
	5. A New Approach to Nucleation .....	13
III.	RESULTS OF CALCULATIONS .....	18
	1. Compositions Inside the Miscibility Gap but Outside the Spinodal .....	18
	2. Compositions Inside the Spinodal .....	20
	3. Symmetric Composition .....	21
	4. Grain Boundary Energy .....	21
	5. Ordering Systems .....	22
	6. Revision of the Diffusion Equation .....	22
	7. First Stage of Transformation in Symmetric Alloy .....	24
	8. First Stage of Transformation in Asymmetric Alloys .....	25
	9. Limitations of Present Treatment .....	25
	10. Second Stage of Transformation .....	26
	11. Purpose of Experimental Work .....	27

<u>Chapter Number</u>		<u>Page Number</u>
IV.	DEFINITION AND CALCULATION OF THE INTERACTION ENERGY .....	30
	1. Classical Definition .....	30
	2. Guggenheim's Definition of the Interaction Energy .....	32
	3. New Definition of the Interaction Energy	33
	4. Estimation of the Interaction Energy ....	39
	5. Discussion of Other Quasi-Chemical Treatments .....	42
V.	X-RAY THEORY OF PERIODIC STRUCTURES .....	45
	1. Previous Work .....	45
	2. Application to FCC Structures .....	50
	3. Treatment of a More General Model .....	52
	4. Application to a Specific Case .....	58
	5. Exact Treatment .....	60
VI.	EXPERIMENTAL WORK .....	63
	1. Preparation of Alloys .....	63
	2. Experimental Technique .....	64
	3. Measurements of the Phase Diagram .....	65
	4. Measurements of Satellites .....	67
VII.	DISCUSSION OF EXPERIMENTAL RESULTS .....	69
	1. Rate of Transformation for the Symmetric Alloy .....	69
	2. Variation of Wave Length with Temperature .....	70
	3. Variation of Wave Length with Composition .....	71
	4. Conclusion from Experimental Work .....	73
	5. The Nature of the Spinodal .....	74

<u>Chapter Number</u>		<u>Page Number</u>
VII.	6. Discussion of Guinier's Model .....	78
VIII.	SUMMARY AND CONCLUSIONS .....	81
	REFERENCES .....	84
	BIOGRAPHICAL SKETCH .....	87
	APPENDIX I .....	88
	APPENDIX II .....	90
	APPENDIX III .....	91



LIST OF FIGURES

<u>Figure Number</u>		<u>Page Number</u>
1.	Equilibrium Diagram and Free Energy of Mixing for System with Miscibility Gap .....	6a
2.	Free Energy Surface for Formation of Fluctuation, Showing the Critical Nucleus According to Different Theories .....	10a
3.	Schematic Plot of the Function $f(x) = x + C \cdot \ln \frac{x}{1-x}$ .....	10b
4.	Solutions to Eq. (13) for a Composition Between the Miscibility Gap and the Spinodal	17a
5.	Solutions to Eq. (13) for a Composition Inside the Spinodal .....	17b
6.	Solution to Eq. (13) for the Symmetric Composition .....	17c
7.	Composition of Successive Atomic Planes for the Most Probable Critical Nucleus when the Alloy Composition is 0.72 (crosses) and 0.76 (dots), Respectively .....	19a
8.	Activation Energy for Nucleation According to Different Theories .....	19b
9.	Solutions to Eq. (13) Showing Periodic Variation of Composition. Positive $\nu$ .....	21a
10.	Solutions to Eq. (13) Showing Periodic Variation of Composition. Negative $\nu$ .....	22a
11.	Variation with Wave Length of the Ratio Between Driving Force and Diffusion Distance	24a
12.	Increase of Q by Lateral Growth of Zone, as Suggested by Guinier .....	49a
13.	Model of Zone in Asymmetric Alloy .....	58a
14.	Calculated Intensity Distribution in Satellites .....	62a
15.	Composition of Alloys Plotted in "Phase Diagram after Slow Cooling" .....	63a

<u>Figure Number</u>		<u>Page Number</u>
15A.	Phase Diagram for the Cu-Ni-Fe System Showing The Miscibility Gap and Tie-Lines for one Alloy at Three Temperatures (According to Köster and Dannöhl) .....	63b
16.	Theoretical Shape of Miscibility Gap According to Zeroth and First Approximation .....	66a
17.	Composition and Temperatures of Annealing Experiments. Miscibility Gap According to First Approximation .....	67a
18.	Growth of Wave Length with Annealing Time at 1080 and 1100°K .....	67b
19.	Growth of Wave Length with Annealing Time at 1050°K .....	67c
20.	Growth of Wave Length with Annealing Time at 1003°K .....	67d
21.	Growth of Wave Length with Annealing Time at 895°K .....	67e
22.	Growth of Wave Length with Annealing Time at 800°K .....	67f
23.	Growth of Wave Length with Annealing Time at 720°K .....	67g
24.	Growth of Wave Length with Annealing Time for Alloy C .....	68a
25.	Growth of Wave Length with Annealing Time for Alloy F .....	68b
26.	Experimental Data for Alloy F Compared with Theoretical "C"-Curve for Symmetric Alloy ...	69a
27.	Variation of Initial Wave Length with Temperature .....	70a
28.	Wave Length of First Transformation Product Compared with the Critical and the Optimum Wave Lengths .....	71a
29.	Experimental "C"-Curve for the Asymmetric Alloy C .....	73a

<u>Figure Number</u>		<u>Page Number</u>
30.	Miscibility Gap for First Approximation with Spinodal for Random Solution .....	75a
31.	Suggested Development of Guinier's Zone .....	80a

LIST OF TABLES

<u>Table Number</u>		<u>Page Number</u>
1	Calculated Values of $\frac{v}{kT}$ .....	32

ACKNOWLEDGMENTS

The author wishes to thank Professors Morris Cohen and Benjamin Averbach for their encouragement during this work and for their assistance in writing the thesis.

Thanks are due to Mr. Robert Goss for his assistance in various parts of the experimental work, and to many other members of the Metallurgy Department, in particular, Professor Carl Wagner, for many helpful discussions.

## I. INTRODUCTION

The theories for homogeneous nucleation in solid, metallic solutions which transform by a redistribution of the atoms on the old lattice sites, is discussed, and a new theory is developed which eliminates some of the short-comings of the older theories. In agreement with Borelius' and Hobstetter's theories, it is found that the free energy of activation for nucleation vanishes inside the spinodal. Moreover, the new theory predicts the nature of the first transformation structure, and can therefore be subjected to a much more thorough test than previous theories. The predicted structures exhibit a periodic variation of the composition, and the wave length of this periodicity is susceptible to experimental verification.

Many investigations have been undertaken in order to test the significance of the spinodal predicted by the above theories. However, most of the work has been concerned with systems which do not transform by a simple redistribution of the atoms on the old lattice sites, and the results are often incompatible with the theories. X-ray data indicate that the Cu-Ni-Fe system might be better suited for a test than most other systems studied previously. A series of alloys covering a whole pseudo-binary section of this ternary system was therefore made in order to test the significance of the spinodal and the predictions concerning the variation with temperature and composition of the wave length of the periodic structures.

The average wave length of the periodicity is measured from X-ray diffraction patterns. The X-ray theory for periodic structures is discussed, and several old treatments have been brought together to form a more general approach. A simple and exact X-ray theory for a specific model of periodic structures is also developed and applied.

The new nucleation theory uses the so-called zeroth approximation of the nearest neighbor interaction model for solutions. This model has recently been tested for solid metallic solutions and considerable deviations have been found. The fundamentals of the model are therefore studied and it is shown that the so-called first approximation can be derived on a purely thermodynamic basis. The result indicates that the recent tests are not quite significant.

A new equation for diffusion is derived in order to explain the stability of structures with a periodic variation in composition. This equation shows that a concentration gradient does not always cause downhill diffusion outside the spinodal or uphill diffusion inside the spinodal.

The nature of coherent grain boundaries in systems with miscibility gaps and of anti-phase domain boundaries in ordering systems is studied and the results indicate that such boundaries do not show any discontinuous change in composition or phase.

The concept of Gibbs free energy will be used frequently in the following treatment. It will be referred to simply as

"free energy," however, since the difference between the Gibbs and Helmholtz free energies usually is insignificant for condensed systems. It is also unnecessary to distinguish between the concepts of energy and enthalpy. Both these concepts will be used, the choice in each case being determined by common practice. The notation for the different thermodynamic quantities adopted by Wagner<sup>(1)</sup> will be used.



## II. THEORY OF NUCLEATION

### 1. The Concept of the "Critical Nucleus"

There are always local fluctuations within a physical system even if it is in a state of equilibrium. The probability of a certain fluctuation is given by statistical thermodynamics as

$$w = C \cdot \exp\left(-\frac{\Delta F}{kT}\right) \quad (1)$$

C is a normalization constant and  $\Delta F$  is the increase of the free energy of the whole system if such constraints are imposed on the system that the fluctuation becomes momentarily fixed. For stable systems  $\Delta F$  usually increases with the size of the fluctuation and the probability of a large fluctuation is thus, according to Eq. (1), less than the probability of a smaller fluctuation.

In a metastable system there will be some kind of fluctuations for which  $\Delta F$  reaches a maximum at a certain size and then decreases with further increase in size until finally a new equilibrium state is reached. Eq. (1) is strictly valid only for stable systems but it can be used as a very good approximation for small fluctuations even in a metastable system. However, it fails for large fluctuations which can grow with a decrease in free energy. Nucleation usually refers to the formation of such large fluctuations, and it is assumed (e.g. by Volmer and Weber<sup>(2)</sup>) that the rate of nucleation is proportional to the probability of formation, according to Eq. (1),

of the least probable state that a fluctuation has to pass through during its growth from a small subcritical size. It is of considerable interest to determine the critical fluctuation, usually called the critical nucleus, and to calculate the corresponding value of  $\Delta F$ , usually denoted  $\Delta F^*$ . The smaller this value, the easier it is for nucleation to take place.

When treating nucleation of liquid droplets from vapors, Becker and Döring<sup>(3)</sup> later took into account also the probability of the reverse reaction, namely the redissolution of large fluctuations. The original approach of Volmer and Weber has been widely used, however, due to its simplicity and it will be adopted here.

## 2. Review of Nucleation Theories

It is usual to distinguish between two kinds of nucleation. Nucleation that occurs at random in a homogeneous phase is called homogeneous nucleation and many theories have been developed for this kind of nucleation. Experience shows, however, that nuclei usually form on preferred sites, for instance on surfaces, grain boundaries and impurities. Such nucleation is referred to as heterogeneous, and one can not expect the theories for homogeneous nucleation to hold in such cases. It must therefore be realized that the usefulness of these theories is quite restricted.

Transformation in alloys usually involves changes in composition and structure. In systems with miscibility gaps, however, there is only a change in composition. The structures

of the two final phases and of the initial phase are identical. It is then possible for the whole transformation to take place simply by an exchange of atoms on the old lattice sites. This is not a common case, but the formation of Guinier-Preston Zones in agehardening alloys seems to be an example of this. There is no accepted name for this kind of transformation. In this work it will be referred to as an exchange transformation. Usually nuclei of a new orientation are formed and grow into the old matrix. This happens in Au-Ni alloys, for instance, and is not significantly different from a transformation which results in new crystal structures.

The present treatment will be limited to homogeneous nucleation of exchange transformations. Several theories have been developed for this special case and they will first be reviewed and examined critically.

The upper part of Fig. 1 shows the equilibrium diagram for a system with a miscibility gap and the lower part demonstrates the variation of the free energy with composition at a temperature of limited solubility. The so-called spinodal is a line along which the second derivative of the free energy with respect to composition,  $d^2F/dx^2$ , is zero. Homogeneous alloys, which are represented by points outside the miscibility gap in the equilibrium diagram, are stable and  $\Delta F$  for all kinds of composition fluctuations increase with the size of the fluctuations in these alloys.

Konobejewski: For homogeneous alloys between the miscibility gap and the spinodal  $\Delta F$  of small composition fluctuations in-

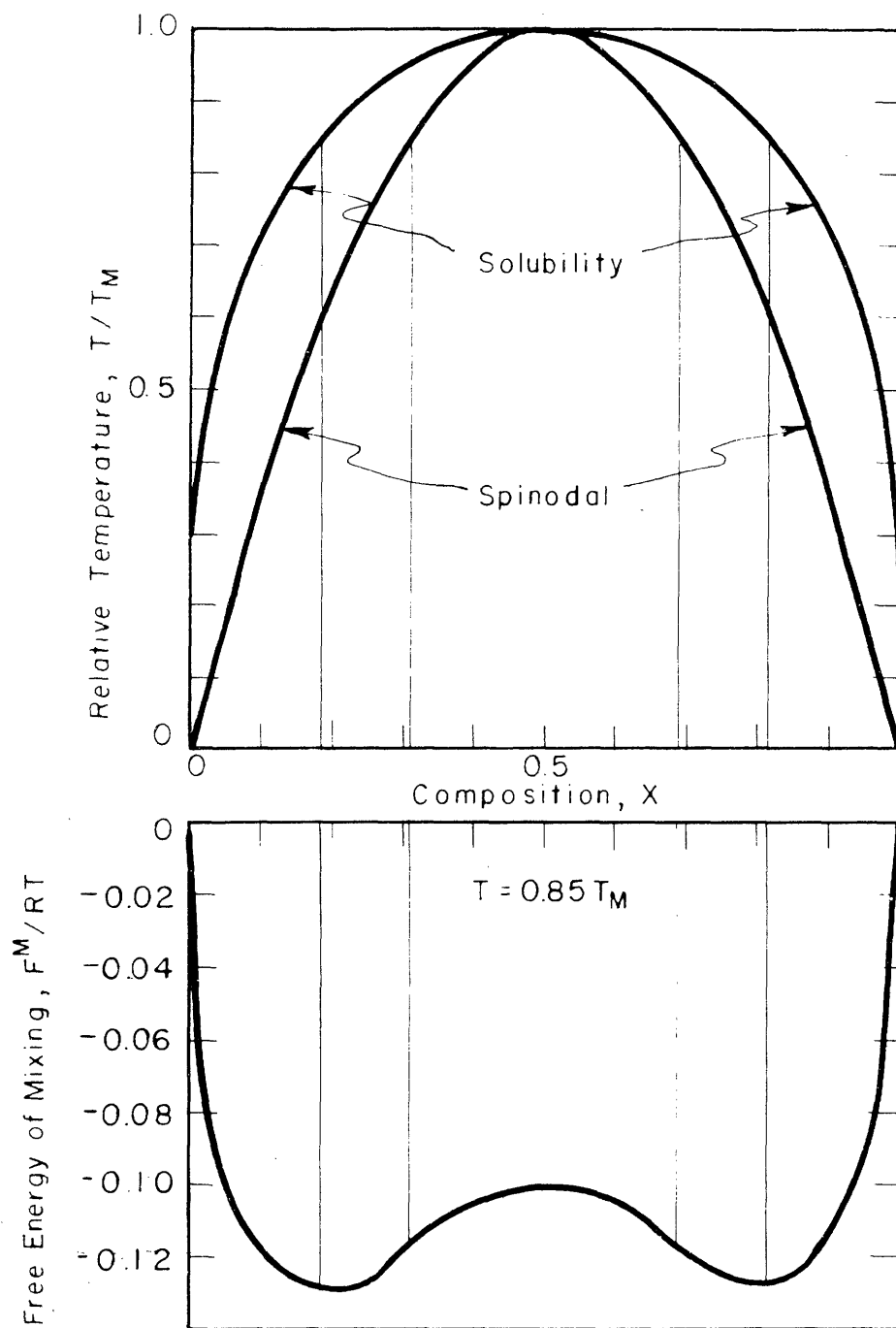


FIG. 1. EQUILIBRIUM DIAGRAM AND FREE ENERGY OF MIXING FOR SYSTEM WITH MISCIBILITY GAP.

crease with the amplitude of the fluctuation since  $d^2F/dx^2$  is positive. Consequently such alloys have some stability but, as was pointed out for instance by Konobejewski<sup>(4)</sup> in 1934,  $\Delta F$  goes through a maximum at some composition of the fluctuation and decreases with further increase in composition. These homogeneous alloys are thus only metastable, and the stable state consists of two phases of different composition, one on each side of the miscibility gap.

Borelius: Borelius<sup>(5,6)</sup> considered the nucleation process in more detail and calculated  $\Delta F$  for a fluctuation of composition  $x$  and containing  $n$  atoms. Neglecting the influence of the discontinuity at the interface between the fluctuation and the rest of the system he found

$$\Delta F(x^0, x, n) = \frac{n}{N_0} \left[ F(x) - F(x^0) - (x - x^0) \frac{dF(x^0)}{dx^0} \right] \quad (2)$$

$N_0$  is Avogadro's number and  $x^0$  is the composition of the alloy. This function goes through a maximum at a certain value of  $x$  for each  $x^0$  in agreement with Konobejewski's statement. The maximum value which is the free energy value for the least probable fluctuation or the critical nucleus, is usually denoted  $\Delta F^*$ .

The maximum,  $\Delta F^*$ , is lower the higher the supersaturation of the alloy i.e. the further inside the miscibility gap the composition of the alloy  $x^0$  is situated.  $\Delta F^*$  decreases to zero at the spinodal, and inside the spinodal  $\Delta F$  decreases with increasing  $x$  without first going through a maximum. The rate of nucleation is thus increased as the supersaturation is increased

until, after crossing the spinodal, there is no resistance against nucleation. These conclusions are in agreement with the fact that  $d^2F/dx^2$  has negative values inside the spinodal, this being the thermodynamic criterion of instability. The significance of the spinodal has also been realized by many other authors e.g. by Becker<sup>(7)</sup> and Dehlinger<sup>(8)</sup>.

Borelius' treatment does not yield any information on the geometric size,  $n^*$ , of the critical nucleus apparently because the influence of the interface is neglected. The value of  $\Delta F^*$  thus contains  $n^*$  as an unknown quantity. Borelius seems to feel that the treatment is quite good in spite of this and attempts have been made to determine  $n^*$  by experimental determinations of  $\Delta F^*$ <sup>(9,10)</sup>.

Hollomon and Turnbull<sup>(11,12)</sup> point out that Borelius' theoretical treatment indicates that the fastest nucleation process should occur via critical nuclei of smallest possible size, namely  $n = 1$ , because this value gives the lowest  $\Delta F^*$  and thus the highest nucleation rate according to Eq. (1). The nucleation rates obtained this way are very high and Hollomon and Turnbull consequently doubt the validity of Borelius' analysis. Becker: Becker<sup>(13)</sup> has treated the same case of nucleation as Borelius but made other assumptions. He took into account the effect of the interface between the fluctuation and the rest of the system by adding another term to Eq. (2)

$$\Delta F(x^0, x, n) = \frac{n}{N_0} \left[ F(x) - F(x^0) - (x - x^0) \frac{dF(x^0)}{dx^0} \right] + A \cdot F_s \quad (3)$$

$A$  is a measure of the area of the interface and  $F_s$  is the interfacial free energy. Using the so-called zeroth approximation

of the nearest neighbor interaction model for solutions and assuming that the interface has no influence on the distribution of the atoms inside the fluctuation, he found

$$\Delta F(x^0, x, n) = n \left[ - Z\nu(x - x^0)^2 \left(1 - \frac{n_p}{Zn}\right) + kT \left( x \ln \frac{x}{x^0} + (1-x) \ln \frac{1-x}{1-x^0} \right) \right] \quad (4)$$

$n_p$  is the number of bonds crossing the interface and can be related to  $n$  by assuming a certain geometric shape of the fluctuations.  $Z$  is the number of nearest neighbors to each atom and  $\nu$  is the so-called interaction energy, which will be further discussed in Chapter IV.

In Becker's original treatment it was assumed that the composition of the fluctuations,  $x$ , was equal to that of the final stable precipitate. It was then found that  $\Delta F$  had a maximum value at a certain critical value of  $n$  and this fluctuation was identified as the critical nucleus.

Hobstetter: Hobstetter<sup>(14)</sup> later combined Borelius' and Becker's theories by allowing  $x$  to vary. For each value of  $x$ ,  $\Delta F$  has a maximum at some value of  $n$  and Hobstetter suggested that the nucleation process passes over the ridge formed by these maxima at the lowest possible point. Such a point must be a saddle point and is found by setting the two derivatives of  $\Delta F$  with respect to  $x$  and  $n$  equal to zero. These two equations allow the determination of both  $x^*$  and  $n^*$  for the critical nucleus.

Scheil<sup>(15)</sup> has in a later paper used the same approach as Hobstetter.

### 3. Comparison of Borelius', Becker's and Hobstetter's Treatments

Fig. 2, where the stars represent the critical nuclei, demonstrates schematically the difference between the three nucleation theories. It is obvious that Hobstetter's treatment gives the lowest  $\Delta F^*$  value and thus the highest nucleation rate.

The advantage of Becker's and Hobstetter's treatment over Borelius' is that they give not only the composition but also the size of the critical nucleus. However, there is a serious objection to Becker's treatment which becomes evident by considering one of the two equations used to find the critical nucleus in Hobstetter's treatment.

$$\frac{d\Delta F}{dx} = n \left[ -2Z\nu(x - x^0) \left(1 - \frac{n_b}{Zn}\right) + kT \left( \ln \frac{x}{1-x} - \ln \frac{x^0}{1-x^0} \right) \right] = 0 \quad (5)$$

which can be written  $f(x) = f(x^0)$

$$\text{where } f(x) = x + C \ln \frac{1-x}{x} \quad \text{and} \quad C = \frac{1}{1 - \frac{n_b}{Zn}} \frac{kT}{2Z\nu}$$

At a sufficiently low temperature the function  $f(x)$  has the appearance shown in Fig. 3 and the construction shows how  $x^*$  can be found for each  $x^0$  in order to satisfy Eq. (5). The solution  $x^* = x^0$  is found at the minimum point, i.e. when

$$0 = \frac{df(x)}{dx} = 1 - \frac{C}{x(1-x)} \quad \text{or} \quad \frac{2kT}{Z\nu} = 4x(1-x) \left(1 - \frac{n_b}{Zn}\right) \quad (6)$$

It is at once seen from Eq. (4) that this solution ( $x^* = x^0$ ) gives  $\Delta F^* = 0$  and thus corresponds to the case of unlimited nucleation because there is no free energy barrier.

If  $n_b$  is set equal to zero in accordance with Borelius' treatment, Eq. (6) gives

$$\frac{2kT}{Z\nu} = 4x(1-x) \quad (7)$$



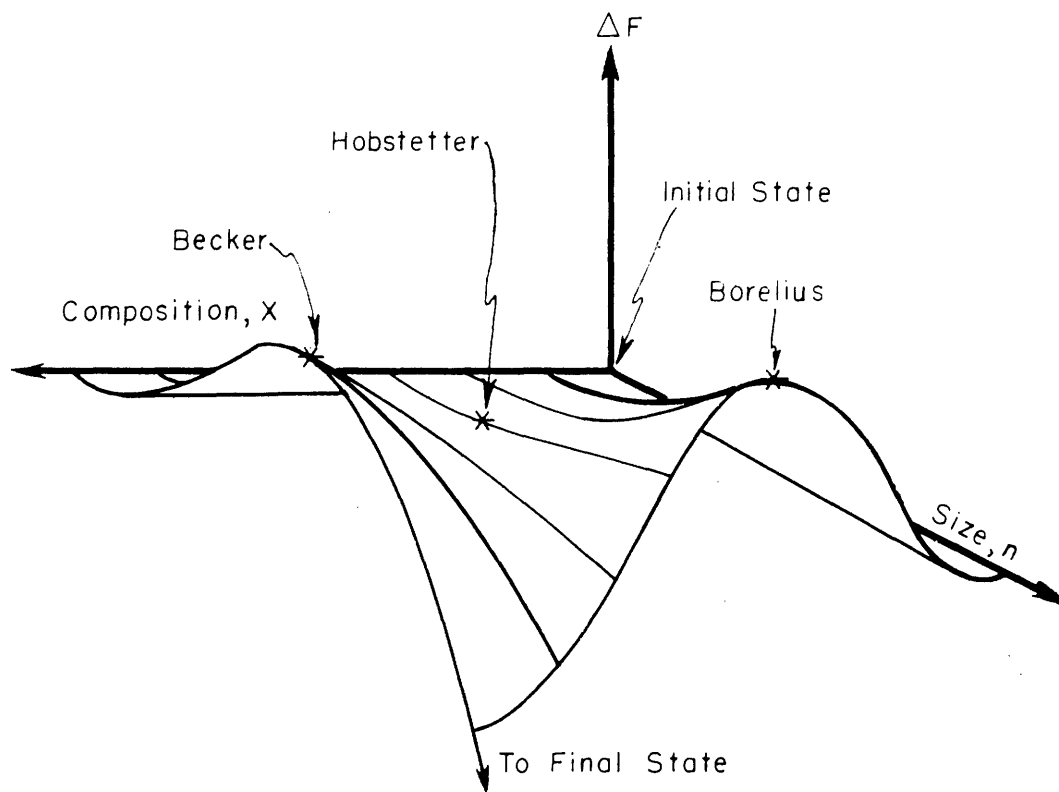


FIG. 2. FREE ENERGY SURFACE FOR FORMATION OF FLUCTUATION, SHOWING THE CRITICAL NUCLEUS ACCORDING TO DIFFERENT THEORIES

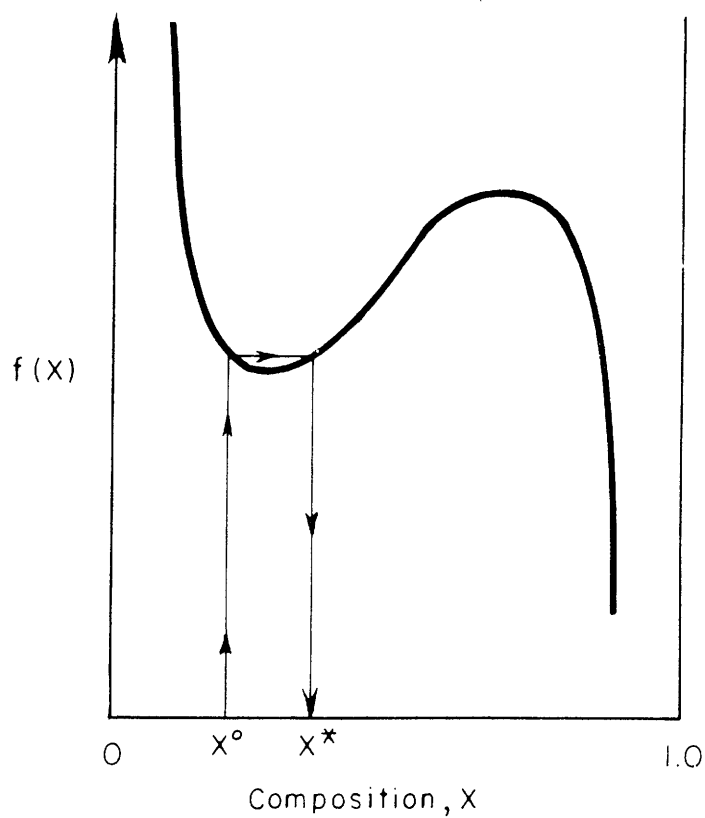


FIG. 3. SCHEMATIC PLOT OF THE FUNCTION  
 $f(x) = x + C \cdot \ln \frac{x}{1-x}$ .

This is recognized as the equation of the spinodal and is thus a mathematical proof of the conclusion from Borelius' treatment that the free energy barrier for the nucleation vanishes at the spinodal. According to Hobstetter's treatment,  $n_b > 0$ ,  $1 - \frac{n_b}{Zn} < 1$ , and the free energy barrier is thus predicted not to vanish until considerably inside the spinodal, unless the size of the critical nucleus,  $n^*$ , is very large. Only then is  $1 - \frac{n_b}{Zn} \cong 1$  and Eq. (6) is transformed into (7), yielding the same result as Borelius' theory. This fact has not been noticed by Hobstetter, however, who due to some error of calculation gives a finite value of  $n^*$  even at the spinodal.

Both Borelius' and Hobstetter's theories are thus, if adequately treated, in agreement with the thermodynamic criterion of instability  $d^2F/dx^2 \leq 0$  which holds at and inside the spinodal. Becker's theory, which does not consider  $x^*$  as a variable, can never give the result  $x^* = x^0$ , and  $\Delta F^*$  obtained from Eq. (4), does not vanish until far inside the spinodal. This is in direct opposition to the criterion of instability.

#### 4. Objections to Becker's and Hobstetter's Treatments

(1) Becker's Eq. (4) does not hold for fluctuations with a limited number of atoms because Stirling's approximation is used in deriving the positional entropy. A correction term can be added to Eq. (4), however, to make it hold for small  $n$  as well and this is found to be

$$-kT \ln \frac{n!}{(nx)!(n(1-x))!} - nkT( x \ln x + (1-x) \ln(1-x) ) \quad (8)$$

Accordingly, Eq. (4) is changed into

$$\Delta F(x^0, x, n) = n \left[ -Z\nu(x - x^0)^2 \left(1 - \frac{n_0}{Zn}\right) - kT \left( x \ln x^0 + (1-x) \ln(1-x^0) \right) \right] - kT \ln \frac{n!}{(nx)! (n(1-x))!} \quad (9)$$

Unfortunately this equation is difficult to handle.

It is worth noting that Poisson's equation

$$w = \frac{(nx^0)^{nx} \exp nx^0}{(nx)!} \quad (10)$$

has erroneously been used by Fink and Smith<sup>(16)</sup> for the probability of finding a certain fluctuation  $nx$  in a group of  $n$  atoms in a random system. The correct probability is obtained by inserting  $\Delta F$  from Eq. (9) in Eq. (1) and setting  $\nu = 0$ , from which

$$w = C \cdot \frac{n!}{(nx)! (n(1-x))!} \cdot (x^0)^{nx} \cdot (1-x^0)^{n(1-x)} \quad (11)$$

(2) Becker and Hobstetter identify the fluctuation with the maximum value of  $\Delta F$  as the critical nucleus, because Eq. (1) seems to tell that this is the least probable fluctuation. However, Eq. (1) contains a normalization constant  $C$  whose value depends upon the constraints that are necessary to make a fluctuation momentarily fixed. These constraints are different for different geometric size and shape of the fluctuation, and  $C$  is therefore dependent on  $n$ . A detailed examination shows that the least probable fluctuation, i.e. the critical nucleus, occurs at a somewhat smaller value of  $n$  than the maximum value of  $\Delta F$ .

(3) All the nucleation theories use the concept "size" of the nuclei. However, in exchange transformations (as defined in Section 2) there is no way of telling whether a certain lattice site belongs to a nucleus or not. Becker and Hobstetter assume that the nuclei must have a certain geometrical shape and thereby avoid this problem. Whether a shell of lattice sites around a nucleus belong to the nucleus or not is determined in their theories by the composition of this shell. It belongs to the nucleus if it has the prescribed nucleus composition and it belongs to the matrix if it has the original composition. These theories, however, do not take into account the fact that the composition of the shell could be different from these two values, and indeed has to change gradually from one of these values to the other in order for the nucleus to grow. Moreover, if one considers a finite nucleus, its composition and also the composition of the shell can only vary in steps because they contain a whole number of each kind of atom. The two compositions can thus be equal only in very special cases.

##### 5. A New Approach to Nucleation

It is evident that not even the assumption of a certain geometrical shape removes the difficulties. It seems to the present author that the concept of size should be completely abandoned in the case of exchange transformations. This would also remove the difficulty mentioned under point (2) in the preceding section. In the following sections it will be shown how a nucleation theory can be developed without making

use of this concept. In order to simplify the calculations only changes in one crystalline direction will be considered. The composition of each atomic plane perpendicular to this direction can then be described with a single  $x$ -value.

We shall use the zeroth approximation of the nearest-neighbor interaction model for solutions, as did Becker and Hobstetter. Denote the composition of succeeding planes  $x^p$ ,  $x^{p+1}$ ,  $x^{p+2}$ , etc. Assuming that the atoms are randomly distributed within each plane one can calculate the difference in free energy between a state specified by a certain set of  $x$  and the homogeneous state in which the composition of all the planes is the same,  $x^0$  (see Appendix I).

$$\Delta F = -\nu_m \sum_p \left[ Z(x^p - x^0)^2 - \zeta (x^p - x^{p+1})^2 \right] + mkT \sum_p \left[ x^p \ln \frac{x^p}{x^0} + (1-x^p) \ln \frac{1-x^p}{1-x^0} \right] \quad (12)$$

$\zeta$  is the number of nearest neighbors, for a given atom, which are situated in a neighboring plane.

In accordance with Hobstetter's treatment we shall attempt to determine the lowest point, i.e. the saddle point, on the free energy ridge, which the nucleation process has to pass over. However, it should be remembered that the total rate of nucleation is equal to the sum of the rate of nucleation for all the possible ways the nucleation process can take. A summation should thus be performed over the whole ridge and the

term "critical nucleus" is not quite an adequate name for the saddle point. It will nevertheless be used in the following approach.

The saddle points in the many-dimensional  $x^p$ -space are found for instance by solving the system of equations

$(\frac{\partial \Delta F}{\partial x^p})_{x^{p'}} = 0$ , where  $x^{p'}$  indicates that all  $x$  are kept constant except  $x^p$  and  $x^{p+1}$ . However, it must be remembered that the same system of equations also gives the minimum points and this treatment will thus yield equilibrium states (metastable and stable) as well as critical nuclei. The equations obtained look the same for all values of  $p$ :

$$x^{p+2} = x^{p-1} + \left(\frac{Z}{3} - 3\right)(x^p - x^{p+1}) + \frac{Z}{43} \frac{T}{T_M} \ln \frac{x^{p+1}(1-x^p)}{x^p(1-x^{p+1})} \quad (13)$$

$T_M$  is the peak temperature of the miscibility gap.

The set of difference equations (13) can be solved explicitly only in the case of small variations in composition from the mean value  $x^0$ . The logarithmic term can then be expanded and the equation becomes

$$x^{p+2} = x^{p-1} - 2L(x^p - x^{p+1})$$

$$\text{where } 2L = \frac{Z}{43} \frac{T}{T_M} \frac{1}{x^0(1-x^0)} + 3 - \frac{Z}{3} \quad (14)$$

One solution is immediately found, namely all  $x^p = x^0$ . This is the case of a homogeneous alloy. Other solutions are described by

$$x^p = C_1 + C_2 \beta^p + C_3 \beta^{-p} \quad (15)$$

where  $C_1$ ,  $C_2$  and  $C_3$  are constants. The value of  $\beta$  is found by inserting this expression of  $x^p$  in Eq. (14), which gives

$$\beta = L - \frac{1}{2} + \sqrt{(L - \frac{1}{2})^2 - 1} \quad (16)$$

For  $|L - \frac{1}{2}| > 1$ ,  $\beta > 1$ , and consequently the impossible result  $x^p \rightarrow \infty$  is obtained when  $p \rightarrow \infty$  and also when  $p \rightarrow -\infty$ , unless  $C_2$  and  $C_3$  are zero. The only possible solution in the case of  $|L - \frac{1}{2}| > 1$  is thus  $x^p = C_1 = x^0$ . It is interesting to note that  $L - \frac{1}{2} = 1$  occurs when  $\frac{T}{4T_M x^0 (1-x^0)} = 1$ , which is the equation of the spinodal. The only solution within small composition variations is thus the homogeneous case when the composition of an alloy is outside the spinodal.

Inside the spinodal  $|L - \frac{1}{2}| < 1$  and  $\beta$  is a complex number. The solution can then be written

$$x^p = x^0 + C_4 \sin(p\varphi) \quad \text{where } \varphi = \tan^{-1} \frac{\sqrt{1 - (L - \frac{1}{2})^2}}{L - \frac{1}{2}} \quad (17)$$

This solution is a sinusoidal variation and the wave length expressed in number of atomic planes is

$$q_{\text{crit}} = \frac{2\pi}{\tan^{-1} \frac{\sqrt{1 - (L - \frac{1}{2})^2}}{L - \frac{1}{2}}} \quad (18)$$

The reason to denote this value  $q_{\text{crit}}$  will be explained in Chapter III. The amplitude,  $2C_4$ , is indeterminate but is very small according to the assumptions.

Solutions with large compositional variations can not be obtained explicitly but can be calculated stepwise by choosing the compositions of three succeeding planes and computing the



following ones one by one with Eq. (13). This process is exceedingly tedious, especially because the mean composition for a solution can not be determined in advance by choosing the three first compositions, but has to be evaluated when the solution is finally found. It therefore takes considerable time to collect data for a certain composition. Moreover, a very high degree of accuracy must be used in the calculations because a small error in the beginning of a calculation may grow as the calculation proceeds and completely distort the final solution. Up to eight decimal figures were employed for the compositions and logarithms.

All the solutions can be described as periodic variations in composition, oscillating around the mean composition. The larger the amplitude, the more the shape will deviate from the ideal sinusoidal shape. Each solution can be specified by its wave length and amplitude and this fact allows us to plot all the solutions for a certain alloy at a certain temperature in a coordinate system of these two parameters, whereas a plot in the many-dimensional  $x^P$ - space would be impossible. Furthermore, the free energy of the solutions can be plotted along a third coordinate as shown in the upper parts of Figs. 4, 5 and 6.

Solutions of different compositions will now be discussed.

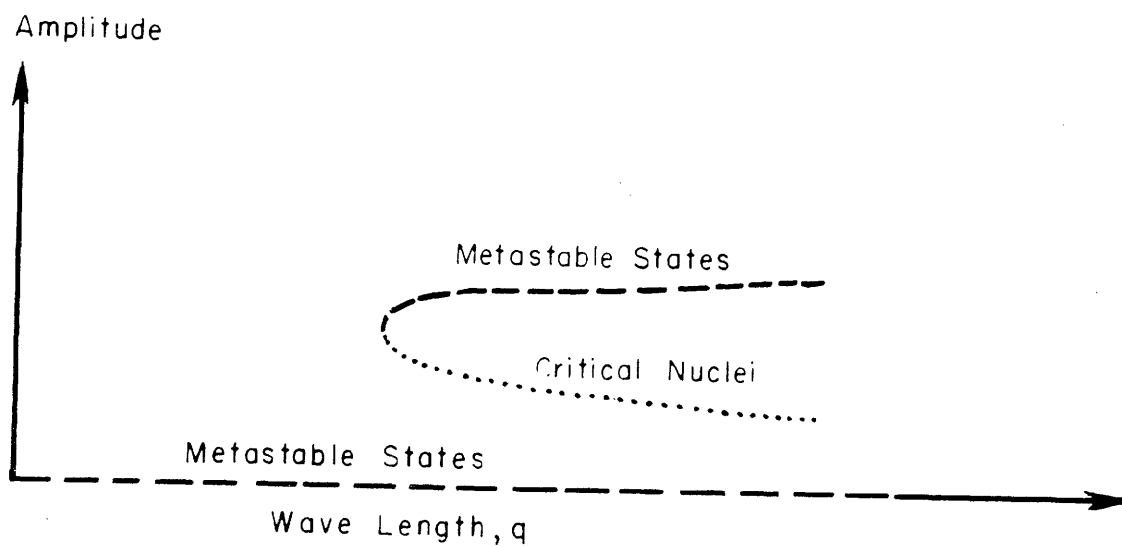
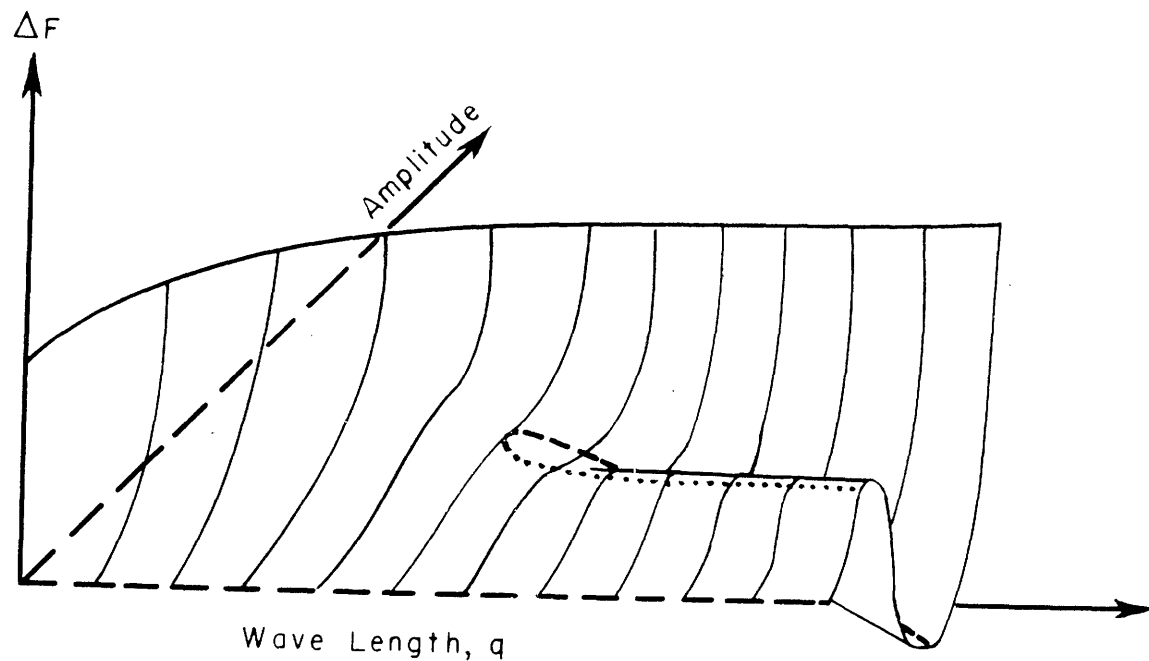


FIG. 4. SOLUTIONS TO EQ. 13 FOR A COMPOSITION BETWEEN THE MISCIBILITY GAP AND THE SPINODAL

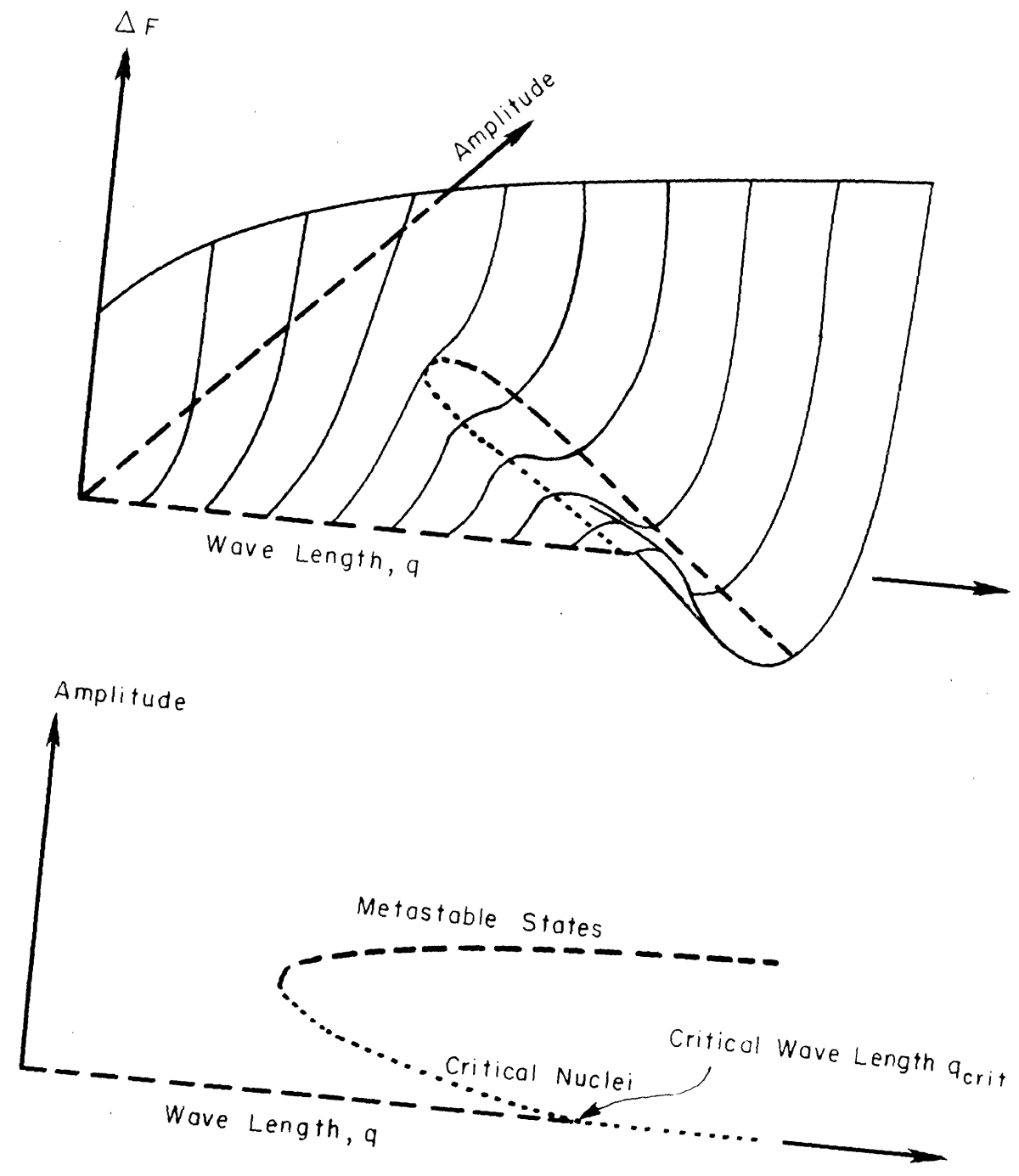


FIG. 5. SOLUTIONS TO EQ. 13 FOR A COMPOSITION INSIDE THE SPINODAL.

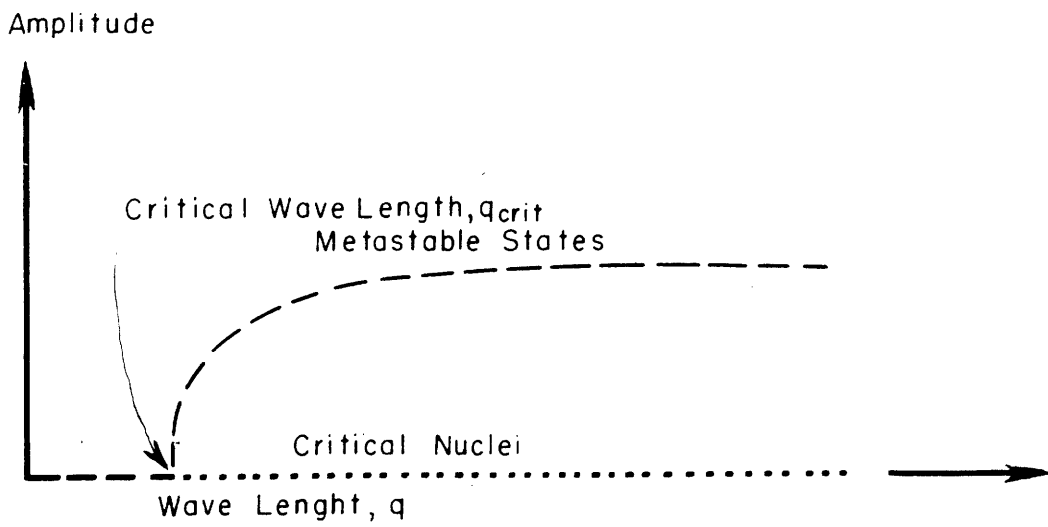
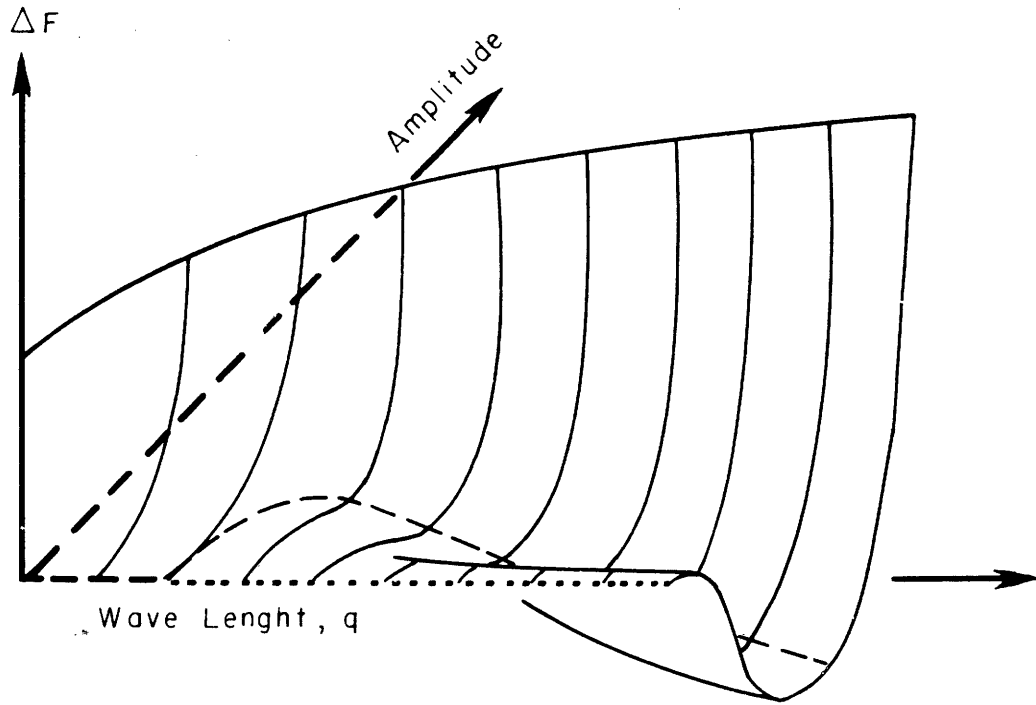


FIG. 6. SOLUTION TO EQ. 13 FOR THE SYMMETRIC COMPOSITION

### III. RESULTS OF CALCULATIONS

#### 1. Compositions Inside the Miscability Gap but Outside the Spinodal

Fig. 4 demonstrates the solutions for this case. There is a whole series of critical nuclei and of metastable states. The critical nuclei form a ridge in this kind of plot extending to infinite wave length\*. This ridge separates two series of metastable states. One of these series is simply represented by the wave length axis. All the states belonging to this series are thus identical to the initial, homogeneous state, because the amplitude of the compositional variation is zero. The other series of metastable states form the bottom of a valley which becomes deeper the longer the wave length. The deepest point must represent the final equilibrium state and is found at infinite wave length. This simply means that the crystal then contains only one region rich in one of the components and this region is surrounded by matrix poor in the same component.

In order to transform into one of the metastable states in the valley, the system must pass from the wave length axis over the ridge of critical nuclei. The most probable way for the transformation is via the lowest point on the ridge and this point is also found at infinite wave length. The characteristics of this most probable critical nucleus can be calculated

---

\*It must be remembered, however, that each point on this ridge represents a saddle point in the many-dimensional  $x^P$ -plot.

by means of our basic Eq. (13) and Fig. 7 shows the result of such a calculation for two different alloy compositions. It is apparent that there is no distinct boundary between the critical nucleus and the matrix. It is also shown that the amplitude of the critical nucleus is decreased when the alloy composition is moved closer to the spinodal. In fact, the amplitude is zero on the spinodal, which means that the ridge in Fig. 4 in this case approaches the wave length axis at infinite wave length.

The activation free energy for nucleation can be computed by means of Eq. (12) after the composition of the atomic layers have been determined. Fig. 8 shows the result of such a computation. It should again be emphasized that this treatment considers variations in composition in one direction only. The activation energy  $\Delta F^*$  is therefore proportional to the number of atoms in each plane. This number has been denoted  $m$  and the quantity  $\Delta F^*/mkT$  has been plotted in Fig. 8. Calculations have also been made from Becker's and Hobstetter's theories, applied to the same case, i.e., with variations in only one direction being considered. A comparison confirms the previous conclusion that Becker's theory does not give vanishing  $\Delta F^*$  values inside the spinodal, as it should; whereas the new approach is in agreement with Hobstetter's and also with Borelius' theory on this essential point. The new approach, however, gives much lower activation free energy values than Hobstetter's theory, apparently because Hobstetter only

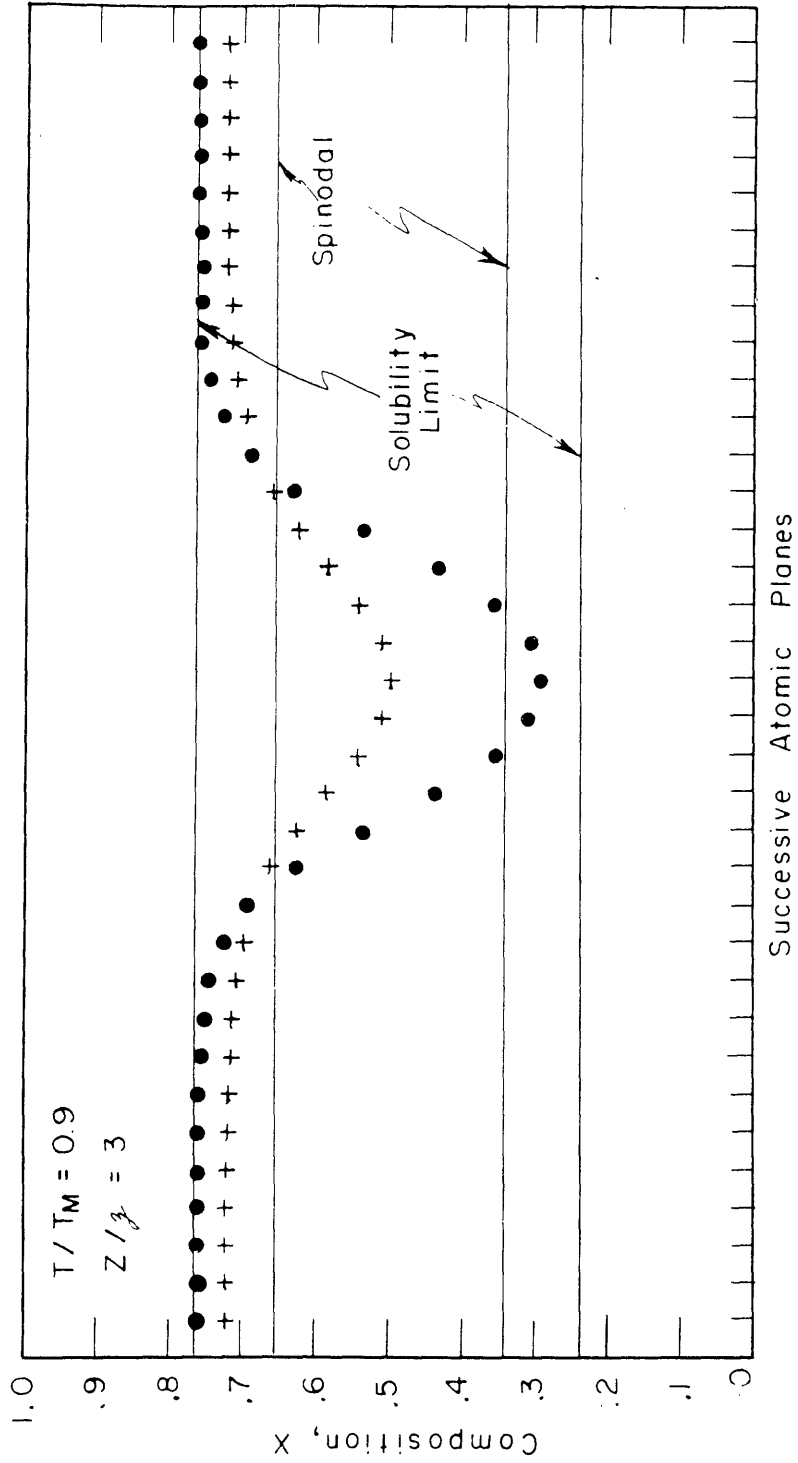


FIG. 7. COMPOSITION OF SUCCESSIVE ATOMIC PLANES FOR THE MOST PROBABLE  
 CRITICAL NUCLEUS WHEN THE ALLOY COMPOSITION IS 0.72 (CROSSES)  
 AND 0.76 (DOTS), RESPECTIVELY.

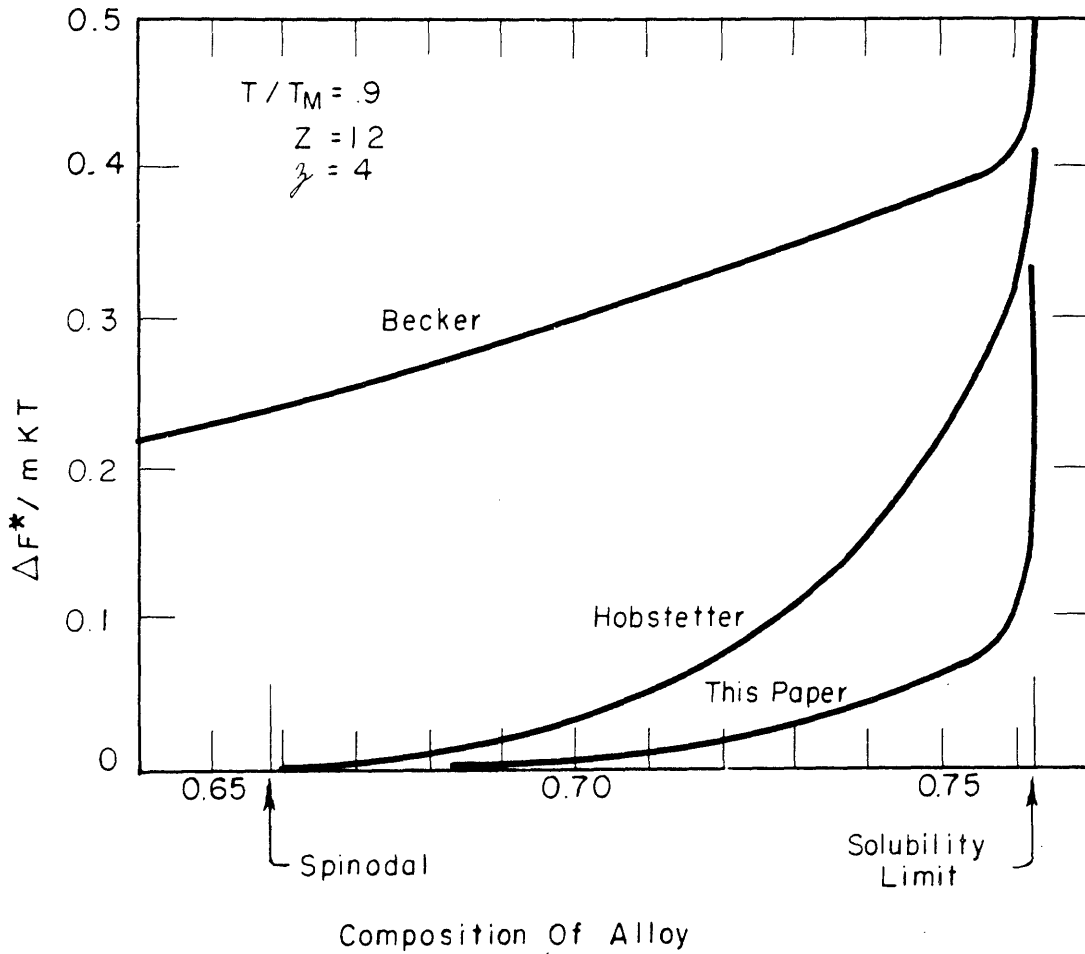


FIG. 8. ACTIVATION ENERGY FOR NUCLEATION ACCORDING TO DIFFERENT THEORIES.



considered fluctuations of a very special kind. It seems justified therefore, to conclude that Hobstetter's theory, also gives much too high activation energy values when applied to variations in three dimensions.

A comparison with Borelius' theory is impossible because this theory does not give any value of  $n^*$ .

## 2. Compositions Inside the Spinodal

It has already been mentioned that the ridge of critical nuclei in Fig. 4 approaches the wave length axis at infinite wave length when the composition is on the spinodal. If the composition is inside the spinodal, the ridge joins the wave length axis at a finite value of the wave length as Fig. 5 demonstrates. This critical wave length value,  $q_{crit}$ , is the one given by Eq. (18). Fig. 5 shows that all metastable states with longer wave lengths than  $q_{crit}$  can be reached from the homogeneous state without passing over any ridge of critical nuclei. There is consequently no activation free energy for the nucleation of these states. However, there are also metastable states, with shorter wave lengths, which are hidden behind a ridge of critical nuclei. A homogeneous alloy inside the spinodal is thus unstable only against fluctuations with wave length longer than a certain critical value,  $q_{crit}$ . It is metastable against fluctuations of shorter wave length down to a certain value and it is stable against fluctuations of even shorter wave lengths.

### 3. Symmetric Composition ( $x^0 = 0.5$ )

The solutions for this case are shown schematically in Fig. 6. All the metastable states can now be reached from the homogeneous state without passing over any ridge. Three of the solutions have been computed for a specific case and are presented in Fig. 9. The value  $Z/3 = 2$  which has been chosen here holds for the  $[100]$  direction in BCC structures along which the ordering in  $\beta$ -brass takes place. All other calculations in this work have been made with  $Z/3 = 3$  which holds for the  $[100]$  direction in FCC structures along which the precipitation in Cu-Ni-Fe alloys takes place.

### 4. Grain Boundary Energy

It was mentioned earlier that the state with infinite wave length represents the final, stable state. The lower part of Fig. 9 therefore shows how the composition varies at a coherent grain boundary\*. It is usually assumed that there is an abrupt change in composition but this is apparently not true. Becker<sup>(13)</sup> calculated the grain boundary energy assuming an abrupt change. A calculation for the case  $T/T_M = 0.9$  and  $Z/3 = 3$  gives the grain boundary energy value  $0.205mkT$  for Becker's model and the grain boundary free energy value  $0.055mkT$  for the new model. Not only is the new value much lower, it also exhibits an appreciable entropy, whereas Becker's model

---

\*It is a common experience that the final state in alloys contains incoherent grain boundaries. However, the zeroth approximation which has been used in the present treatment, assumes that the atoms are all of the same size, and a coherent boundary might then have lower energy than an incoherent.

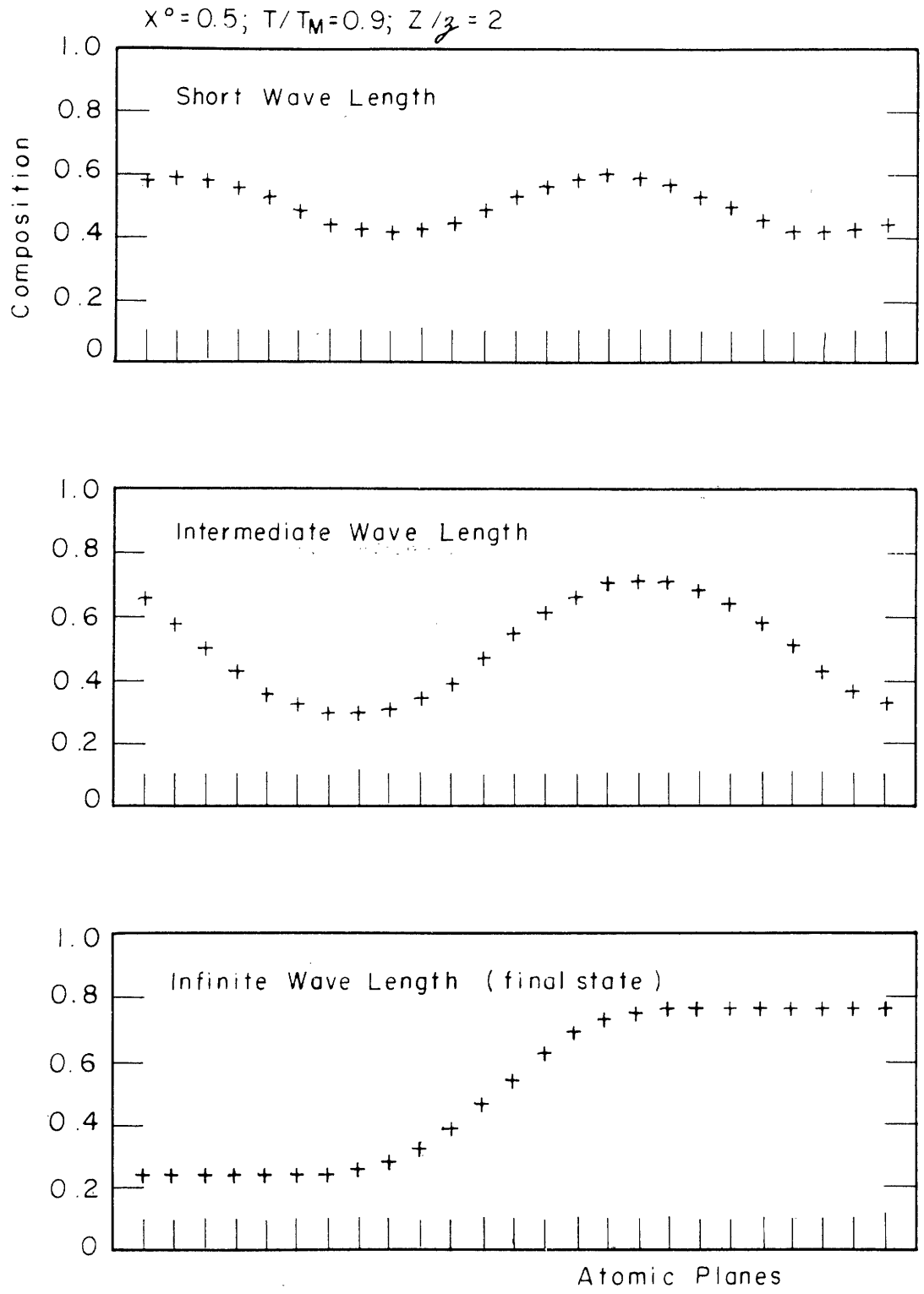


FIG. 9. SOLUTIONS TO EQ. 13 SHOWING PERIODIC VARIATION OF COMPOSITION. POSITIVE  $\nu$ .

exhibits only an enthalpy.

### 5. Ordering Systems

This work is concerned with alloy systems with miscibility gaps. However, the mathematical treatment applies equally well to ordering systems. The ordering reaction is also an exchange transformation. The only difference in the mathematics is that the interaction energy  $\nu$ , which entered into Eq. (5), is negative for ordering systems. Three of the metastable states have been computed for an ordering system with symmetric composition and are presented in Fig. 10. These states can also be described as periodic variations of the composition and can be characterized by a wave length and an amplitude. A comparison with Fig. 9 shows a striking similarity which can be expressed mathematically as  $x_{\text{pos}}^{\text{D}\nu^{-\frac{1}{2}}} = (-1)^{\text{P}} \cdot (x_{\text{neg}\nu^{-\frac{1}{2}}})$ . This relation holds only for the symmetric composition, however.

The state with infinite wave length is shown at the bottom of Fig. 10 and is identical to the case of two ordered domains joined by an anti-phase domain boundary. It is evident that there is not a sharp phase change at such a boundary but a gradual change, quite equivalent to the gradual change in composition found for grain boundaries.

### 6. Revision of the Diffusion Equation

It has long been realized that a concentration gradient causes diffusion in the direction against the gradient (up-hill diffusion) if the composition is inside the spinodal,

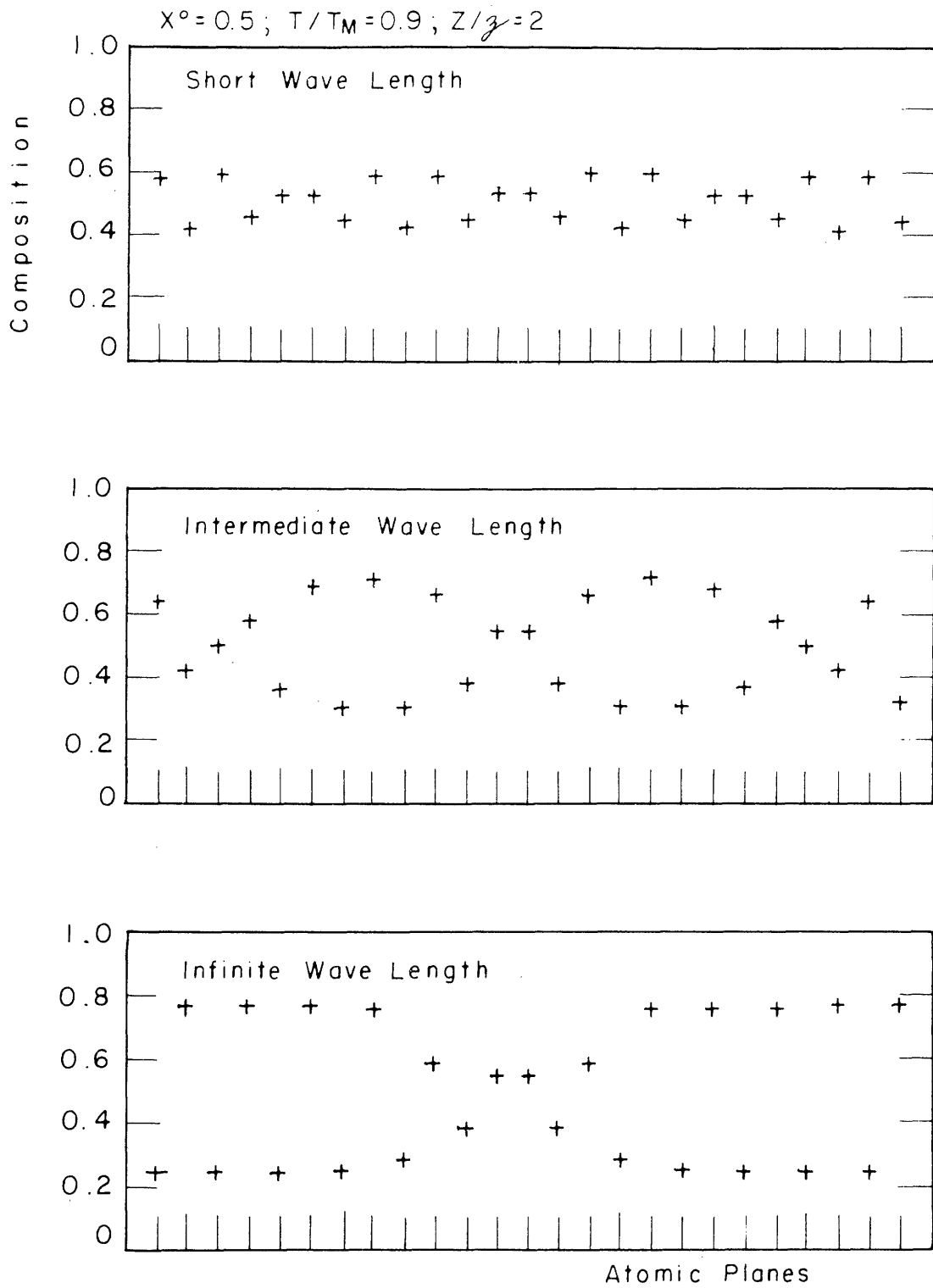


FIG.10. SOLUTIONS TO EQ.13 SHOWING PERIODIC VARIATION OF COMPOSITION. NEGATIVE  $\nu$ .

whereas it otherwise causes diffusion down the gradient (down-hill diffusion). This is a consequence of the fact that the change in free energy can be considered as the driving force for diffusion, and was pointed out by Becker<sup>(7)</sup> in the case of equal mobility of the two components in a binary metallic system and by Darken<sup>(17)</sup> in the case of different mobilities. However, from the previous sections it is clear that concentration gradients can exist without giving rise to any diffusion, since the periodic structures are metastable states. In order to account for this phenomenon one must consider the diffusion process on a microscopic scale. We shall here derive the diffusion equation for the case of a reasonably small concentration gradient, i.e.  $x^p \cong x^{p+1}$ . Only the case of equal mobility will be treated and the zeroth approximation will again be used. The change in free energy when A and B atoms are exchanged between two neighboring atomic planes was derived in Section II.5. The flow of atoms is now obtained using Eqs. (12) to (14).

$$J = Bx(1-x) \left( \frac{\partial \Delta F}{\partial x^p} \right) x^p = mBx(1-x) \left[ \left( \frac{kT}{x(1-x)} - 2Z\nu \right) (x^p - x^{p+1}) + 2Z\nu(x^{p+2} - 3x^{p+1} + 3x^p - x^{p-1}) \right] \quad (19)$$

where  $m$  is the number of atoms per plane and  $B$  is the mobility.

If Becker's<sup>(7)</sup> and Darken's<sup>(17)</sup> equations are applied to the same case, one finds

$$J = mBx(1-x) \left( \frac{kT}{x(1-x)} - 2Z\nu \right) (x^p - x^{p+1}) \quad (20)$$

The two equations differ only in the last term in the bracket. This term is zero if the concentration gradient is constant. In fact, it corresponds to the third derivative of the concentration and is therefore negligibly small in most cases. However, it is of great importance for processes which take place on a very small scale, such as those treated here.

#### 7. First Stage of Transformation in Symmetric Alloy

The question which wave length will first be formed in a specimen, when it is quenched from above the miscibility gap and annealed at a temperature inside the spinodal, is difficult to answer. All wave lengths longer than the critical value,  $q_{crit}$ , can be formed without any nucleation difficulties and the formation of them can thus start without any incubation time. The decisive factor might then be the rate of development of the metastable states with different wave lengths. This rate should be higher, the larger the decrease in free energy,  $-\Delta F$ , and it should be lower the longer distance the atoms must be transported. This distance is proportional to the wave length,  $q$ , and it can therefore be expected that the rate is highest in the vicinity of the maximum of  $(-\Delta F)/q$ . This quantity was calculated for a case with symmetric composition and is plotted in Fig. 11. It could thus be expected that the initial transformation in this case leads to a wave length a few times longer than the critical value  $q_{crit}$ . We shall in the following refer to this as the optimum wave length,  $q_{opt}$ .

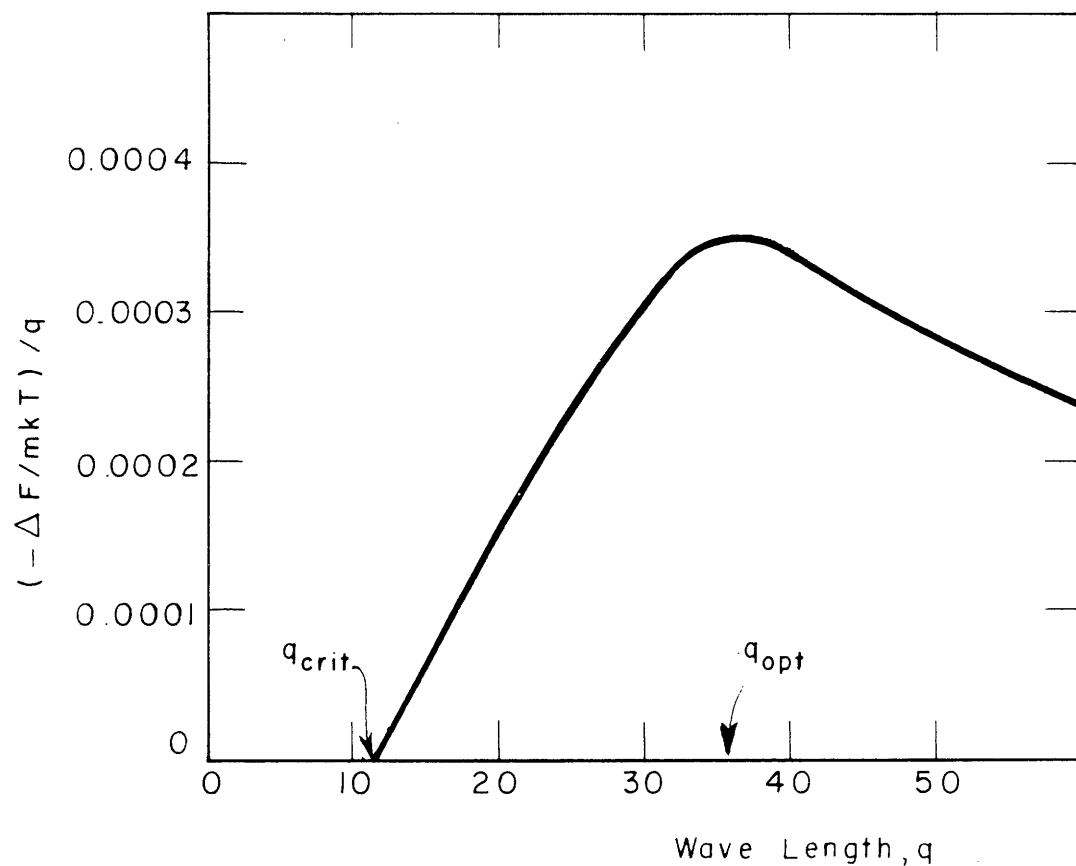


FIG. II. VARIATION WITH WAVE LENGTH OF THE RATIO BETWEEN DRIVING FORCE AND DIFFUSION DISTANCE.



The atoms need to move only from one plane to the neighboring one in the case of ordering. The optimum wave length is thus very high in this case.

#### 8. First Stage of Transformation in Asymmetric Alloys

No calculation of  $(-\Delta F)/q$  has been made for asymmetric compositions because it would be much more tedious than in the symmetric case. It is, however, evident that the optimum wave length,  $q_{opt}$ , will be longer as the composition is made more asymmetric, and it approaches infinity as the composition approaches the solubility limit.

It is doubtful that this method gives a good estimate of the first wave length when the composition is very asymmetric. The optimum wave length is then shorter than the critical wave length which approaches infinity already on the spinodal. (See Fig. 28.) The metastable state with the optimum wave length is then hidden behind the ridge of critical nuclei and can not be formed without nucleation. It is still possible that the time of formation, including the incubation time for nucleation, could be shorter for some wave length behind the ridge than for the wave lengths longer than  $q_{crit}$ .

#### 9. Limitations of Present Treatment

The present treatment compares the homogeneous state with states where the composition varies in one direction only. It is probable that in a specific case some state with variations in two or three directions is even more favorable than the structures found here. In particular, the activation free

energy for nucleation of metastable states behind the ridge of critical nuclei is proportional to the number of atoms in each plane,  $m$ . The nuclei should thus have a limited extension in the two directions of the planes. It is impossible at the present to tell how such a limited extension will modify the predictions made here for the compositional variations in the considered direction.

It was mentioned in Section II.5 that the name "critical nucleus" is not quite adequate because the transformation can pass over the ridge in the many-dimensional  $x^p$ -space at any point and we consider only the saddle points. Points close to the saddle points have almost as low activation free energy as the saddle points themselves. The chance that the transformation goes exactly over a saddle point is thus negligible, and one should never expect to obtain a structure with an ideal periodicity but rather a spectrum of wave lengths.

#### 10. Second Stage of Transformation

Suppose a system has been completely transformed into a metastable state in the valley of Fig. 6. It can not be transformed into another state of still lower free energy without a difficult nucleation process. In essence, it has to climb back uphill to the wave length axis and can then choose a new longer wave length and fall downhill into the valley deeper than before. This is the reason why the wave length axis was marked as a ridge of critical nuclei outside  $q_{crit}$ .

The increase of the wave length from its first value could thus be expected to be an exceedingly slow process. However, it was mentioned in the last section that an ideal periodic structure is very improbable. As soon as there is a spectrum of wave lengths it is easy to imagine that the mean wave length increases continuously simply by a disappearance of the shorter wave lengths and creation of longer wave lengths by interference between the remaining wave lengths.

#### 11. Purpose of Experimental Work

It is a common feature of the present treatment and Borelius' and Hobstetter's theories that the activation energy for nucleation is zero on and inside the spinodal. Many investigations have been undertaken in order to test this significance of the spinodal (12, 18 - 25). However, most of the examined transformations have not been exchange transformations and the results should therefore not be used to test the above theories. The only case of exchange transformation that has been examined previously is the formation of Guinier-Preston zones in age-hardening systems. Such systems might contain metastable miscibility gaps, the positions of which can be calculated from thermodynamic data of the solid solutions. They are not possible to determine experimentally because of the formation of more stable phases. Such thermodynamic data are not known with any accuracy and our knowledge of the metastable miscibility gaps is therefore limited and the position of the spinodals can not be calculated with any accuracy.

Moreover, only one side of the metastable miscibility gap can be examined experimentally, due to the presence of other phases.

It would be highly desirable to investigate an exchange transformation in a system with complete miscibility at high temperatures and a stable miscibility gap at lower temperature. This seems to be possible in the ternary system Cu-Ni-Fe. This system is known to have a miscibility gap and it has been found that alloys in a certain composition range show exchange transformation when quenched into the miscibility gap. Moreover, the transformation product has been examined by means of X-ray diffraction, and the diffraction patterns have been interpreted as caused by a structure with a periodic variation of the composition. The wave length can easily be evaluated and it would be very interesting to test how well our theoretical treatment can account for the variation with temperature and composition of the wave length of the first formed structure. Previous measurements are not sufficiently accurate for such a test. They have mainly been made with a single composition, only a few temperatures have been used, and the interest has not been focussed on the first transformation product.

It is apparent that the advantage of the present treatment over Borelius' and Hobstetter's theories is that it not only predicts spontaneous transformation inside the spinodal but also the characteristics of the structure. Such predictions might be easier to test experimentally.

It should be remembered that all the nucleation theories considered here treat homogeneous nucleation only, and it is in fact very difficult to prove directly by experiments if a certain nucleation process is homogeneous or heterogeneous. It is consequently difficult to disprove a nucleation theory. Lack of agreement with experiments may very well be due to the fact that the theory treats one kind of nucleation and the examined process is of the other kind.

The Cu-Ni-Fe system is not an ideal system for a test of the nucleation theories because it is a ternary system and the theories treat binary systems. However, the alloys in the interesting composition range behave almost pseudo-binarily, one of the two components being copper.

The experiments undertaken will be described in Chapter VI after a discussion of the interaction energy concept in Chapter IV and of the X-ray theory for periodic structures in Chapter V.

#### IV. DEFINITION AND CALCULATION OF THE INTERACTION ENERGY

##### 1. Classical Definition

There is a certain class of solid-solution theories which assume that an energy can be ascribed to the bond between every two atoms in a crystal. The heat of mixing can then be calculated by considering the change in the number of the different kinds of bonds on mixing the pure components. A basic assumption is that the heat of mixing is unaffected by a change in temperature, if the configuration of the atoms in the crystal can be retained during the temperature change. This is almost equivalent to the Kopp-Neumann rule, which, however, is concerned with the equilibrium state at every temperature. The usefulness of these theories depends on the assumption that the bond energies are independent of temperature, composition and configuration. For the sake of simplicity it is usually considered that all bonds except those between the nearest neighbors can be neglected, and the pertinent quantity is the so-called interaction energy  $\nu$ , which is defined as

$$\nu = E_{AB} - \frac{1}{2} (E_{AA} + E_{BB}) \quad (21)$$

Cowley<sup>(26)</sup>, however, has also taken into account the next nearest neighbor bonds.

Using the above assumptions, it is possible in principle to calculate the equilibrium configuration at every temperature in terms of the bond energies, which in turn allows a calculation of the entropy, enthalpy and free energy of mixing. These calculations are very difficult and certain simplifications are

used. Guggenheim<sup>(27)</sup> has reviewed these theories recently.

In the so-called zeroth approximation, it is assumed that the atoms are randomly distributed in the crystal. However, if the interaction energy  $\nu$  is positive, there should be fewer AB bonds than in the random case because the enthalpy is thereby decreased; if  $\nu$  is negative, there should be more AB bonds. This is taken into account in an approximate way by the so-called first approximation, which is also called the quasi-chemical theory. This leads to an expression for the different kinds of bonds of the following form which resembles the chemical law of mass action.

$$\frac{P_{AB}^2}{P_{AA} P_{BB}} = 4 \exp\left(-\frac{2\nu}{kT}\right) \quad (22)$$

where  $P_{AA}$  is the number of AA bonds, etc.

It is possible to calculate the thermodynamic quantities accurately in terms of power series in  $\left(\frac{\nu}{kT}\right)$ . Unfortunately these series converge rather slowly and the use of the simpler quasi-chemical theory, which gives a correct result up to the third term, is thus justified.

The long-range program, of which this investigation is a part, was originally designed to test the quasi-chemical theory for metallic solid solutions. The experimental results have demonstrated that high excess entropy is normal if there is a considerable difference in atomic size or valency between the components. The quantity,  $\nu$ , is then dependent on temperature. It was also found that  $\nu$  may vary considerably with

composition when there is a difference in valency. These results are in conflict with the assumptions leading to the quasi-chemical theory. Moreover, a comparison of the values of  $\frac{\nu}{kT}$  calculated from X-ray data and from experimental values of the thermodynamic quantity  $H^M$  does not show good agreement, as is seen from Table I. Consequently, the validity of the quasi-chemical theory and the concept of an interaction energy,  $\nu$ , appear doubtful.

TABLE 1  
Calculated Values of  $\frac{\nu}{kT}$

<u>Alloy</u>	<u>Temp. °K</u>	<u>Calculation Based on <math>H^M</math></u>	<u>Calculation Based on <math>F^M</math></u>	<u>Calculation Based on X-ray Data</u>
Au <sub>0.5</sub> Ni <sub>0.5</sub> (30)	1173	+0.55	+0.15	-0.06
Al <sub>0.9</sub> Ag <sub>0.1</sub> (33)	820	+0.1	0	+0.6
Al <sub>0.185</sub> Ag <sub>0.815</sub>	820	-0.1	-0.4	-0.4*

\*This value is for 733°K

## 2. Guggenheim's Definition of the Interaction Energy

The difficulty of the temperature dependency of  $\nu$  can be removed, as was shown by Guggenheim<sup>(28)</sup>, who suggested that the interaction energy can be defined on a purely isothermal basis by using the quasi-chemical equation as a definition of  $\nu$ . The only assumption Guggenheim makes is that this quantity  $\nu$  is independent of configuration and composition. We shall go a step further and derive the quasi-chemical theory without any assumption concerning  $\nu$ .



### 3. New Definition of the Interaction Energy

A binary alloy is usually considered as consisting of the two kinds of atoms and its molar free energy is therefore described by the partial molar free energies and mole fractions of the components

$$F_m = x_A \bar{F}_A + x_B \bar{F}_B \quad (23)$$

where  $x_A + x_B = 1$ .

Realizing that the alloy could as well be described by means of the nearest-neighbor bonds, one could describe the free energy per mole of atoms in terms of partial molar free energies and mole fractions of the bonds.

$$F_m = \frac{Z}{2} \left[ x_{AA} \bar{F}_{AA} + x_{AB} \bar{F}_{AB} + x_{BA} \bar{F}_{BA} + x_{BB} \bar{F}_{BB} \right] \quad (24)$$

where  $x_{AA} + x_{AB} + x_{BA} + x_{BB} = 1$ .  $Z$  is the number of nearest neighbors to each atom and  $\frac{Z}{2}$  is thus the number of moles of bonds per mole of atoms. One has to distinguish between AB and BA because an AB-bond can be placed in two different ways between two atom sites, which is not the case for AA- or BB-bonds. As an average  $x_{AB}$  and  $x_{BA}$  will be equal, and so will  $\bar{F}_{AB}$  and  $\bar{F}_{BA}$ . The previously used symbol  $P_{AB}$  referred to the number of AB bonds regardless of their direction. One therefore obtains per mole of atoms  $P_{AB} = \frac{1}{2}ZN (x_{AB} + x_{BA}) = ZNx_{AB}$ .

It is easy to show that

$$\begin{aligned} x_A &= x_{AA} + \frac{1}{2}x_{AB} + \frac{1}{2}x_{BA} \\ x_B &= x_{BB} + \frac{1}{2}x_{BA} + \frac{1}{2}x_{AB} \end{aligned} \quad (25)$$

The relative molar free energy (free energy of mixing) of an alloy is defined by

$$F^M = F_M - x_A F_A^0 - x_B F_B^0 \quad (26)$$

where  $F_A^0$  and  $F_B^0$  are the free energies per mole of pure A and B, respectively. In pure A there are only AA-bonds. Therefore Eq. (24) gives  $F_A^0 = \frac{Z}{2} F_{AA}^0$  and also  $F_B^0 = \frac{Z}{2} F_{BB}^0$ . Eqs. (24)

and (26) now yield

$$F^M = \frac{Z}{2} \left[ x_{AA} \bar{F}_{AA} + x_{AB} \bar{F}_{AB} + x_{BA} \bar{F}_{BA} + x_{BB} \bar{F}_{BB} - x_A F_{AA}^0 - x_B F_{BB}^0 \right] \quad (27)$$

When the equilibrium is attained in a  $(x_A, x_B)$  alloy, the free energy change for the reaction



has to be zero. Thus

$$\bar{F}_{AB} + \bar{F}_{BA} - \bar{F}_{AA} - \bar{F}_{BB} = 0 \quad (28)$$

One can therefore form the expression,

$$\frac{x_{AB} x_{BA}}{x_{AA} x_{BB}} = \exp \left( \ln \frac{x_{AB} x_{BA}}{x_{AA} x_{BB}} \right) = \exp \frac{-1}{RT} \left[ \left( \bar{F}_{AB} - RT \ln x_{AB} \right) + \left( \bar{F}_{BA} - RT \ln x_{BA} \right) - \left( \bar{F}_{AA} - RT \ln x_{AA} \right) - \left( \bar{F}_{BB} - RT \ln x_{BB} \right) \right] \quad (29)$$

The quantities  $-R \ln x_{AA}$ ,  $-R \ln x_{AB}$ ,  $-R \ln x_{BA}$  and  $-R \ln x_{BB}$  are recognized as the partial, positional entropy for four components in random mixing. The integral positional entropy is then, per mole of atoms

$$S^P = - \frac{Z}{2} R \left[ x_{AA} \ln x_{AA} + x_{AB} \ln x_{AB} + x_{BA} \ln x_{BA} + x_{BB} \ln x_{BB} \right] \quad (30)$$

In the case of bonds, however, there is a restriction on the distribution, since at each atom site all bonds must be either AA and AB (in the case of an A atom) or BB and BA (in the case of a B atom). A correction term must therefore be added to the expression for  $S^P$  in Eq. (30). The correction can be calculated for the case of random distribution of the atoms, i.e., when  $x_{AA} = x_A^2$ ,  $x_{AB} = x_A x_B$ ,  $x_{BA} = x_A x_B$  and  $x_{BB} = x_B^2$ , because  $S^P$  then has to be equal to  $-R [x_A \ln x_A + x_B \ln x_B]$ . The correction term is thus found to be  $(Z-1) \cdot R \cdot [x_A \ln x_A + x_B \ln x_B]$ . Assuming the correction term to be independent of the degree of randomness, one can get  $S^P$  at any value of  $x_{AA}$ ,  $x_{AB}$ ,  $x_{BA}$  and  $x_{BB}$

$$S^P = -\frac{Z}{2} \cdot R \left[ x_{AA} \ln x_{AA} + x_{AB} \ln x_{AB} + x_{BA} \ln x_{BA} + x_{BB} \ln x_{BB} \right] + (Z-1)R \left[ x_A \ln x_A + x_B \ln x_B \right] \quad (31)$$

This is exactly the expression for the entropy of mixing according to the quasi-chemical theory. It has also been derived by Takagi<sup>(29)</sup>. The foregoing assumption is obviously very poor when the degree of randomness is low. For instance, Eq. (31) gives the quite impossible negative entropy value  $(\frac{Z}{2} - 1)R \cdot$

$\left[ x_A \ln x_A + x_B \ln x_B \right]$  when  $x_{AB} = x_{BA} = 0$ . However, at small

deviations from ideal randomness it is a good approximation which is shown by a comparison with the more accurate power-series expansion. (27)

The partial positional entropies are now obtained from Eq. (31)

$$\begin{aligned}
 S_{AA}^P &= -R \ln x_{AA} + (2 - \frac{2}{Z}) R \ln x_A \\
 S_{AB}^P &= -R \ln x_{AB} + (2 - \frac{2}{Z}) R (\frac{1}{2} \ln x_A + \frac{1}{2} \ln x_B) \\
 S_{BA}^P &= -R \ln x_{BA} + (2 - \frac{2}{Z}) R (\frac{1}{2} \ln x_A + \frac{1}{2} \ln x_B) \\
 S_{BB}^P &= -R \ln x_{BB} + (2 - \frac{2}{Z}) R \ln x_B
 \end{aligned} \tag{32}$$

Partial excess free energy for a component A is defined<sup>(1)</sup> as

$$F_A^E = \bar{F}_A - F_A^\circ - RT \ln x_A \tag{33}$$

where  $-R \ln x_A$  is the ideal value of the partial entropy of mixing for the component. The corresponding values for the bonds are those given by Eq. (32), however, and the partial excess free energy of the bonds should thus be defined as

$$F_{AA}^E = \bar{F}_{AA} - F_{AA}^\circ - RT \ln x_{AA} + (2 - \frac{2}{Z}) RT \ln x_A \tag{34a}$$

$$F_{AB}^E = \bar{F}_{AB} - F_{AB}^\circ - RT \ln x_{AB} + (1 - \frac{1}{Z}) RT (\ln x_A + \ln x_B) \tag{34b}$$

$$F_{BA}^E = \bar{F}_{BA} - F_{BA}^\circ - RT \ln x_{BA} + (1 - \frac{1}{Z}) RT (\ln x_A + \ln x_B) \tag{34c}$$

$$F_{BB}^E = \bar{F}_{BB} - F_{BB}^\circ - RT \ln x_{BB} + (2 - \frac{2}{Z}) RT \ln x_B \tag{34d}$$

It may be convenient to define  $F_{AB}^\circ$  and  $F_{BA}^\circ$  as  $\bar{F}_{AB}$  and  $\bar{F}_{BA}$  in a completely ordered alloy of composition  $x_A = x_B = \frac{1}{2}$ .

In any event, adding (b) and (c), and subtracting (a) and (d) gives

$$\begin{aligned} & (\bar{F}_{AB} - RT \ln x_{AB}) + (\bar{F}_{BA} - RT \ln x_{BA}) - (\bar{F}_{AA} - RT \ln x_{AA}) - (\bar{F}_{BB} - RT \ln x_{BB}) = \\ & F_{AB}^{\circ} + F_{BA}^{\circ} - F_{AA}^{\circ} - F_{BB}^{\circ} + F_{AB}^E + F_{BA}^E - F_{AA}^E - F_{BB}^E \end{aligned} \quad (35)$$

The left-hand side is recognized as the bracket in Eq. (29), which can now be replaced by the right-hand side of Eq. (35). Using the relations  $x_{AB} = x_{BA}$  and  $\bar{F}_{AB} = \bar{F}_{BA}$  together with the definitions

$$\begin{aligned} N_0 \nu^{\circ} &= F_{AB}^{\circ} - \frac{1}{2} (F_{AA}^{\circ} + F_{BB}^{\circ}) \\ N_0 \nu^E &= F_{AB}^E - \frac{1}{2} (F_{AA}^E + F_{BB}^E) \end{aligned} \quad (36)$$

$$\nu = \nu^{\circ} + \nu^E$$

where  $N_0$  is Avogadro's number, one may write Eq. (27)

$$F^M = \frac{Z}{2} \left[ 2x_{AB} N_0 \nu^{\circ} + x_{AA} F_{AA}^E + 2x_{AB} F_{AB}^E + x_{BB} F_{BB}^E \right] - TS^P \quad (37)$$

$$\text{or } F^M = \frac{Z}{2} \left[ 2x_{AB} N_0 \nu + x_A F_{AA}^E + x_B F_{BB}^E \right] - TS^P \quad (38)$$

where  $S^P$  is given by Eq. (31) and  $x_{AB}$  by (29), which by means of (35) can be transformed into

$$\frac{x_{AB}^2}{x_{AA} x_{BB}} = \exp \left( -\frac{2\nu}{kT} \right) \quad (39)$$

or

$$x_{AB} = \frac{-1 + \sqrt{1 + 4x_A x_B \left( \exp \frac{2\nu}{kT} - 1 \right)}}{2 \left( \exp \frac{2\nu}{kT} - 1 \right)} \quad (40)$$

This is identical to the quasi-chemical equation, Eq. (22). It is interesting to note, however, that the quantity  $\nu$  is a free energy according to this derivation.

$\nu$  has been defined here for a constant temperature and composition, and it is in principle unnecessary to make any assumptions concerning the independence of  $\nu$  relative to these two variables. The experimental results for the Al-Ag system indicating  $\nu$  to vary with both temperature and composition are thus not in opposition to the theory. However, the usefulness of this theory is quite limited, because of the two unknown quantities  $F_{AA}^E$  and  $F_{BB}^E$  in Eq. (38). In view of Eq. (36) it is to be expected that these quantities vary with composition if  $\nu$  does, and it is then impossible to determine  $\nu$  accurately from thermodynamic data.

Eqs. (36) to (38) show clearly that the interaction energy  $\nu$  is actually a free energy and its magnitude should not be calculated from experimental enthalpy values but from free energy values. This has not been done in the past, and the systems Au-Ni and Al-Ag should, therefore, be reconsidered. Assuming that  $F_{AA}^E$  and  $F_{BB}^E$  are negligible,  $\frac{\nu}{RT}$  was calculated from  $F^M$  for these two systems and the results are compared in Table 1 with values calculated from X-ray measurements. Values based on the erroneous use of  $H^M$  are also given.

Au and Ni have considerably different atomic sizes and it has therefore been suggested that strains play an important role in solid Au-Ni solutions<sup>(30,31,32)</sup>. Attempts have even

been made to account for the discrepancy between the values of  $\frac{\nu}{kT}$  calculated from  $H^M$  and X-ray data by a separate calculation of the effect of the strains. However, Table 1 shows that the agreement is improved considerably through the use of  $F^M$  instead of  $H^M$  for the alloy  $Au_{0.5}Ni_{0.5}$ . There is still a difference in sign which cannot be removed without the assumption that the excess quantities,  $F_{AA}^E$  and  $F_{BB}^E$ , have non-vanishing values. It seems quite reasonable that this should be the case when the strains play an important role.

For the alloy  $Al_{0.185}Ag_{0.815}$  the agreement is improved by the use of  $F^M$ , for the alloy  $Al_{0.9}Ag_{0.1}$  the agreement is slightly worse. No definite improvement is thus obtained for the Al-Ag system, probably because there is no appreciable difference in the atomic sizes. It is obvious that  $F_{AA}^E$  and  $F_{BB}^E$  cannot be neglected in this system, which indeed should be expected in view of Eq. (36) because  $\nu$  shows a substantial variation with composition.<sup>(33)</sup> This variation is probably caused by the difference in valence between Al and Ag.

#### 4. Estimation of the Interaction Energy

The preceding analysis indicates that there is not necessarily anything fundamentally wrong with the interaction-energy concept despite the apparent disagreement found in the earlier investigations. The use of this concept in Chapter II therefore seems justified, especially for systems without appreciable differences in atomic size (as was the case for Au-Ni)

or valency (as was the case for Al-Ag). In alloys between transition elements in the same series one could consequently expect that  $\nu$  is fairly constant with both temperature and composition, and it should be possible to make a good estimation of  $\nu$  from thermodynamic data.

If no thermodynamic data are available for a system, it is possible to estimate the thermodynamic properties from the phase diagram. Some assumptions must then be made concerning the shape of the enthalpy and entropy functions, but these assumptions can not generally be tested. Hardy<sup>(34)</sup> has suggested a certain shape for these functions, which can be written

$$F^E = x_A x_B \left[ A_0 + A_1 \cdot (x_A - x_B) \right] \quad (41)$$

where  $A_0$  and  $A_1$  may be temperature dependent. Hardy also presented a test for this "subregular solution model" for systems with a miscibility gap. However, if more terms are used in the expression for  $F^E$ ,

$$F^E = x_A x_B \left[ A_0 + A_1 \cdot (x_A - x_B) + A_2 \cdot (x_A - x_B)^2 + A_3 \cdot (x_A - x_B)^3 \dots \right] \quad (42)$$

one can derive the following two equations.

$$\frac{RT}{2(x_A^I - x_A^{II})} \ln \frac{x_A^I x_B^I}{x_A^{II} x_B^{II}} - \frac{3RT\varepsilon}{(x_A^I - x_A^{II})} \left[ (x_A^I + x_A^{II}) \ln \frac{x_A^I}{x_A^{II}} + (x_B^I + x_B^{II}) \ln \frac{x_B^I}{x_B^{II}} \right] =$$

$$= A_0 + A_2 (-4\varepsilon^2 + 4\varepsilon - 8x_A^I x_A^{II} + 1) + A_3 \cdot 4\varepsilon (-4\varepsilon^2 + 2\varepsilon - 4x_A^I x_A^{II} + 1) \dots \quad (43)$$



and

$$\frac{RT}{(x_A^{II} - x_A^I)^3} \left[ (x_A^I + x_A^{II}) \ln \frac{x_A^I}{x_A^{II}} + (x_B^I + x_B^{II}) \ln \frac{x_B^I}{x_B^{II}} \right] =$$

$$= A_1 + A_2 4\mathcal{E} + A_3 (12\mathcal{E}^2 + 4\mathcal{E} - 8x_A^I x_A^{II} + 1) \dots \quad (44)$$

where  $x_A^I$  and  $x_A^{II}$  are the compositions of the two coexisting phases at a temperature  $T$ , and  $\mathcal{E}$  is defined as  $x_A^I - x_B^I$ .

Eq. (44) becomes identical to that used in Hardy's test if one sets  $A_2 = A_3 = \dots = 0$ . He plotted  $RT \left[ (x_A^I + x_A^{II}) \ln x_A^I / x_A^{II} + (x_B^I + x_B^{II}) \ln x_B^I / x_B^{II} \right]$  versus  $(x_A^{II} - x_A^I)^3$ , and suggested that a straight-line relationship indicates all coefficients higher than  $A_1$  to be negligibly small. However, we see from Eq. (44) that a straight line simply indicates the whole right-hand side to be constant over the temperature range under consideration. For the systems Ag-Cu, Ag-Pt, Al-Zn and Au-Pt, the quantities  $4\mathcal{E}$  and  $(12\mathcal{E}^2 + 4\mathcal{E} - 8x_A^I x_A^{II} + 1)$  have rather low values and vary little with temperature within the temperature region where solubility data are available. Moreover, the possibility that  $A_1$  itself varies with temperature must also be considered. Without very accurate solubility measurements over a wide temperature range, it therefore seems unwarranted to use Hardy's plot as a test that  $A_2 = A_3 = \dots = 0$ . Unfortunately, such data are usually not available.

The chances of validating an assumed shape for the enthalpy and entropy functions are thus remote, and consequently it seems just as proper to use the simplest possible shape as more

complicated ones. Hence, the zeroth approximation, which was employed in the theory derived in Chapter II can be used for evaluation of  $\nu$ . The free energy of mixing is then

$$F^M = x_A x_B N Z \nu + RT(x_A \ln x_A + x_B \ln x_B) \quad (45)$$

and from the second derivative one finds the relation

$$\nu = \frac{RT_M}{2NZx_A x_B} \quad (46)$$

where  $T_M$  is the maximum temperature of the miscibility gap. Only this information is needed from the phase diagram.

#### 5. Discussion of Other Quasi-Chemical Treatments

Scheil and Wegener: Scheil and Wegener<sup>(35)</sup> have developed a theory for the short-range configuration of atoms in solid solutions. They do not refer to the quasi-chemical theory but their treatment turns out to be in principle identical to the quasi-chemical theory with the Z value 1. This value holds only for two-atomic gas molecules, and the Scheil-Wegener treatment is thus unnecessarily restrictive, especially since the quasi-chemical theory can handle systems with any Z value. However, their analysis is interesting in connection with the preceding section, where it was shown that the expression for the free energy of mixing,  $F^M$ , should contain the terms  $\frac{Z}{2}(x_{AA} F_{AA}^E + 2x_{AB} F_{AB}^E + x_{BB} F_{BB}^E)$ . (See Eq. (37).) Scheil and Wegener give an equation (their number 9), which in the present notation is equivalent to

$$F^M = 2x_{AB}N_0 \nu^0 + a_1 x_{AA}(1-x_{AA}) + a_2 x_{BB}(1-x_{BB}) + a_{12} x_{AA} x_{BB} - TS^P \quad (47)$$

where  $a_1$ ,  $a_2$  and  $a_{12}$  are constants. This equation should be compared with Eq. (37). It is worth noting that their expression for  $S^P$  is identical to the one given here with  $Z = 1$ , whereas a factor of  $\frac{1}{2}$ , coming from  $\frac{Z}{2}$ , is missing in the first term of Eq. (47).

The use of the three constants  $a_1$ ,  $a_2$  and  $a_{12}$  apparently implies the assumption of a very special concentration dependency of the three quantities  $F_{AA}^E$ ,  $F_{AB}^E$  and  $F_{BB}^E$  in Eq. (37). Scheil and Wegener make calculations using certain values for the three constants, and their results are quite contrary to the results of a calculation to be presented here in a later section. The physical significance of the constants is difficult to interpret, and it is therefore impossible at the moment to tell whether the discrepancy is due only to an unlucky choice of the constants in the Scheil-Wegener calculation or to the very use of these constants.

Dehlinger and Knapp: The quasi-chemical theory (i.e. the so-called first approximation) gives information about the excess number of AA, AB or BB bonds compared with the random case. Dehlinger and Knapp<sup>(36,37)</sup> have in essence tried to calculate the same thing by modifying the zeroth approximation. They assume that there is a certain excess number of AA bonds and that these are gathered in clusters containing only component A. All the clusters are assumed to be of the same size and the zeroth approximation is assumed to hold for the distribution of

the rest of the atoms in the matrix and also for the distribution of the clusters in the specimen. The size and number of the clusters can be calculated by minimizing the free energy of the whole system.

It is apparent that this theory is only an approximation for the quasi-chemical theory, which does not contain any restrictions about the geometric arrangement of the excess number of bonds. Dehlinger and Knapp themselves claim that their treatment gives the final state reached at cold hardening of age-hardening alloys, especially Al-Ag alloys, and this view has been accepted by Hardy and Heal<sup>(38)</sup> and by Guinier<sup>(39)</sup>. However, the above discussion shows that the quasi-chemical theory in any case might be a better approximation than the Dehlinger-Knapp treatment and it does not seem likely that the cold hardening process involves only the adjustment with temperature of the local atomic arrangement predicted by the quasi-chemical theory.

## V. X-RAY THEORY OF PERIODIC STRUCTURES

### 1. Previous Work

A periodic variation in composition can be detected by X-ray diffraction only if the scattering power of the atomic planes or the distance between them varies with the composition. The effect of a periodic variation of the distance has actually been treated theoretically by Dehlinger<sup>(40)</sup> and by Kochendorfer<sup>(41)</sup> in another connection. On considering the influence of elastic strains, caused by cold working, on the broadening of X-ray reflections, they calculated the effect of a sinusoidal variation of the lattice spacing in one direction in a crystal and found that the main reflections should be surrounded by satellites.

Daniel and Lipson<sup>(42)</sup> reported that such satellites were observed by Bradley after an annealing treatment of a Cu-Ni-Fe alloy. This alloy lies within a miscibility gap with a peak at 800°C. It was previously found by Bradley, Cox and Goldschmidt<sup>(43)</sup> that the same alloy on slow cooling from above the miscibility gap did not separate into two FCC phases as it should according to the phase diagram. Instead two slightly tetragonal face centered phases were observed, one with the c-axis a little larger than the two a-axes, the other with the c-axis a little shorter. Their a-axes were identical. The structure could be explained by assuming that the transformation on slow cooling lead to a lamellar structure consisting of plates of one of the stable phases alternating with

plates of the other stable phase. The most copper rich of these phases has a little larger unit cell than the copper poor phase and the tetragonality could thus be explained as a consequence of retained coherency between the different lamellae.

Daniel and Lipson annealed homogenized and quenched specimens inside the miscibility gap and found that the early stages of the transformation gave rise to satellites to the main reflections; these grew closer to the main reflections as the annealing was continued. At the same time satellites of higher order appeared outside the first set of satellites. As all the satellites moved closer to the main reflection the intensity of the higher order satellites increased and the diffraction pattern gradually changed into that for two tetragonal phases.

Daniel and Lipson suggested that the annealing causes a periodic variation of the composition along the  $[100]$  direction. There should then be a periodic variation of both the scattering power and the lattice spacing. The variation in scattering power can be calculated from the atomic scattering powers. The variation in lattice spacing can be calculated from the known variation of the molar volume with composition<sup>(43)</sup>, assuming that the spacings perpendicular to the direction of the periodic variation are unchanged due to coherency in the crystal. Daniel and Lipson treated the effect of these two variations separately, using some approximations, and they found that both give rise to satellites. However, the variation of the lattice

spacing does not give any satellites at the zeroth reflection, whereas the variation of the scattering power does. Inasmuch as such satellites were not observed, it was concluded that only the variation of the lattice spacing is important. This was to be expected because Cu, Ni and Fe have very similar atomic scattering powers.

The distance in reciprocal space between the first order satellites and the main reflection is equal to  $\frac{1}{Q}$  where  $Q$  is the wave length of the periodic variation, measured in number of unit cells. Daniel and Lipson derived the equation,

$$Q = h \tan \theta / (h^2 + k^2 + l^2) \Delta \theta \quad (48)$$

which relates the wave length  $Q$  and the difference in Bragg angle,  $\Delta \theta$ , between a satellite and its main reflection.  $h$ ,  $k$  and  $l$  are the three indices of the main reflection,  $h$  being the index for the  $a_1$  direction, in which the periodic variation takes place. This equation shows that the wave length  $Q$  is increased as the satellites move closer to the main reflection. Daniel and Lipson<sup>(44)</sup> pointed out that the X-ray diffraction would simply show the presence of two tetragonal phases when the wave length  $Q$  is large enough. Both the satellites and the tetragonal diffraction patterns could thus be explained on the same basis.

By assuming that the periodic variation is sinusoidal, Daniel and Lipson could calculate theoretically the intensity of the satellites at different main reflections, but they did not obtain agreement with measured data without the use of a

somewhat arbitrary correction for extinction. Hargreaves<sup>(45)</sup> suggested that the composition always changes abruptly from one extreme value to the other. Even the early stages of the transformation, which give rise to satellites, can then be described as lamellar structures. He also showed that the intensities could be accounted for without the use of the extinction correction, suggested by Daniel and Lipson. Instead Hargreaves had to assume that there may be untransformed regions in a specimen.

It was observed by Hargreaves that the satellites on the two sides of a main reflection have somewhat different intensities. Such asymmetry should occur when the variations in scattering power and lattice spacing are both significant but a quantitative calculation indicated that the variation in scattering power was too low to account for the observed intensity. Hargreaves therefore suggested that the asymmetry is due to an asymmetric location of the alloy in the miscibility gap. This would give rise to a difference in the amount of the two stable phases and consequently a difference in thickness of the two kinds of lamellae. All the X-ray treatment by Daniel and Lipson and by Hargreaves assumed that the composition of the alloy was located exactly in the middle of the miscibility gap.

Balli and Zakharova<sup>(46)</sup> followed Hargreaves suggestion and treated theoretically the case of different thickness of the two kinds of lamellae. They derived an expression for the



asymmetry, which showed that the asymmetry should increase with the wave length  $Q$ , and also reported<sup>(47)</sup> that a specimen was observed to display considerable asymmetry but only after a long annealing treatment.

There is difficulty in understanding how the wave length of the periodic structure can increase continuously, as the measurements by Daniel and Lipson indicate. It was pointed out by Guinier<sup>(39)</sup> that if a specimen has been completely transformed to a perfect periodic structure of a certain wave length, the wave length can increase to a slightly higher value only by a complete dissolution of the old structure and formation of a completely new one.

Guinier suggested that the early stages of the transformation consist of zones, each of which contains a central lamella of one of the extreme compositions, surrounded by two lamellae of the other extreme composition. The value  $Q$ , measured on the diffraction pattern, is then approximately equal to the width of such a zone. As long as the different zones are far apart, the value of  $Q$  can increase continuously simply by a lateral growth of the zones, Fig. 12. This model also predicts an appreciable width of the satellites, whereas the previous models predict sharp satellites. It has in fact been observed that the satellites are much broader than the main reflections and this supports Guinier's viewpoint.

An attempt will be presented here to treat theoretically a more general model which covers all the models reviewed above

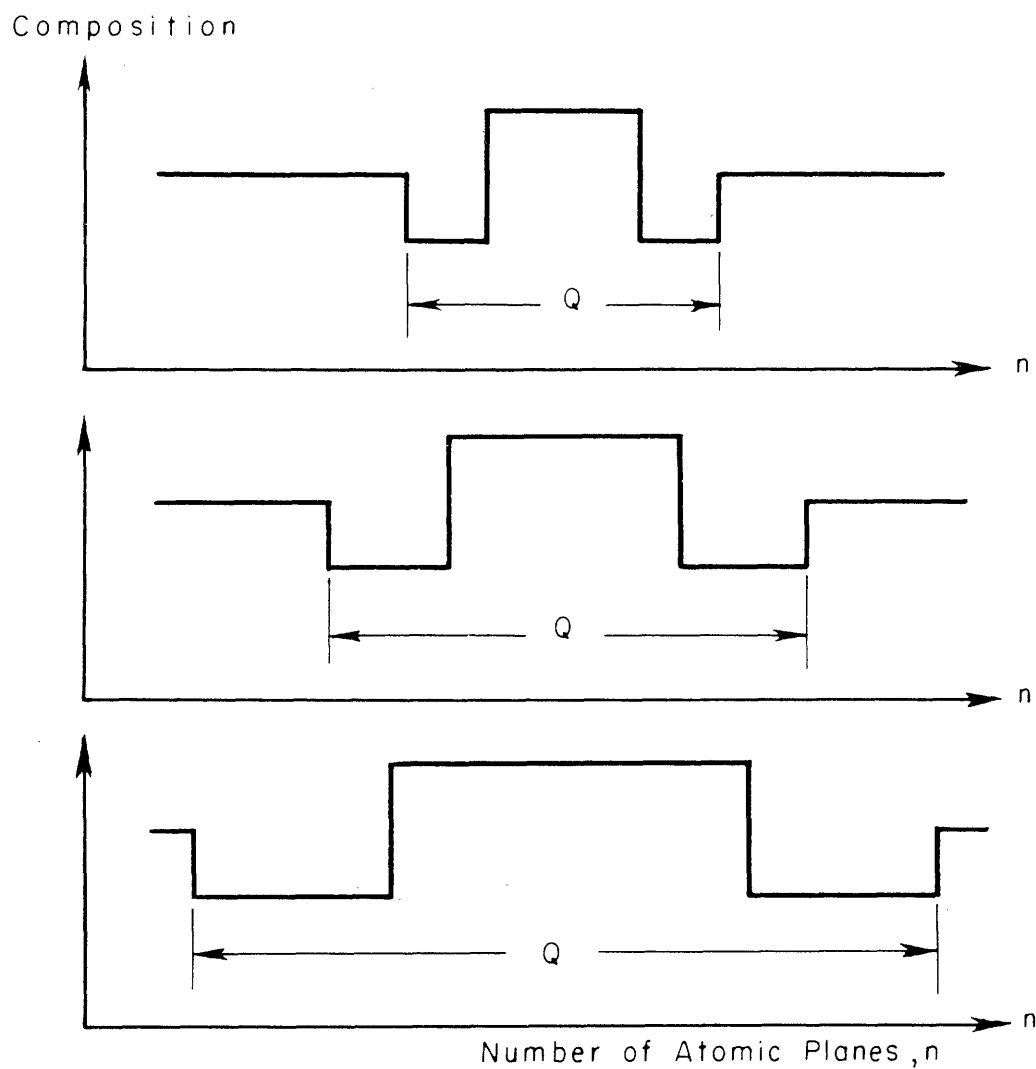


FIG. 12. INCREASE OF Q BY LATERAL GROWTH OF ZONE, AS SUGGESTED BY GUINIER

and also holds for an arbitrary number of lamellae in each transformed region.

## 2. Application to FCC Structures

Previous theoretical treatments have only been concerned with simple cubic systems and it was assumed that the effect of a periodic variation of the lattice spacing is the same for the Cu-Ni-Fe alloys which have a FCC structure. The conditions for this to be true will first be examined.

The amplitude of the scattered x-radiation in a certain direction from a FCC crystal is proportional to the structure factor,

$$F(R) = \sum_{N_1} \sum_{N_2} \sum_{N_3} \left[ 1 + e^{\pi i R(a_1 + a_2)} + e^{\pi i R(a_2 + a_3)} + e^{\pi i R(a_3 + a_1)} \right] \cdot e^{2\pi i R(n_1 a_2 + n_2 a_2 + n_3 a_3)} \quad (49)$$

where R is the vector in reciprocal space, and  $a_1$ ,  $a_2$  and  $a_3$  are the three vectors defining the unit cell.  $N_1$ ,  $N_2$  and  $N_3$  are the numbers of unit cells along the sides of the crystal, assuming it has the shape of a rectangular prism. F(R) can be rearranged

$$F(R) = \frac{e^{2\pi i R a_2 N_2 - 1}}{e^{2\pi i R a_2 - 1}} \frac{e^{2\pi i R a_3 N_3 - 1}}{e^{2\pi i R a_3 - 1}} \cdot \sum_{N_1} \left[ (1 + e^{\pi i R(a_2 + a_3)}) + e^{\pi i R(a_1 + a_2)} \cdot (1 + e^{\pi i R(a_3 - a_2)}) \right] \cdot e^{2\pi i R n_1 a_1} \quad (50)$$

The first two factors show that  $F(R)$  has appreciable values only when  $Ra_2$  and  $Ra_3$  are whole numbers. Then

$$F(R) = \frac{e^{\frac{2\pi i Ra_2 N_{2-1}}{2\pi i Ra_2}}}{e^{\frac{2\pi i Ra_2 N_{2-1}}{2\pi i Ra_2}}} \frac{e^{\frac{2\pi i Ra_3 N_{3-1}}{2\pi i Ra_3}}}{e^{\frac{2\pi i Ra_3 N_{3-1}}{2\pi i Ra_3}}} (1 + e^{\pi i R(a_2 + a_3)}) \cdot \sum_{N_1} (1 + e^{\pi i R(a_1 + a_2)}) \cdot e^{2\pi i R n_1 a_1} \quad (51)$$

When there is a distortion  $a_1 Y(n_1)$  along the  $a_1$  direction, one instead obtains

$$F(R) = \frac{e^{\frac{2\pi i Ra_2 N_{2-1}}{2\pi i Ra_2}}}{e^{\frac{2\pi i Ra_2 N_{2-1}}{2\pi i Ra_2}}} \frac{e^{\frac{2\pi i Ra_3 N_{3-1}}{2\pi i Ra_3}}}{e^{\frac{2\pi i Ra_3 N_{3-1}}{2\pi i Ra_3}}} (1 + e^{\pi i R(a_2 + a_3)}) \cdot \sum_{N_1} (1 + e^{2\pi i R [a_1(\frac{1}{2} + Y(\frac{1}{2})) + \frac{1}{2}a_2]}) \cdot e^{2\pi i R a_1 (n_1 + Y(n_1))} \quad (52)$$

If the distortion is so small that  $a_1(\frac{1}{2} + Y(\frac{1}{2}))$  can be approximated by  $\frac{1}{2}a_1$ , this can be written as

$$F(R) = \frac{e^{\frac{2\pi i Ra_2 N_{2-1}}{2\pi i Ra_2}}}{e^{\frac{2\pi i Ra_2 N_{2-1}}{2\pi i Ra_2}}} \frac{e^{\frac{2\pi i Ra_3 N_{3-1}}{2\pi i Ra_3}}}{e^{\frac{2\pi i Ra_3 N_{3-1}}{2\pi i Ra_3}}} \left[ 1 + e^{\pi i R(a_1 + a_2)} + e^{\pi i R(a_2 + a_3)} + e^{\pi i R(a_3 + a_1)} \right] \cdot \sum_{N_1} e^{2\pi i R a_1 (n_1 + Y(n_1))} \quad (53)$$

This seems to be a very good approximation for the Cu-Ni-Fe alloys and it is thus justifiable to study only the part of the structure factor,  $F(R)$ , which depends upon the distortion in the  $a_1$ -direction. James<sup>(48)</sup> has denoted this quantity  $G(R)$ . We find

$$G(R) = \sum_{N_1} e^{2\pi i R a_1 (n_1 + Y(n_1))} \quad (54)$$

### 3. Treatment of a More General Model

A basic assumption in all the previous work has been that the lattice parameter is proportional to the composition and the same assumption will be adopted here. We shall consider a distortion  $Y(n)$  which is zero except between the values  $n^0$  and  $n^0 + \Delta n$  wherein it is a periodic function with a wave length  $Q$ .  $\Delta n$  is thus assumed to be a multiple of  $Q$ , say  $\Delta n/Q = v$ . The distortion in the region  $n^0$  to  $n^0 + \Delta n$  can thus be expressed as a Fourier series. We shall write

$$2\pi R a_1 Y(n) = \sum_m \left[ \alpha_m \cos 2\pi n m / Q + \beta_m \sin 2\pi n m / Q \right] \quad (55)$$

It is then possible to write also the exponential function as a Fourier series.

$$\begin{aligned} e^{2\pi i R a_1 Y(n)} &= M - iN + 2 \sum_p \left[ (R_p - iS_p) \cos 2\pi n p / Q + \right. \\ &+ (T_p - iU_p) \sin 2\pi n p / Q = M - iN + \sum_p \left\{ (R_p + U_p) - i(S_p - T_p) \right\} e^{2\pi i n p / Q} + \\ &\left. + \left\{ (R_p - U_p) - i(S_p + T_p) \right\} e^{2\pi i n p / Q} \right] \quad (56) \end{aligned}$$

where the set of coefficients  $M$ ,  $N$ ,  $R_p$ ,  $S_p$ ,  $T_p$ , and  $U_p$  can be calculated from the set of coefficients  $\alpha_m$  and  $\beta_m$ . Eq. (54) now gives

$$\begin{aligned}
 G(R) &= \sum_{n=-n^0}^{N_1-1-n^0} e^{2\pi i R a_1 n} + \sum_{n=0}^{\Delta n-1} (e^{2\pi i R a_1 Y(n)} - 1) e^{2\pi i R a_1 n} = \\
 &= e^{-2\pi i R a_1 n^0} \cdot \frac{e^{2\pi i R a_1 N_1-1}}{e^{2\pi i R a_1-1}} - (1 - M + iN) \frac{e^{2\pi i R a_1 \Delta n-1}}{e^{2\pi i R a_1-1}} + \\
 &+ \sum_p \left[ \left\{ (R_p + U_p) - i (S_p - T_p) \right\} \frac{e^{2\pi i (R a_1 + \frac{p}{Q}) \Delta n-1}}{e^{2\pi i (R a_1 + \frac{p}{Q})-1}} + \right. \\
 &\left. + \left\{ (R_p - U_p) - i (S_p + T_p) \right\} \frac{e^{2\pi i (R a_1 - \frac{p}{Q}) \Delta n-1}}{e^{2\pi i (R a_1 - \frac{p}{Q})-1}} \right] \quad (57)
 \end{aligned}$$

The intensity of the scattered radiation is proportional to the product  $G(R)G(R)^*$ . This product gives sharp intensities for  $R a_1 = h$ , where  $h$  is any whole number, but it also contains terms which represent diffuse intensities if  $\Delta n$  is small. The largest of these diffuse terms are

$$\begin{aligned}
 &\left[ (1 - M)^2 + N^2 \right] \frac{\sin^2 \pi R a_1 \Delta n}{\sin^2 \pi R a_1} + \sum_p \left[ \left\{ (R_p + U_p)^2 + (S_p - T_p)^2 \right\} \cdot \right. \\
 &\left. \cdot \frac{\sin^2 \pi (R a_1 + \frac{p}{Q}) \Delta n}{\sin^2 \pi (R a_1 + \frac{p}{Q})} + \left\{ (R_p - U_p)^2 + (S_p + T_p)^2 \right\} \frac{\sin^2 \pi (R a_1 - \frac{p}{Q}) \Delta n}{\sin^2 \pi (R a_1 - \frac{p}{Q})} \right] \quad (58)
 \end{aligned}$$

The first term is symmetric around the main reflection, the other terms have their maxima at  $R a_1 = h \pm \frac{p}{Q}$ . These terms

represent satellites to the sharp reflections at  $Ra_1 = h$ . The intensity of each satellite decreases from the maximum value at  $Ra_1 \pm \frac{p}{Q} = h$  to zero when  $(Ra_1 \pm \frac{p}{Q}) \Delta n = h\Delta n - 1$ . The width of a satellite as expressed by the distance between these two points is thus

$$h \pm \frac{p}{Q} - \left[ \frac{1}{\Delta n} (h\Delta n - 1) \pm \frac{p}{Q} \right] = \frac{1}{\Delta n} = \frac{1}{vQ} \quad (59)$$

The width is thus equal to the distance between adjoining satellites when there is only one period in the distorted region, i.e. when  $v = 1$ . This is the model suggested by Guinier. We can now see that the satellites become rapidly sharper if  $v$  is increased. Actually, this equation can be used to calculate  $v$  from the width, assuming that all the distorted regions in a sample have the same value of  $Q$ .

The asymmetry of the intensities of the satellites is

$$\left( \frac{\Delta I}{I_{\text{mean}}} \right)_p = 2 \cdot \frac{I_{-p} - I_{+p}}{I_{-p} + I_{+p}} = 4 \cdot \frac{R_p U_p - S_p T_p}{R_p^2 + U_p^2 + S_p^2 + T_p^2} \quad (60)$$

For any quantitative comparison of the intensities, it is necessary to evaluate the coefficients  $M$ ,  $N$ ,  $R_p$ ,  $S_p$ ,  $T_p$ , and  $U_p$  in Eq. (58) from the coefficients  $\alpha_m$  and  $\beta_m$ , which describe the distortion  $Y(n)$  in Eq. (55). This can be done by means of the relations

$$e^{i\alpha_m \cos 2\pi n m / Q} = J_0(\alpha_m) + 2iJ_1(\alpha_m) \cos 2\pi n / Q - 2J_2(\alpha_m) \cos 4\pi n / Q - 2iJ_3(\alpha_m) \cos 6\pi n / Q \dots \quad (61)$$

$$e^{i\beta_m \sin 2\pi n m / Q} = J_0(\beta_m) + 2iJ_1(\beta_m) \sin 2\pi n / Q + \\ + 2J_2(\beta_m) \cos 4\pi n / Q + 2iJ_3(\beta_m) \sin 6\pi n / Q \dots \quad (62)$$

where the J's are Bessel functions.  $e^{2\pi i R a_1 Y(n)}$  is thus the product of these series for all the m values. This whole product is very complicated and we shall therefore study separately the two parts of it which are made up of only the  $\alpha$  terms and of only the  $\beta$  terms.

These partial products can be written

$$\exp i \sum_{m=0}^{\infty} \alpha_m \cos 2\pi n m / Q = A_0 - iB_0 + \sum_p (A_p - iB_p) \cos 2\pi n p / Q \quad (63)$$

$$\exp i \sum_{m=1}^{\infty} \beta_m \sin 2\pi n m / Q = C_0 + \sum_p (C_p \cos 2\pi n p / Q - iD_p \sin 2\pi n p / Q) \quad (64)$$

In order to make the distortion small at  $n = n^0$  and  $n = n^0 + \Delta n$ ,  $\alpha_0$  must be very close to  $\sum_{m=1}^{\infty} \alpha_m$  whereas  $\beta_0 = 0$ .

For reasonably small distortions one finds that  $C_0 = 1$ ,  $A_0 = \cos \alpha_0$  and  $B_0 = -\sin \alpha_0$  and all the other constants are very small. The largest terms in the full product are therefore  $C_0 A_0 - iC_0 B_0 = \cos \alpha_0 + i \sin \alpha_0$ . One finds for the first two coefficients in Eq. (56)

$$M = \cos \alpha_0 \\ N = -\sin \alpha_0 \quad (65)$$



According to Eq. (58) the diffuse intensity close to the main reflection is then proportional to

$$\begin{aligned}
 (1 - M)^2 + N^2 &= 1 + \cos^2 \alpha_0 - 2\cos \alpha_0 + \sin^2 \alpha_0 = \\
 &= 2 - 2\cos \alpha_0 = 4\sin^2 \frac{1}{2} \alpha_0 \qquad (66)
 \end{aligned}$$

However, no such intensity has been observed experimentally and hence we shall conclude that the distortion is such that  $\alpha_0 = 0$ . It is then natural to assume, as did Guinier, that all  $\alpha_m = 0$  in view of the relation  $\alpha_0 = \sum_{m=1}^{\infty} \alpha_m$ . These conditions are fulfilled if  $Y(n) = -Y(-n)$ . We can then immediately identify the coefficients in Eq. (64) with those in Eq. (56) and we find

$$\begin{aligned}
 M = C_0 &= \prod_m J_0(\beta_m) \left[ 1 - 2J_3^1 J_1^3 \dots \dots \dots \right] \\
 R_1 = C_1 &= \prod_m J_0(\beta_m) \left[ - 2J_1^1 J_1^2 - 2J_3^1 J_1^2 \dots \dots \dots \right] \\
 U_1 = D_1 &= \prod_m J_0(\beta_m) \left[ - 2J_1^1 + 2J_3^1 J_2^2 - 2J_2^1 J_1^3 \dots \dots \dots \right] \\
 R_2 = C_2 &= \prod_m J_0(\beta_m) \left[ 2J_2^1 + 2J_2^1 J_2^2 - 2J_1^1 J_1^3 \dots \dots \dots \right] \\
 U_2 = D_2 &= \prod_m J_0(\beta_m) \left[ - 2J_1^2 \dots \dots \dots \right] \\
 N = S_p &= T_p = 0
 \end{aligned} \qquad (67)$$

where the following shorthand notation has been used

$$J_p^m = \frac{J_p(\beta_m)}{J_0(\beta_m)} \quad (68)$$

All terms with m or p larger than 3 have been neglected which is a very good approximation for the earlier stages of the transformation, when Q is small.

The expression for the asymmetry, Eq. (60), can now be written

$$\left(\frac{\Delta I}{I_{\text{mean}}}\right)_p = \frac{4R_p U_p}{R_p^2 + U_p^2} \quad (69)$$

The only way of having no asymmetry is to have  $\beta_m = 0$  for all even m, which is fulfilled if  $Y(n) = -Y(n + \frac{1}{2}Q)$ . This results in  $R_p = 0$  for all odd p and  $U_p = 0$  for all even p. The product  $R_p U_p$  is thus zero for all p. For small degrees of asymmetry, one can use the approximation

$$\left(\frac{\Delta I}{I_{\text{mean}}}\right)_{p \text{ odd}} = 4 \frac{R_p}{U_p} \quad \left(\frac{\Delta I}{I_{\text{mean}}}\right)_{p \text{ even}} = 4 \frac{U_p}{R_p} \quad (70)$$

and one finds for instance

$$\left(\frac{\Delta I}{I_{\text{mean}}}\right)_{p=1} = 4 \frac{-J_1^1 J_1^2}{-J_1^1} = 4J_1^2 = 4 \frac{J_1(\beta_2)}{J_0(\beta_2)} \approx 2\beta_2 \quad (71)$$

#### 4. Application to a Specific Case

The general treatment presented here can be applied to any specific model by evaluating the  $\alpha_m$  and  $\beta_m$  coefficients and choosing the appropriate value for  $\nu$ . The value  $\nu = \infty$  holds for the models suggested by Daniel and Lipson, Hargreaves, and Balli and Zakharova,  $\nu = 1$  holds for Guinier's model. The model suggested by Daniel and Lipson simply gives all  $\alpha_m = 0$ ,  $\beta_1 = \text{constant}$ , and  $\beta_m = 0$  for all  $m > 1$ .

Both Hargreaves, Balli and Zakharova, and Guinier assumed that there is an abrupt change in composition between the two kinds of lamellae. Fig. (13) shows such a model with one zone ( $\nu = 1$ ). Using the approximation

$$a_1 \cdot Y(n') = \sum_{n=n^0}^{n'} (a - a_1) = \int_{n^0}^{n'} (a - a_1) dn \quad (72)$$

for the distortion in a certain plane,  $n'$ .  $a$  is the variable spacing in the  $a_1$  direction. One finds for the coefficients in Eq. (55)

$$\alpha_m = 0$$

$$\beta_m = \frac{(-1)^m}{\pi m^2} 2Ra_1 Q(\epsilon_1 + \epsilon_2) \sin \pi m \frac{\epsilon_2}{\epsilon_1 + \epsilon_2} \quad (73)$$

where  $\epsilon_1$  and  $\epsilon_2$  are the relative changes in lattice spacing in the two kinds of lamellae. In Chapter III some indication was found that there is no abrupt change in composition. However, taking a somewhat more gradual change into account will affect the  $\beta_m$  values comparatively little.

The  $\beta_m$  values given by Eq. (73) can now be used to calculate

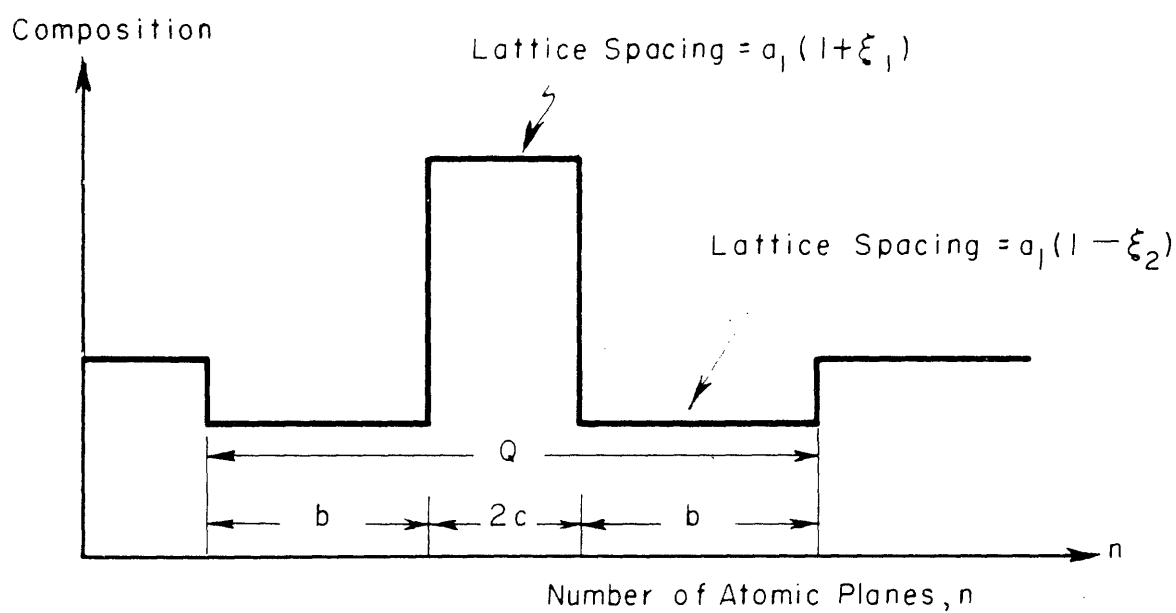


FIG. 13. MODEL OF ZONE IN ASYMMETRIC ALLOY

the set of coefficients,  $M$ ,  $N$ ,  $R_p$ ,  $S_p$ ,  $T_p$  and  $U_p$  from Eq. (67) and Eq. (68), and the relative intensities of the satellites can then be computed from Eq. (58).

It is seen immediately from Eq. (73) that the condition for no asymmetry is  $\epsilon_1 = \epsilon_2$ , because this makes  $\beta_m = 0$  for all even  $m$ . The condition is thus that the composition of the alloy lies in the middle of the miscibility gap, as would be expected. This is the case treated by Hargreaves and Guinier.

$(\epsilon_1 + \epsilon_2)$  is of the order of 0.02 in the case of Cu-Ni-Fe alloys and the highest reflection we shall consider has  $Ra_1 = h = 3$ . It is then found that  $J_1(\beta_1)$  is much larger than all the Bessel functions of higher order, when  $Q < 50$ . It is therefore a good approximation to neglect all higher orders for small  $Q$ . Only the first order satellites ( $p = 1$ ) then have appreciable intensity. However, if  $Q$  grows to larger values the intensity of the first order satellites starts to decrease, as they move closer to the main reflection, and higher order satellites become visible. Finally, for very large  $Q$ , the low order satellites have negligible intensity and the only visible ones are those which are situated where the sharp reflections for lattices with the spacings  $a_1(1 + \epsilon_1)$  and  $a_1(1 - \epsilon_2)$  fall, which of course is to be expected. The diffraction pattern then simply shows the presence of two coherent, tetragonal phases. Such late stages of the transformation for which higher orders of the Bessel functions cannot be neglected are very

difficult to treat quantitatively with the above method, using the Bessel expansions. An exact treatment is then simpler and will therefore be presented in the next section.

### 5. Exact Treatment

We shall treat the same kind of variation in composition as is shown in Fig. (13). Suppose the center strip contains  $2c$  unit cells with the spacing  $a_1(1 + \epsilon_1)$  and the side strips contain  $b$  unit cells each, with the spacing  $a_1(1 - \epsilon_2)$ . Let the origin be in the middle of the center strip. Then

$$\sum_{-(b+c-\frac{1}{2})}^{(b+c-\frac{1}{2})} e^{2\pi Ra_1(n + Y(n))} = \sum_{c+\frac{1}{2}}^{b+c-\frac{1}{2}} + \sum_{\frac{1}{2}}^{c-\frac{1}{2}} + \sum_{-(c-\frac{1}{2})}^{-\frac{1}{2}} + \sum_{-(b+c-\frac{1}{2})}^{-(c+\frac{1}{2})} =$$

$$e^{2\pi i Ra_1(b + c - \frac{1}{2} + \frac{1}{2}\epsilon_2)} \cdot \frac{e^{-2\pi i Ra_1(1 - \epsilon_2)b} - 1}{e^{-2\pi i Ra_1(1 - \epsilon_2)} - 1} +$$

$$+ e^{2\pi i Ra_1(\frac{1}{2} + \frac{1}{2}\epsilon_1)} \cdot \frac{e^{2\pi i Ra_1(1 + \epsilon_1)c} - 1}{e^{2\pi i Ra_1(1 + \epsilon_1)} - 1} +$$

$$+ e^{-2\pi i Ra_1(\frac{1}{2} + \frac{1}{2}\epsilon_1)} \cdot \frac{e^{-2\pi i Ra_1(1 + \epsilon_1)c} - 1}{e^{-2\pi i Ra_1(1 + \epsilon_1)} - 1} +$$

$$+ e^{-2\pi i Ra_1(b + c - \frac{1}{2} + \frac{1}{2}\epsilon_2)} \cdot \frac{e^{2\pi i Ra_1(1 - \epsilon_2)b} - 1}{e^{2\pi i Ra_1(1 - \epsilon_2)} - 1} =$$

$$= 2 \cos \pi Ra_1(1 + \epsilon_1)c \cdot \frac{\sin \pi Ra_1(1 + \epsilon_1)c}{\sin \pi Ra_1(1 + \epsilon_1)} +$$

$$+2\cos \pi Ra_1 \left[ (1 - \epsilon_2)b - Q \right] \cdot \frac{\sin \pi Ra_1 (1 - \epsilon_2)b}{\sin \pi Ra_1 (1 - \epsilon_2)} \quad (74)$$

Suppose there are  $v$  periods like the one shown in Fig. (13) immediately following each other in the distorted region. Then

$$\begin{aligned} G(R) &= \sum_{N_1} e^{2\pi i Ra_1 (n + Y(n))} = \\ &= e^{2\pi i Ra_1 u} \cdot \frac{\sin \pi Ra_1 N_1}{\sin \pi Ra_1} - \frac{\sin \pi Ra_1 Qv}{\sin \pi Ra_1} + \\ &+ \frac{\sin \pi Ra_1 Qv}{\sin \pi Ra_1 Q} \left\{ 2\cos \pi Ra_1 (1 + \epsilon_1)c \cdot \frac{\sin \pi Ra_1 (1 + \epsilon_1)c}{\sin \pi Ra_1 (1 + \epsilon_1)} + \right. \\ &\left. + 2\cos \pi Ra_1 \left[ (1 - \epsilon_2)b - Q \right] \cdot \frac{\sin \pi Ra_1 (1 - \epsilon_2)b}{\sin \pi Ra_1 (1 - \epsilon_2)} \right\} \quad (75) \end{aligned}$$

The quantity  $u$  is the distance from the center of the distorted region to the center of the specimen. The factor in front of the bracket shows that the intensity has a series of maxima close to  $Ra_1 = m/Q$ , where  $m$  is any whole number. One can as well write  $Ra_1 = h \pm \frac{p}{Q}$  where  $p$  is any whole number less than  $\frac{1}{2}Q + 1$ . These maxima are thus the centers of the satellites. At the ideal position of the satellites,  $Ra_1 = h \pm \frac{p}{Q}$ , Eq. (75) simplifies to

$$G(R) = v \cdot \left\{ \frac{\sin \pi Ra_1 (1 + \epsilon_1)2c}{\sin \pi Ra_1 (1 + \epsilon_1)} + \frac{\sin \pi Ra_1 (1 - \epsilon_2)2b}{\sin \pi Ra_1 (1 - \epsilon_2)} \right\} \quad (76)$$

which also can be written

$$G(R) = v \cdot \sin \pi R a_1 (1 + \varepsilon_1) 2c \left\{ \operatorname{cosec} \pi R a_1 (1 + \varepsilon_1) - \right. \\ \left. - \operatorname{cosec} \pi R a_1 (1 - \varepsilon_2) \right\} \quad (77)$$

It is thus very simple to calculate the intensities of higher order satellites with this equation.

Eq. (77) has been used to calculate the influence of the quantity  $v$  on the width of the satellites, and Fig. (14) shows the result in a very asymmetric case. It is obvious that an increase of  $v$  from 1 to 2 could easily be observed whereas a further increase of  $v$  affects the width comparatively little. Fig. (14) will be used in a later section for an evaluation of  $v$  from experimental observations of the width of satellites.

"Unit cell" has been used by all previous authors as the unit length for the wave length  $Q$ , being the natural unit in the X-ray theory. The natural unit in the thermodynamic treatment is atomic plane, however, and the symbol  $q$  was therefore used in Chapters II and III in order to avoid confusion. There is always a simple relation between the two units. When the considered direction is  $[100]$  in a FCC structure, there are two atomic planes per unit cell.



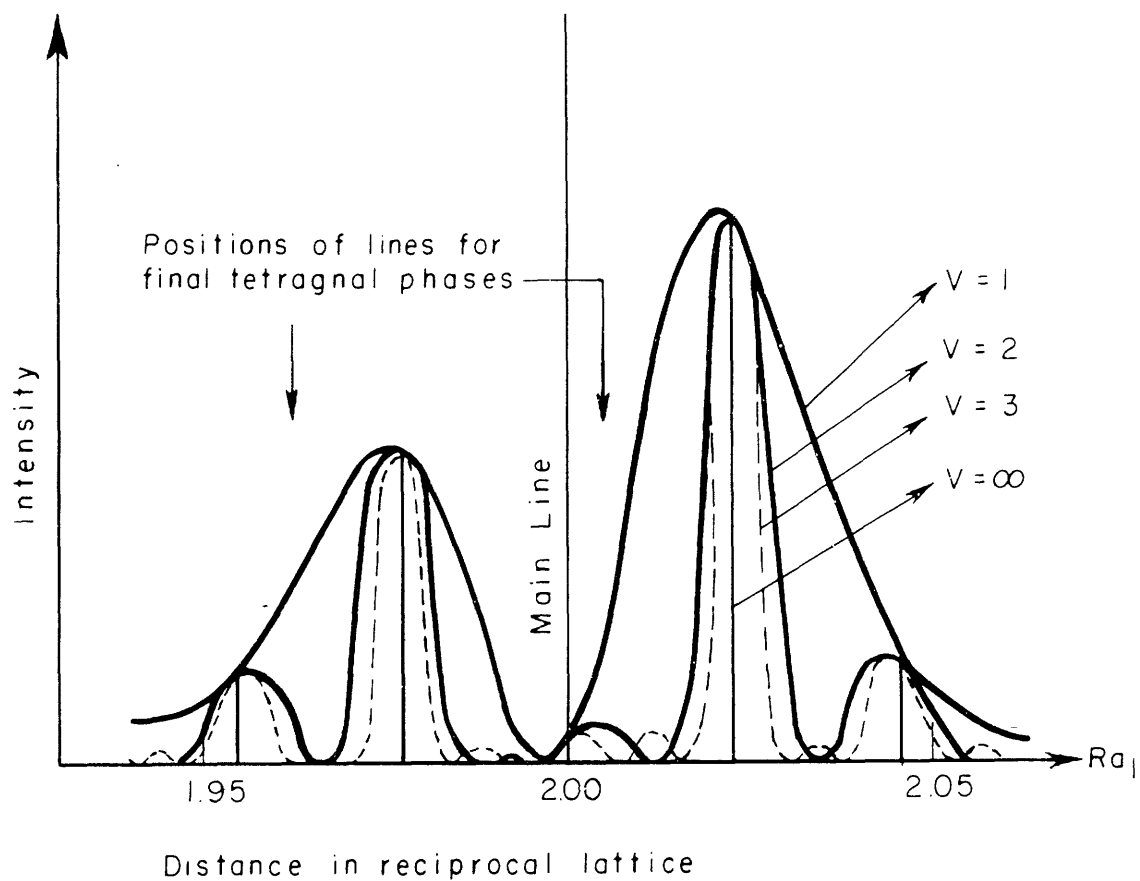


FIG. 14. CALCULATED INTENSITY DISTRIBUTION IN SATELLITES

## VI. EXPERIMENTAL WORK

### 1. Preparation of Alloys

It was desired to make up a complete series of alloys in a pseudo-binary section of the ternary system. The tie-lines in the miscibility gap have been determined by means of magnetic and resistance measurements by Köster and Dannöhl<sup>(49)</sup>. Their results show that the tie-lines point almost directly toward the Cu-corner. See Fig. (15A). The deviation varies with the temperature and there is consequently no true pseudo-binary section. A section through the Cu-corner was selected.

The alloys were made from carbonyl nickel, spectrographic copper and a specially purified iron received from the Battelle Memorial Institute. A high-frequency vacuum furnace was used and the melts were cast in a copper mold under vacuum. This procedure minimized segregation. The castings were sealed under vacuum in separate Vycor tubes and given a homogenization anneal at 950°C for 10 days. They were quenched into brine by breaking the Vycor tubes under the liquid surface and were then ground with a carborundum wheel. The metallic powder could be separated from the carborundum with a magnet and the fraction passing through a 325 mesh sieve was used for these experiments. Coarser fractions were used for chemical analysis, and these analyses are listed in Appendix II. Fig. (15) shows the compositions of all these alloys and also the phase diagram after slow cooling determined by Bradley, Cox and Goldschmidt<sup>(43)</sup>.

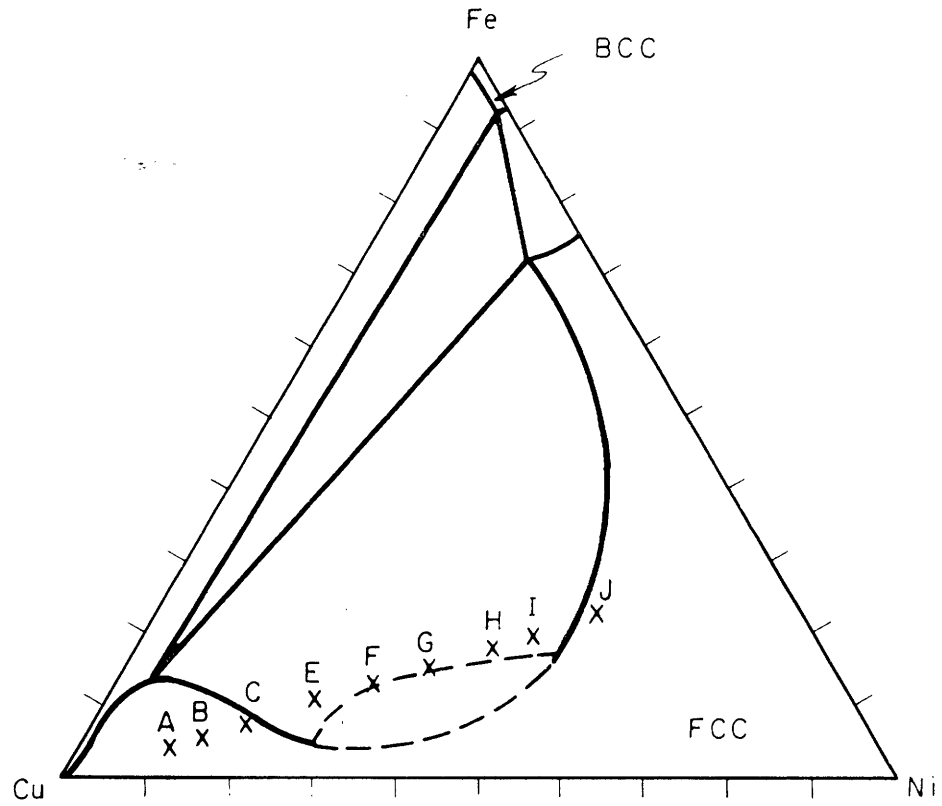


FIG. 15. COMPOSITION OF ALLOYS PLOTTED IN "PHASE DIAGRAM AFTER SLOW COOLING"

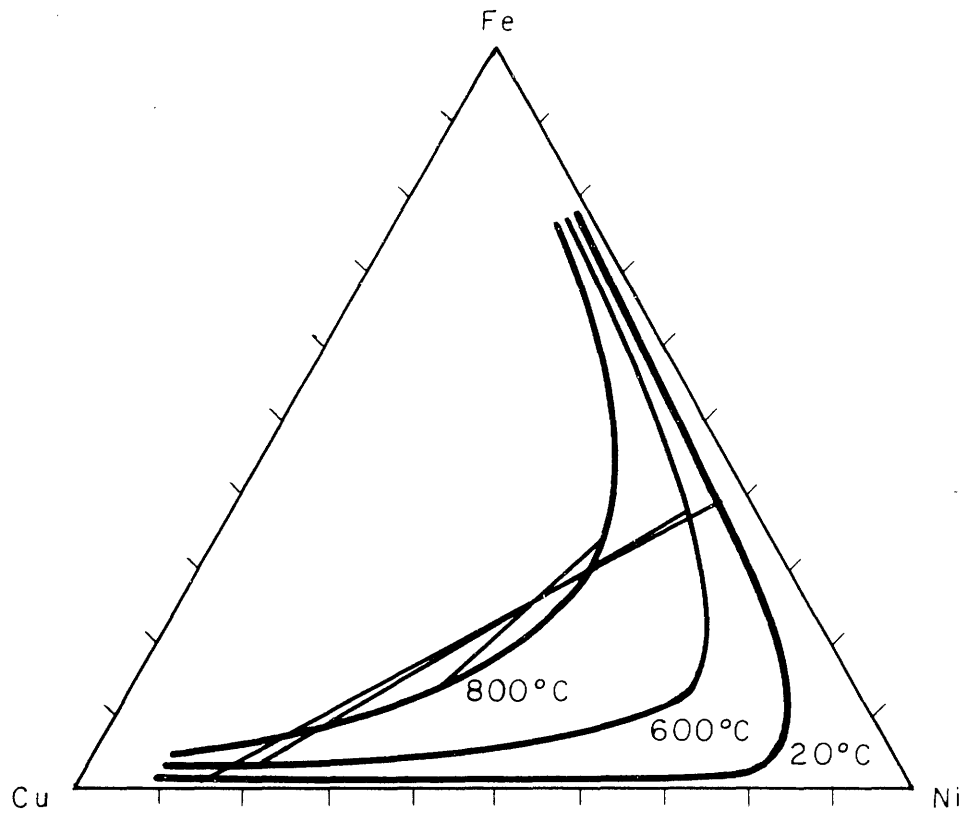


FIG. 15A. PHASE DIAGRAM FOR THE Cu-Ni-Fe SYSTEM SHOWING THE MISCIBILITY GAP AND TIE-LINES FOR ONE ALLOY AT THREE TEMPERATURES (ACCORDING TO KÖSTER AND DANNÖHL).

All the current alloys lie very close to the section through the Cu-corner and the point  $\text{Ni}_{0.7}\text{Fe}_{0.3}$ , and their compositions can therefore be written  $\text{Cu}_{1-x}(\text{Ni}_{0.7}\text{Fe}_{0.3})_x$ . The value of  $x$  will be used in the following to characterize each alloy.

## 2. Experimental Technique

The first annealing experiments revealed that the transformation is very fast in a certain temperature range. The following technique was used for most of the experiments in order to make certain that the specimens would come to temperature equilibrium with their surroundings very rapidly.

Capillaries with an outer diameter of about 0.7 mm and an inner diameter of about 0.4 mm were drawn from thicker quartz tubes. They were filled with metallic powder to a length of about 7 mm and sealed under an atmosphere of about 50 mm He. These tubes were dropped down into a 5 mm thick quartz tube leading into a furnace held at a temperature  $100^\circ\text{C}$  above the peak of the miscibility gap. The quartz tube was lifted out of its furnace after at least 2 hours and the samples were "poured" into another quartz tube leading into another furnace held at a temperature within the miscibility gap. The samples were removed after different annealing times by the same method and quenched in brine. The thin quartz capillaries could now be broken and the metallic powder which had sintered to a rod could be used directly in a 19cm Debye-Scherrer camera. An exposure time of 4 hours was usually adopted.

The distance between satellites was measured optically. The uncertainty of this measurement depends on the width of

the satellites, which is appreciable compared to their distance. One part of this width is inherent and will be discussed later, another part is the width of the main reflection, which is inherited by the satellites. This part is considerable if one does not eliminate the  $K\alpha_2$  from the  $K\alpha_1$  radiation, which can be done with the technique employed by Hargreaves<sup>(45)</sup>. The intensity of the remaining  $K\alpha_1$  radiation is greatly decreased, and Hargreaves did not find it convenient to use his refined technique when the satellites themselves were weak. This is the case at the early stages of the transformation. In the present investigation the interest is focussed on these stages and therefore the primitive technique used by Daniel and Lipson<sup>(42)</sup> was employed. Most of the measurements were made on the satellites of the (200) line in order to minimize the effect of this instrumental broadening on the width of the satellites. The (311) reflection was used in some cases, when the satellites were very weak, because of the higher intensity of this reflection and its satellites.

### 3. Measurements of the Phase Diagram

The composition and temperature of the peak of the miscibility gap was determined by annealing samples F and G at 1119 and 1111°K. Only the F sample at 1111°K separated into two phases and the peak was calculated from a measurement of the lattice parameter of these two phases, using the relation between lattice parameter and composition determined by Bradley, Cox and Goldschmidt<sup>(43)</sup> and assuming that the shape of the upper part

of the miscibility gap is that given by the zeroth approximation. The result was  $T_M = 1116^\circ\text{K}$  and  $x_M = 0.47$ . This miscibility gap is thus unusually symmetric and it may thus be a good approximation to assume that the interaction energy is independent of composition.

No accurate determination was made of the miscibility gap at lower temperatures but it was established that it follows fairly well the miscibility gap predicted by the zeroth or first approximation. These two approximations predict almost the same shape of the miscibility gap and their spinodals are also rather close to each other as is shown in Fig. (16). The miscibility gap and spinodal for the zeroth approximation were computed from the well known equations<sup>(27)</sup>

$$\text{Miscibility gap: } \frac{T_M}{T} \cdot \frac{2}{Z} = \frac{\chi}{kT} = \frac{1}{Z(x_A - x_B)} \ln \frac{x_A}{x_B} \quad (78)$$

$$\text{Spinodal: } \frac{T_M}{T} \cdot \frac{2}{Z} = \frac{\chi}{kT} = \frac{1}{2Zx_A x_B} \quad (79)$$

The following equations were derived for the first approximation.

$$\text{Miscibility gap: } \frac{T_M}{T} \ln \frac{Z}{Z-2} = \frac{\chi}{kT} = \frac{1}{Z} \ln \frac{x_A}{x_B} + \ln \left( \frac{\frac{x_A}{x_B} - 1}{\frac{x_A}{x_B} - \left(\frac{x_A}{x_B}\right)^{2/Z}} \right)^{2/Z} \quad (80)$$

$$\text{Spinodal: } \frac{T_M}{T} \ln \frac{Z}{Z-2} = \frac{\chi}{kT} = \frac{1}{2} \ln \left( \frac{1}{x_A x_B} \cdot \frac{Z-1}{(Z-2)^2} + 1 \right) \quad (81)$$

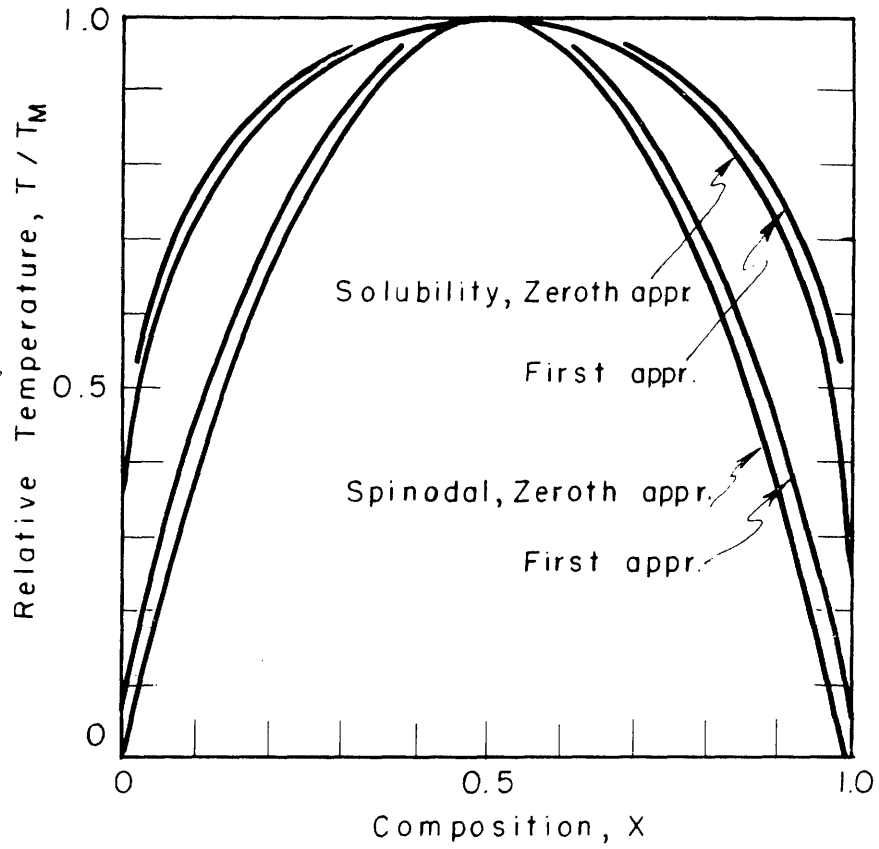


FIG. 16. THEORETICAL SHAPE OF MISCIBILITY GAP ACCORDING TO ZEROth AND FIRST APPROXIMATION.



#### 4. Measurements of Satellites

Fig. (17) shows all the compositions and temperatures, at which the development of the satellites was followed. The check marks represent runs where no reaction was ever found. They may lie outside the real miscibility gap and thus indicate a slight asymmetry in agreement with the experimental value of the peak composition. The miscibility gap according to the first approximation is also shown. Each point usually represents a series of four different annealing times. The average wave lengths of the periodic structures were calculated from the measured distance between the center of the satellites by means of Eq. (48), and the results are presented in Figs. (18) to (23). The numerical values are given in Appendix III.

Daniel and Lipson plotted their wave length data versus the logarithm of the annealing time. We are interested in extrapolating the data to zero time and have therefore plotted the data against the square root of the annealing time. It is possible to represent the measured data with straight lines for low annealing times in this kind of a plot, and it seems justified to assume that the wave length of the first structure to form is given fairly well by the intersections of these straight lines with the wave length axis. These extrapolated values are also given in Appendix III.

The results for the C and F alloy are also presented on a logarithmic plot in Figs. (24) and (25) because this plot

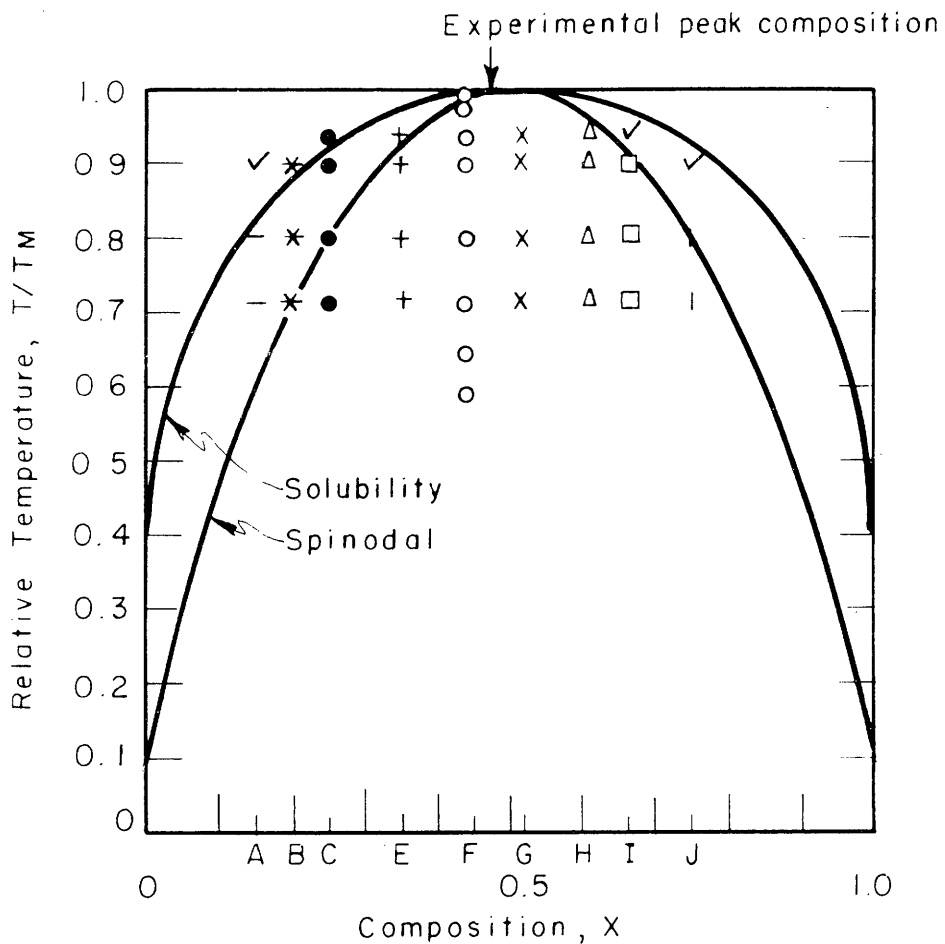


FIG. 17. COMPOSITION AND TEMPERATURES OF ANNEALING EXPERIMENTS. MISCIBILITY GAP ACCORDING TO FIRST APPROXIMATION

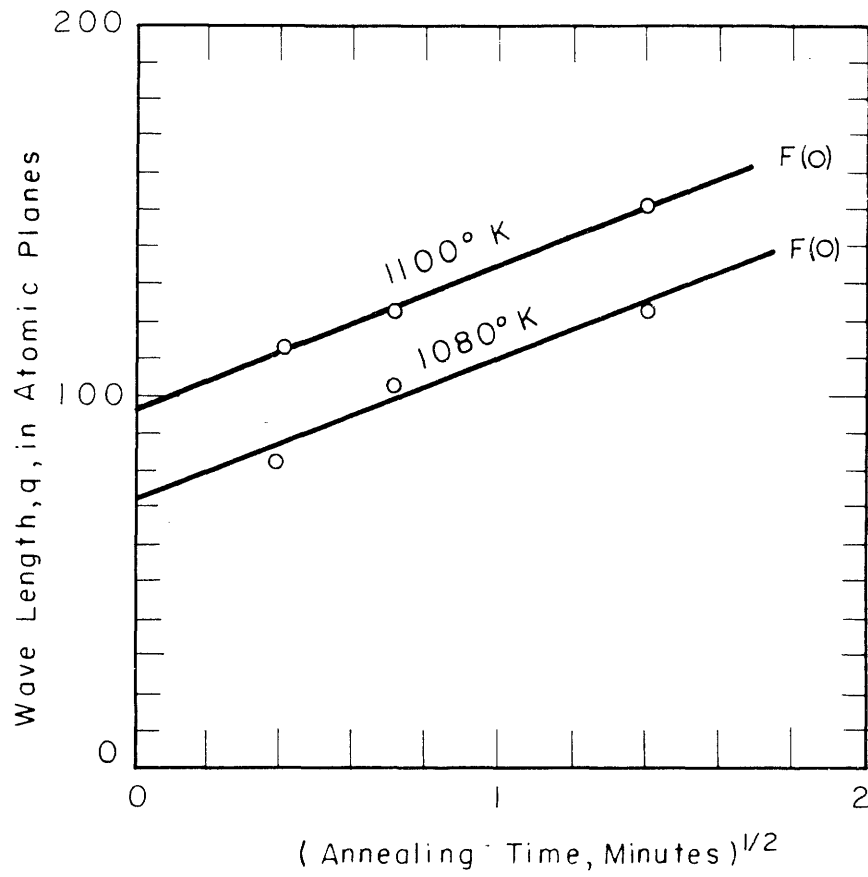


FIG. 18. GROWTH OF WAVE LENGTH WITH ANNEALING TIME AT 1080 AND 1100° K.

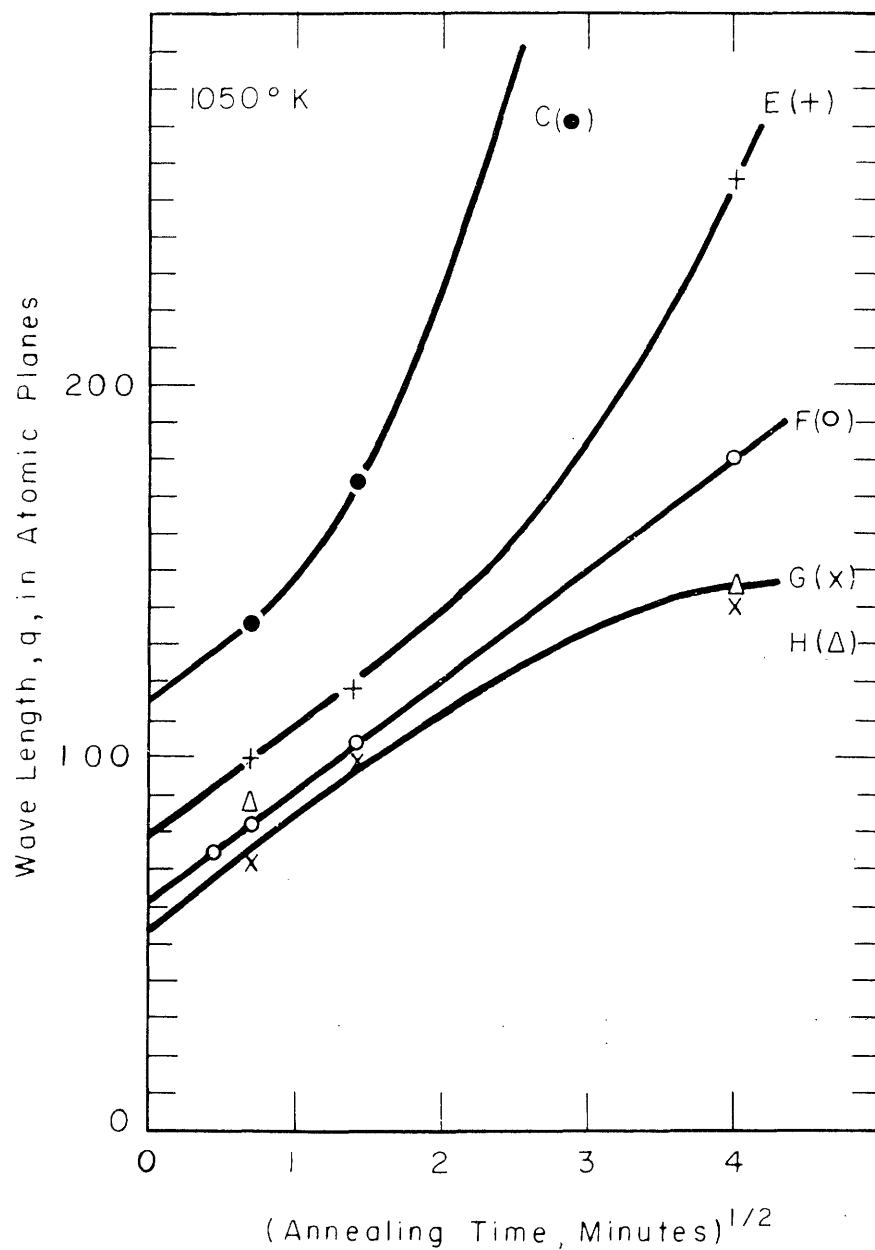


FIG. 19. GROWTH OF WAVE LENGTH WITH ANNEALING TIME AT  $1050^\circ \text{K}$ .

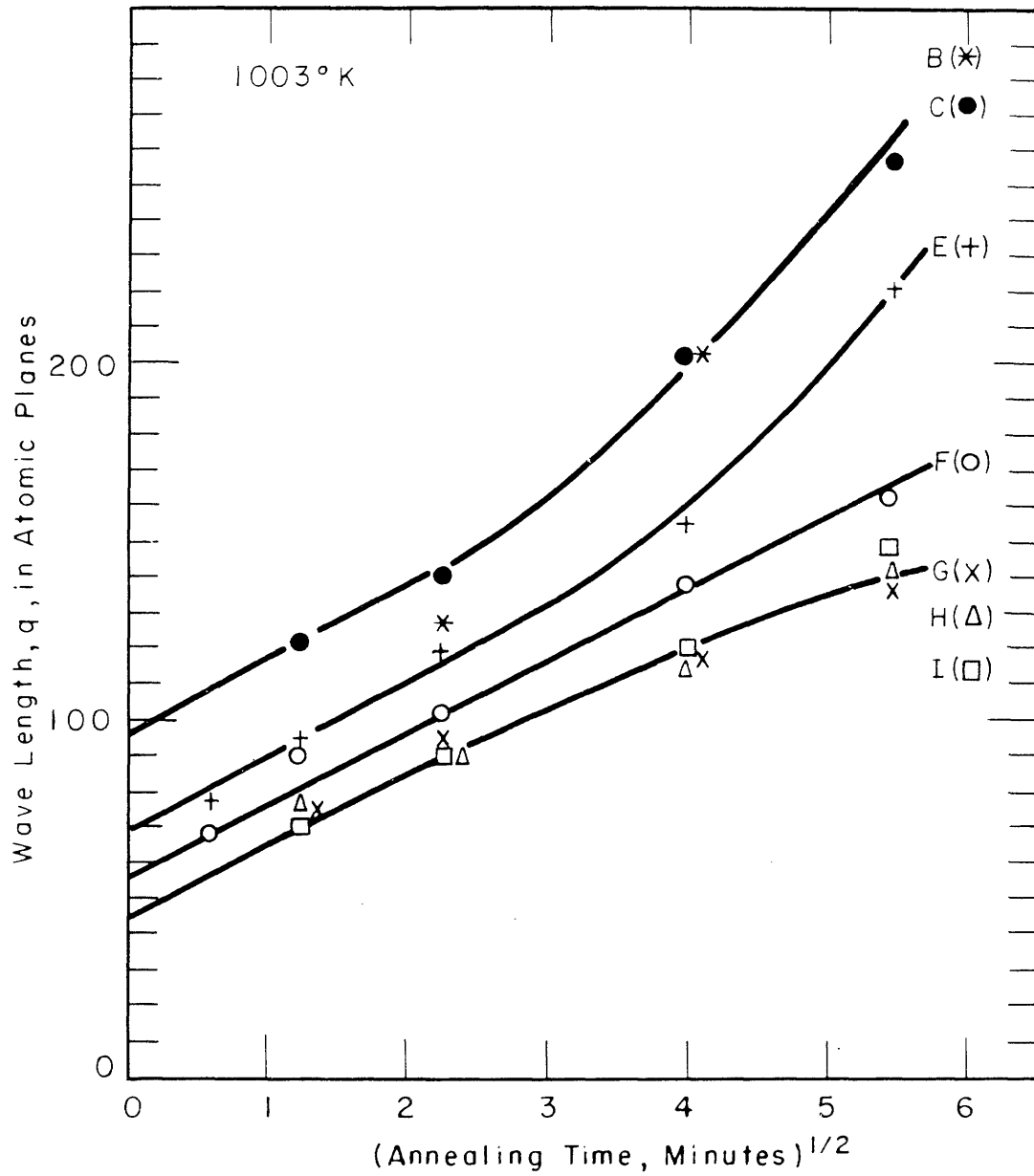


FIG. 20. GROWTH OF WAVE LENGTH WITH ANNEALING TIME AT  $1003^\circ \text{K}$ .

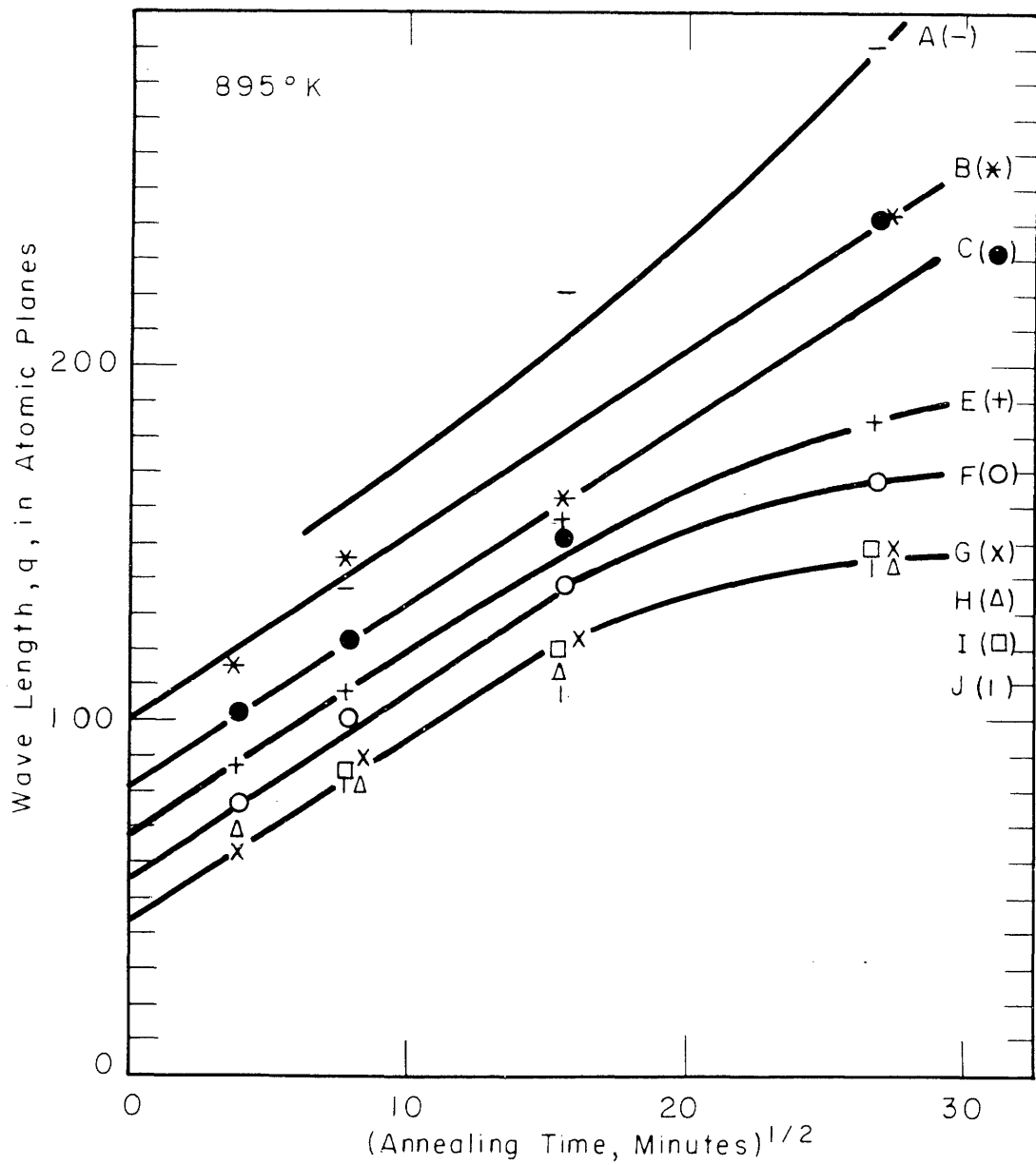


FIG. 21. GROWTH OF WAVE LENGTH WITH ANNEALING TIME AT 895 °K.

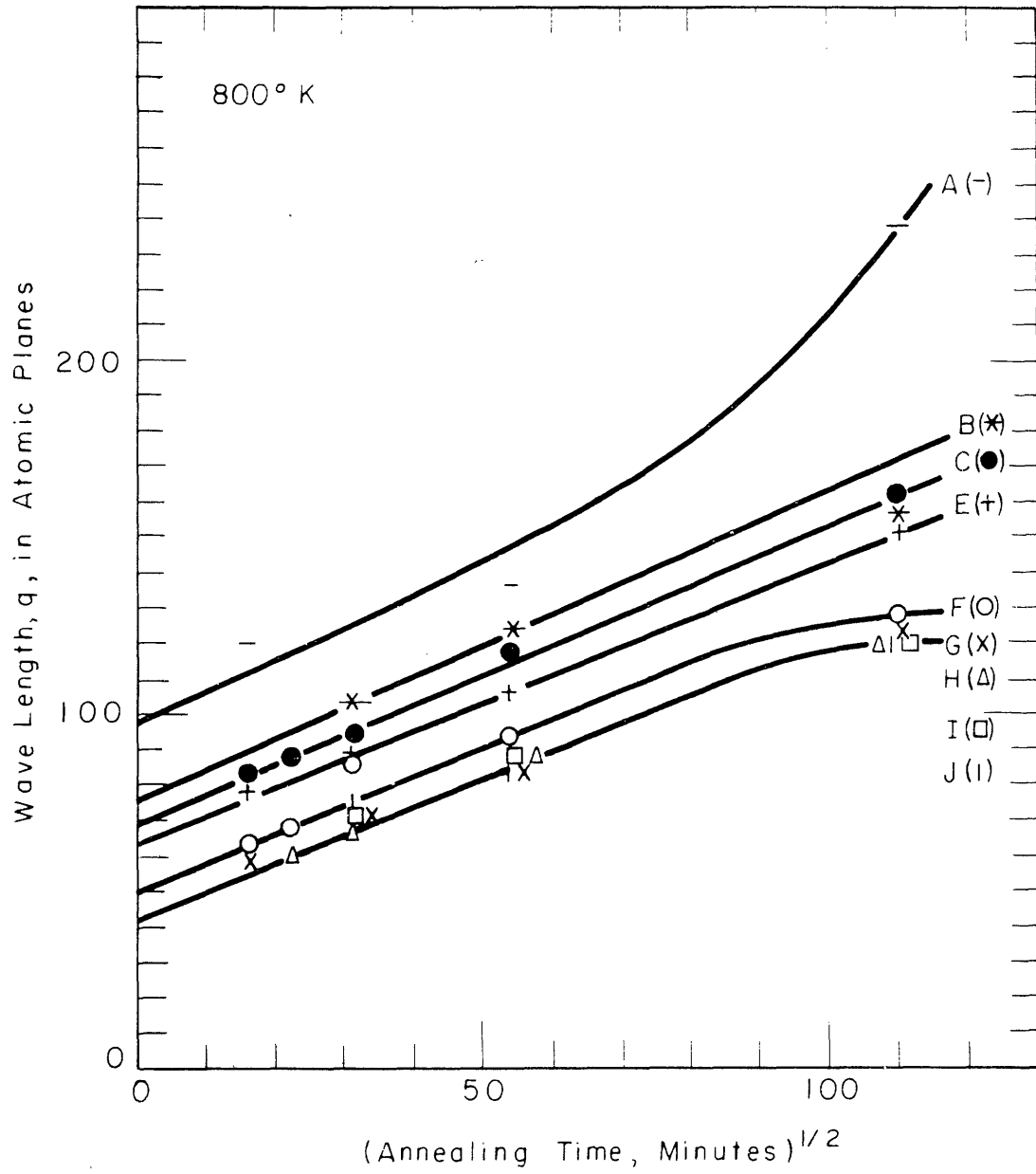


FIG. 22. GROWTH OF WAVE LENGTH WITH ANNEALING TIME AT 800° K.

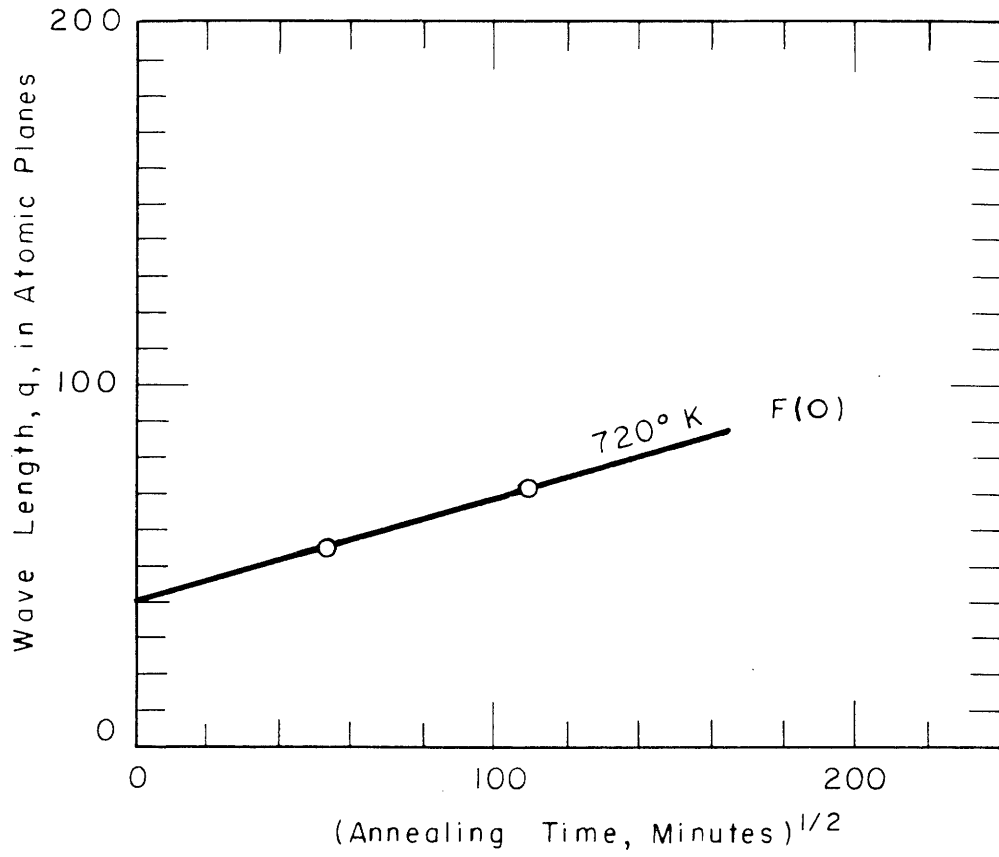


FIG. 23. GROWTH OF WAVE LENGTH WITH ANNEALING TIME AT  $720^\circ \text{K}$



allows the data from a wide range of temperatures to be represented in the same diagram.

It was always attempted to extend the measurements at each temperature to as short annealing times as possible. The first measurement in each series was, therefore, made on very weak satellites and the accuracy is not very high. The data obtained for the longest annealing times are also of rather poor accuracy because the satellites then are very close to the main reflections.

Daniel and Lipson<sup>(44)</sup> found that the growth of the wave length with time could be represented by an equation

$$Q = C_1 + C_2 \log t \quad (82)$$

where  $C_1$  is a function of the temperature, and  $C_2$  is a constant. The present measurements were extended to a larger range of times and temperatures and the results plotted in Figs. (24) and (25) clearly show that the data are not well represented by straight lines in the logarithmic plot, and also that the slope of the curves, which is the constant  $C_2$  in Daniel's and Lipson's equation, in fact decreases with temperature.

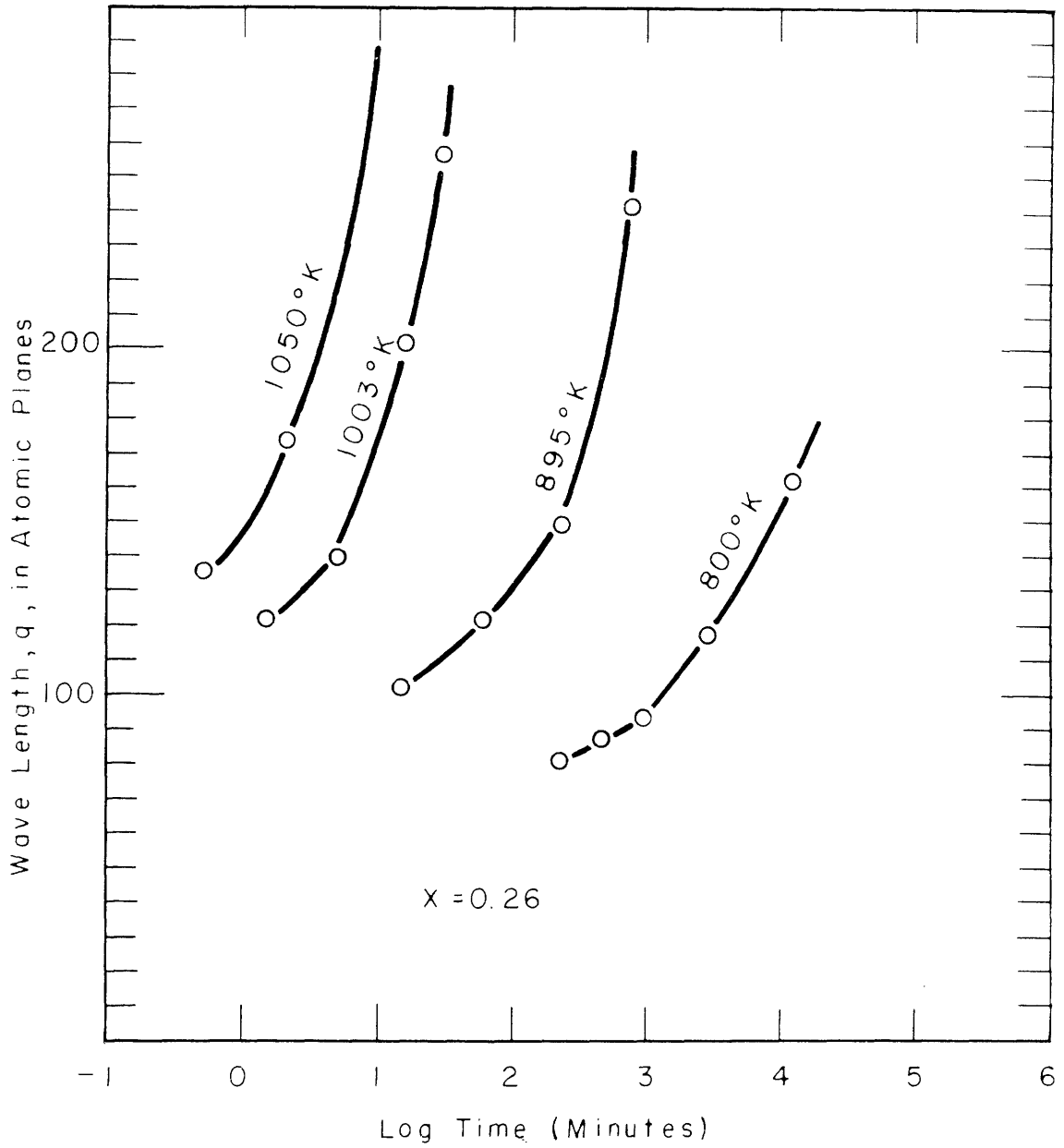


FIG. 24. GROWTH OF WAVE LENGTH WITH ANNEALING TIME FOR ALLOY C.

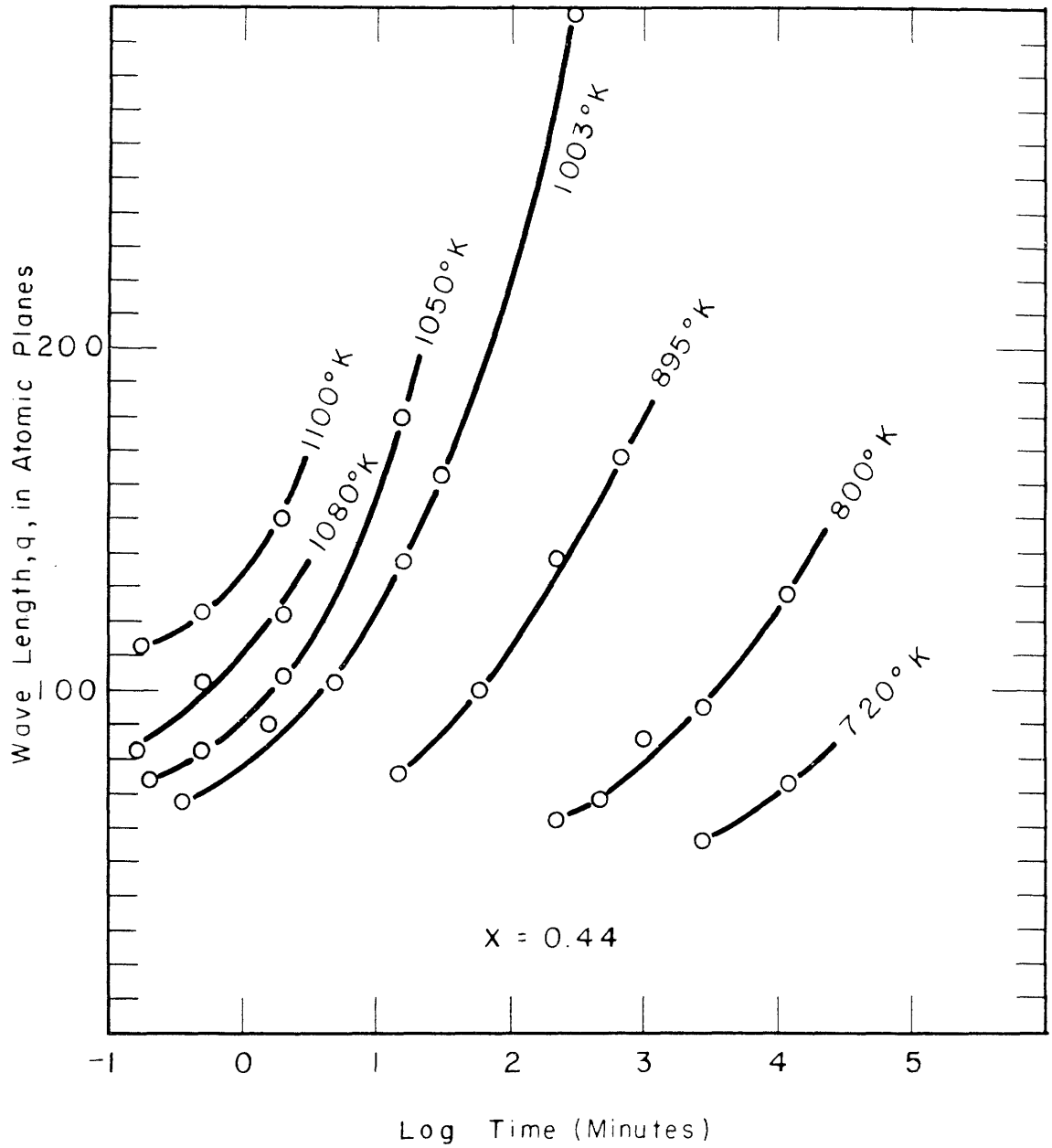


FIG. 25. GROWTH OF WAVE LENGTH WITH ANNEALING TIME FOR ALLOY F.

## VII. DISCUSSION OF EXPERIMENTAL RESULTS

### 1. Rate of Transformation for the Symmetric Alloy

The shortest time at which the satellites were detected for each temperature is plotted logarithmically against the inverse temperature in Fig. (26) for the most symmetric alloy F. A theoretical growth rate has also been plotted in the same figure. It was calculated under the rather crude assumption that the rate of transformation would be proportional to the diffusion coefficient,  $D$ , and to the difference in free energy,  $\Delta F$ , between the initial, homogeneous state and the final, stable state.

$$G = \text{const. } \Delta F \cdot D \quad (83)$$

The wave length,  $q$ , which was considered in Section III.7, is here included in the constant, because it varies only slightly with temperature. The diffusion coefficient has been determined by Daniel<sup>(50)</sup>. No calculation of the absolute rate could be made from these simple assumptions, and only the variation with temperature of the theoretical curve is therefore significant. It was displaced horizontally to give the best fit with the experimental points.

There is a close agreement between the theoretical growth rate curve and the experimental points. It thus seems possible to explain the variation with temperature of the measured rate of formation on the basis of a variation in the rate of development of nuclei into a detectable structure. This process of development may involve an increase in the degree of segregation,

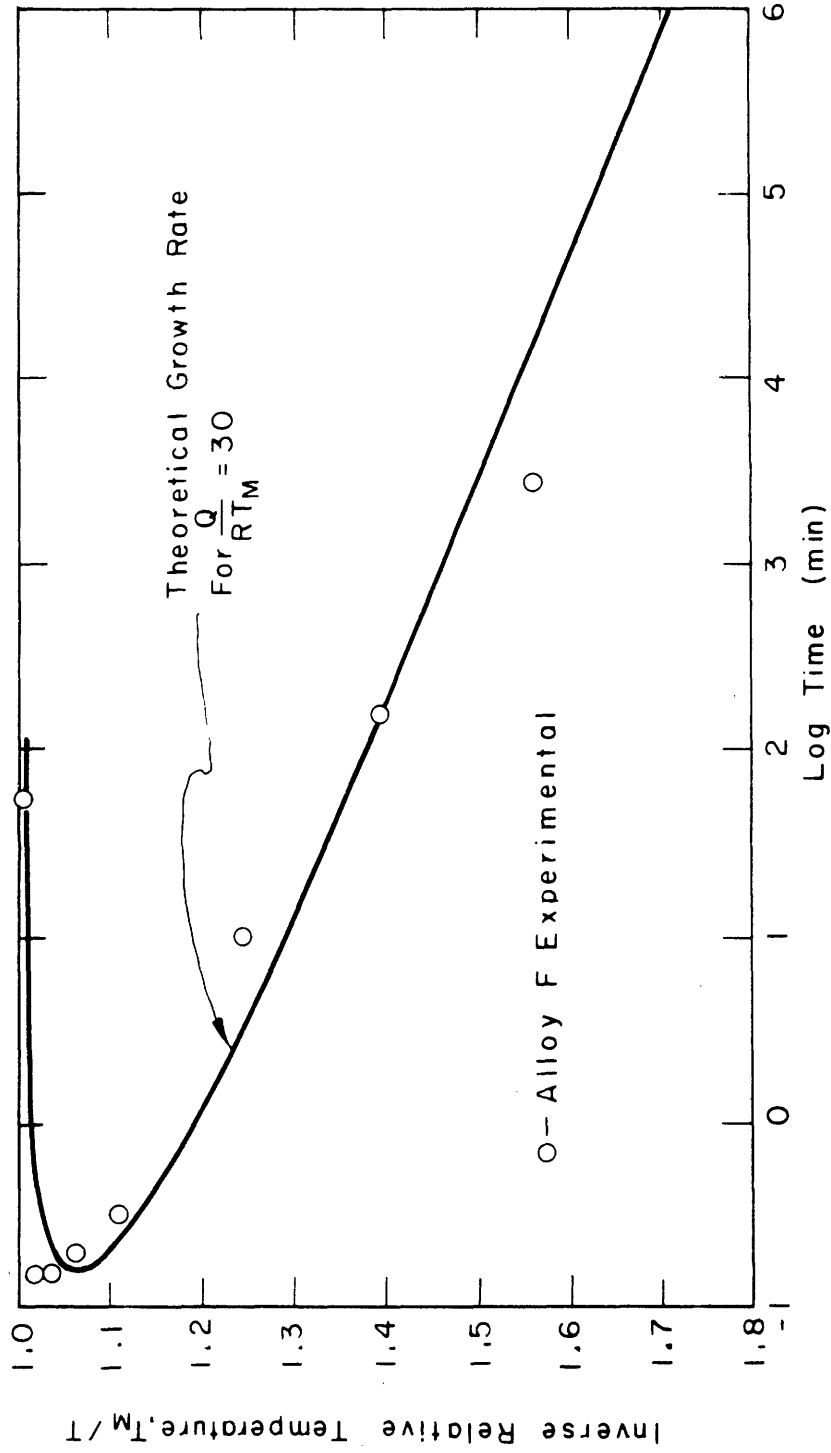


FIG 26 EXPERIMENTAL DATA FOR ALLOY F COMPARED WITH THEORETICAL "C" - CURVE FOR SYMMETRIC ALLOY

i.e., the amplitude, as well as a geometrical growth. Eq. (83) might apply fairly well to both of these processes. There is consequently no experimental indication of a difference in the nucleation process at the different temperatures. This is in accordance with the predictions of the nucleation theories, because the symmetric alloy is always inside the spinodal when it is inside the miscibility gap and there should consequently be no differences in the nucleation process.

Borelius and co-workers<sup>(19)</sup> have used a method to evaluate the spinodal temperature from C-curves, which results in a temperature below the nose of the C-curve. On the other hand, some authors<sup>(24)</sup> have interpreted the temperature of the nose as the temperature below which there is no retardation due to nucleation difficulties. These interpretations do not seem warranted in view of the above results. It is possible of course, that they would be fairly correct if applied to a C-curve measured for an extremely early stage of the transformation. However, at present there does not seem to be any available method sensitive enough for such measurements, and all experimental observations therefore seem to be largely determined by the growth process.

## 2. Variation of Wave Length with Temperature

The extrapolated wave length values for the most symmetric alloy F are plotted versus the temperature in Fig. (27). The theoretical curves for the critical wave length,  $q_{crit}$ , and the optimum wave length,  $q_{opt}$ , as calculated for the symmetric

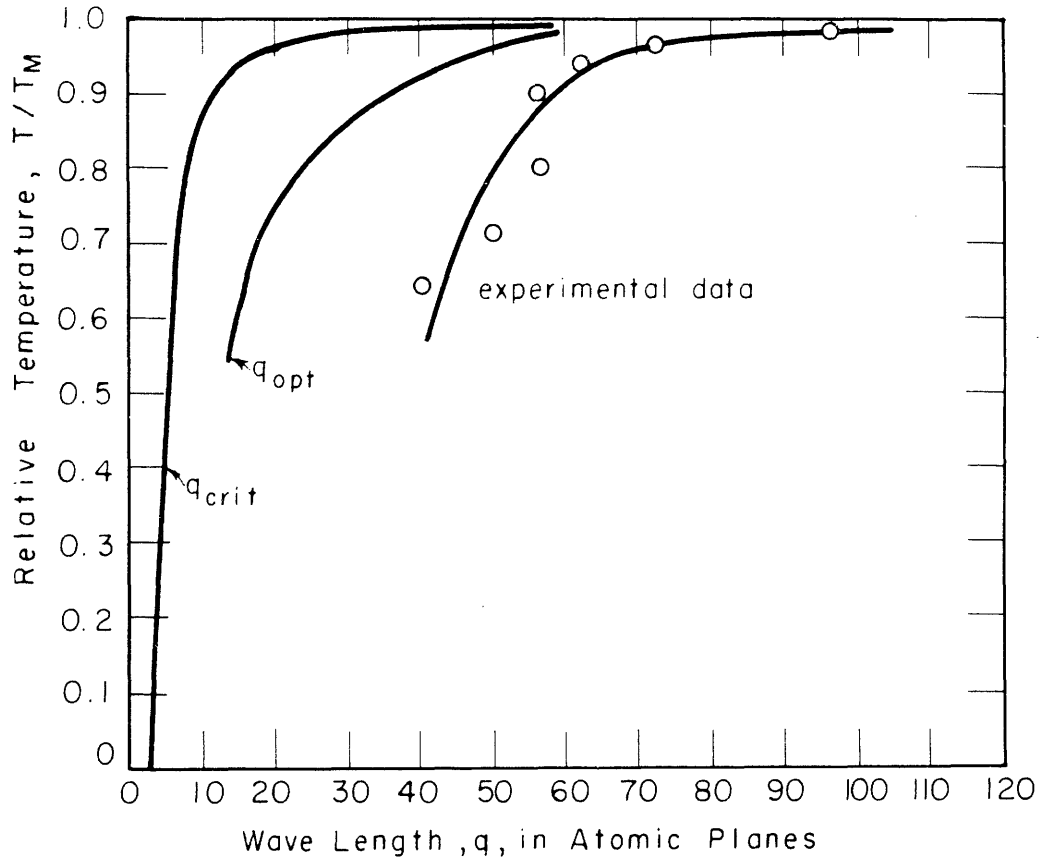


FIG. 27. VARIATION OF INITIAL WAVE LENGTH WITH TEMPERATURE

composition, are also presented. Any wave length larger than  $q_{crit}$  can be nucleated without any activation barrier, and  $q_{opt}$  is the wave length of the structure which in Section III.7 was assumed to develop to a detectable stage in shortest time. The experimental values fall quite close to  $q_{opt}$  at the higher temperatures and show a similar variation with temperature. This again indicates that the nucleation process might occur according to the nucleation theory but the growth process determines what will be observed experimentally.

The somewhat poorer agreement at the lower temperatures may be due to an ineffective quenching through the higher temperature region. Long wave lengths could be nucleated during the quenching and later grow to a detectable stage at the lower annealing temperature. In order to test this, some specimens were quenched from above the miscibility gap into brine and later heated to the low annealing temperature. However, they showed the same wave lengths as specimens which were dropped directly into the annealing furnace from the high temperature.

### 3. Variation of Wave Length with Composition

The extrapolated wave length values at  $1003^{\circ}\text{K}$  are plotted versus the composition in Fig. (28). The theoretical curves for  $q_{crit}$  and  $q_{opt}$  are also presented.  $q_{opt}$  was calculated only for the symmetric composition. It is known to approach the solubility limits asymptotically, however, and could thus be drawn tentatively.  $q_{crit}$  was calculated accurately from



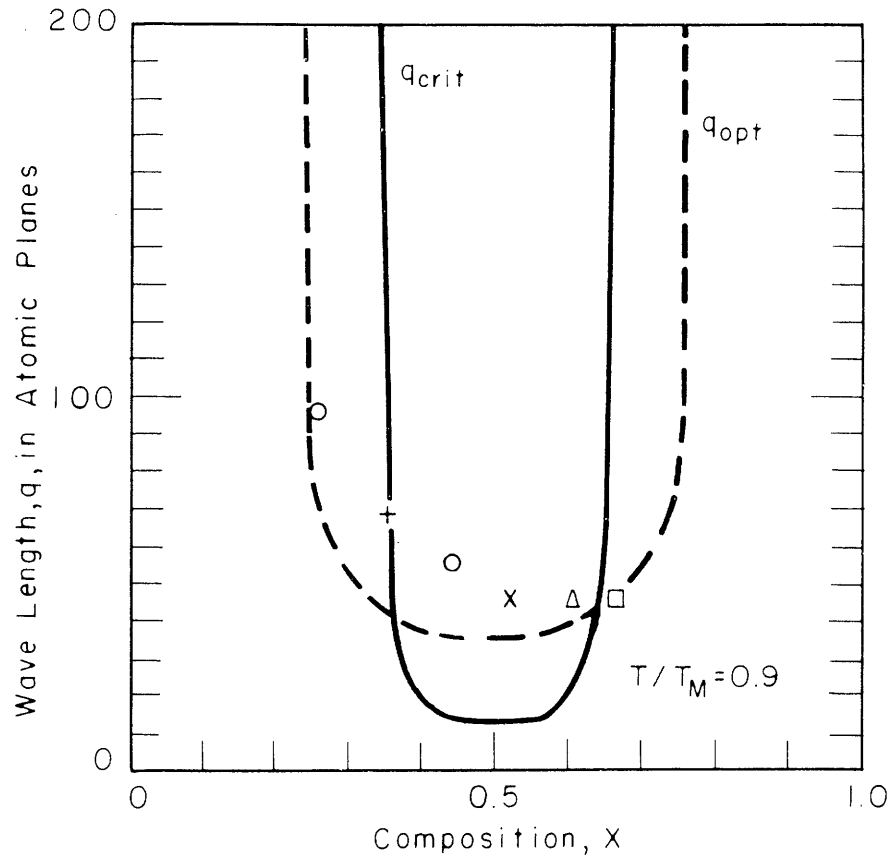


FIG. 28. WAVE LENGTH OF FIRST TRANSFORMATION PRODUCT COMPARED WITH THE CRITICAL AND THE OPTIMUM WAVE LENGTHS.

Eq. (18). It goes to infinity at the spinodal and no wave length can be nucleated outside the spinodal without an activation free energy. It should be noticed that the critical wave length,  $q_{crit}$ , is defined as the shortest wave length which can be nucleated without any activation barrier and not as the shortest wave length that is stable. Only for the symmetric alloy are these two definitions identical, as is shown by Figs. (5) and (6).

The experimental points show the same behavior as the curve for the optimum wave length,  $q_{opt}$ , both inside and outside the spinodal and there is no noticeable change at the spinodal. The shortest annealing time which gave detectable satellites was approximately the same for all the alloys and did not show any discontinuity at the spinodal, either. These facts again may indicate that the growth conditions are predominant. Consider for instance an alloy inside the spinodal but very close to it. Any wave length longer than  $q_{crit}$  can be nucleated at once without any retardation. However, it may develop so slowly that it does not become measurable before a wave length shorter than  $q_{crit}$  has had time both to nucleate and develop. In other words, the incubation time for nucleation of wave lengths shorter than  $q_{crit}$  may be short compared with the time it takes to develop a structure to a measurable stage. The composition of the alloy could thus be changed to fall outside the spinodal without any main difference in the transformation process, and the incubation time may still be much too short to be measurable.

The suggestion that the incubation time for nucleation is very short close to the spinodal is supported by Fig. (8). This figure shows that the activation barrier for alloys outside the spinodal does not decrease sharply toward zero if the composition is changed toward the spinodal. Instead the activation free energy approaches the value zero very slowly and there is in fact no sharp discontinuity at the spinodal.

An alternative explanation of the experimental observations is that the spinodal is not uniquely defined for a real system with imperfections. No discontinuity should then be expected at the theoretical spinodal. This explanation will be further discussed in a later section.

The experimental C-curve for the alloy C is shown in Fig. (29), and no discontinuity can be detected at the theoretical spinodal in this case either.

#### 4. Conclusions from Experimental Work

It seems possible to explain all the experimental observations in accordance with the nucleation theories, but they do not provide any critical test of these theories, because the growth process seems predominant. They do not even provide a test of the significance of the spinodal, which is predicted by Borelius<sup>1</sup>, Hobstetter's and the present theories.

The present theory is the only one which makes any predictions about the transformation product and is more susceptible to testing. The measured wave lengths show a fair agreement with these predictions and thus lend some support to the present

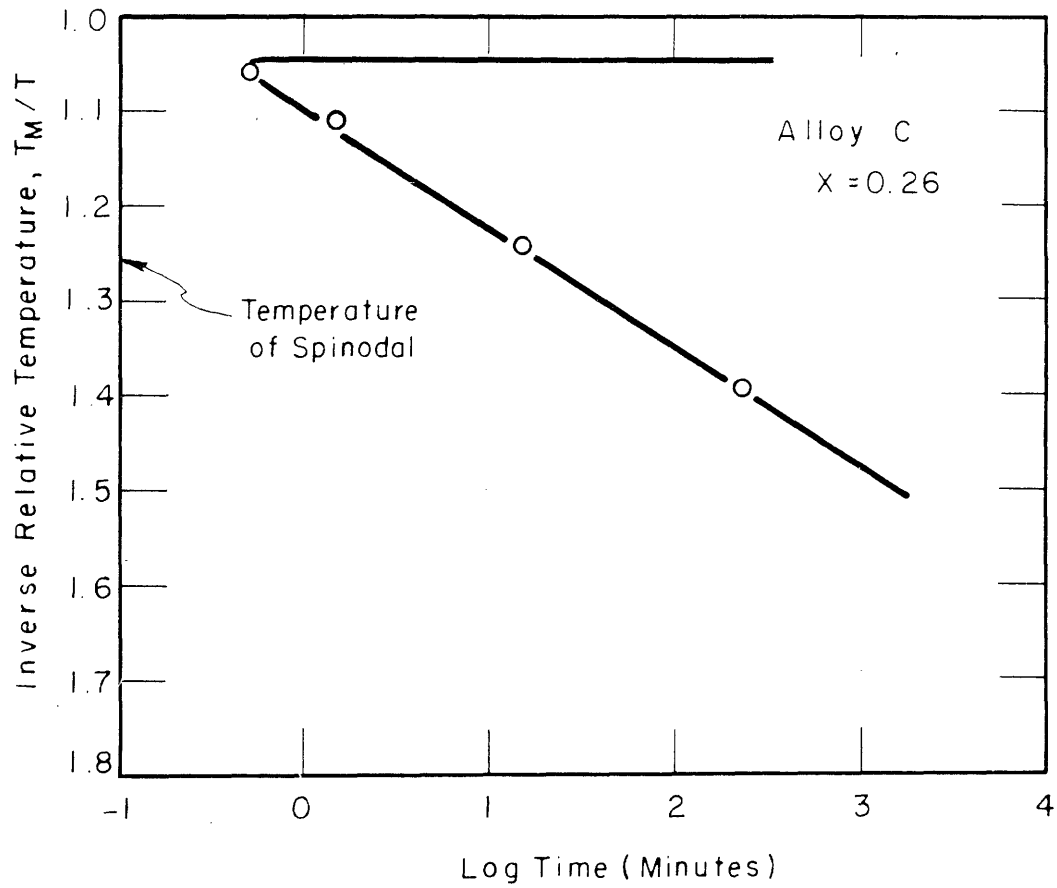


FIG. 29. EXPERIMENTAL "C"-CURVE FOR THE ASYMMETRIC ALLOY C.

theory. The very existence of the periodic structures in the Cu-Ni-Fe alloys could be taken as a support for this theory. It must be remembered, however, that the theory only treats compositional variations in one direction and it does not predict that periodic structures should form in preference to any other structure which involves compositional changes in all three directions.

In view of the above results, it seems even more hopeless to test the significance of the spinodal by measurements on other than exchange transformations. This has been tried many times, however<sup>(9,18,23,24)</sup>.

##### 5. The Nature of the Spinodal

The experiments undertaken have not been able to prove the significance of the spinodal. This result was explained in the preceding sections as due to the predominance of the growth process. It was still assumed that the spinodal may be significant for the nucleation process itself. In this section, several factors will be discussed which might even remove the significance of the theoretical spinodal.

(1) By definition, the spinodal is the locus of all points where  $d^2F/dx^2 = 0$ , which gives a well defined curve in the temperature-composition diagram if one considers equilibrium states. However, when a specimen is quenched from a high temperature down into the spinodal, the short-range arrangement of the atoms is much more random than the equilibrium state at the new temperature. The first approximation of the nearest-

neighbor interaction model predicts an increased clustering as the temperature is lowered, and the theoretical spinodal at each temperature holds only for systems with the prescribed degree of clustering. It takes some time for the atoms to rearrange, and before this happens the actual spinodal might approximate that for a random solution. This spinodal is given by Eq. (79) and has been plotted in the phase diagram of Fig. (30) according to the first approximation, assuming a constant interaction energy,  $\nu$ . Fig. (30) shows that the actual spinodal in this case is displaced outwards when the temperature is close to the peak of the miscibility gap. It is thus possible for a quenched specimen between the two spinodals of Fig. (30) to start transforming without any retardation.

Scheil and Wegener<sup>(35)</sup> have also calculated the spinodal for random solution but they found it to fall inside the equilibrium spinodal. It seems that their calculation is in error and two possible explanations for the discrepancy are given in Section IV.5.

(2) It is usually assumed that the interaction energy  $\nu$  is independent of the configuration of the atoms on the lattice sites. The thermodynamic quantities (e.g. Eq. (38)), the shape of the miscibility gap (Eqs. (78) and (79)) and the short-range arrangement of the atoms in a homogeneous solution (Eq. (40)) can then all be computed from the same value of  $\nu$ . However, if there is a considerable difference in size between the two kinds of atoms in a binary solution, the strains might play an important role. The strain energy of a randomly mixed

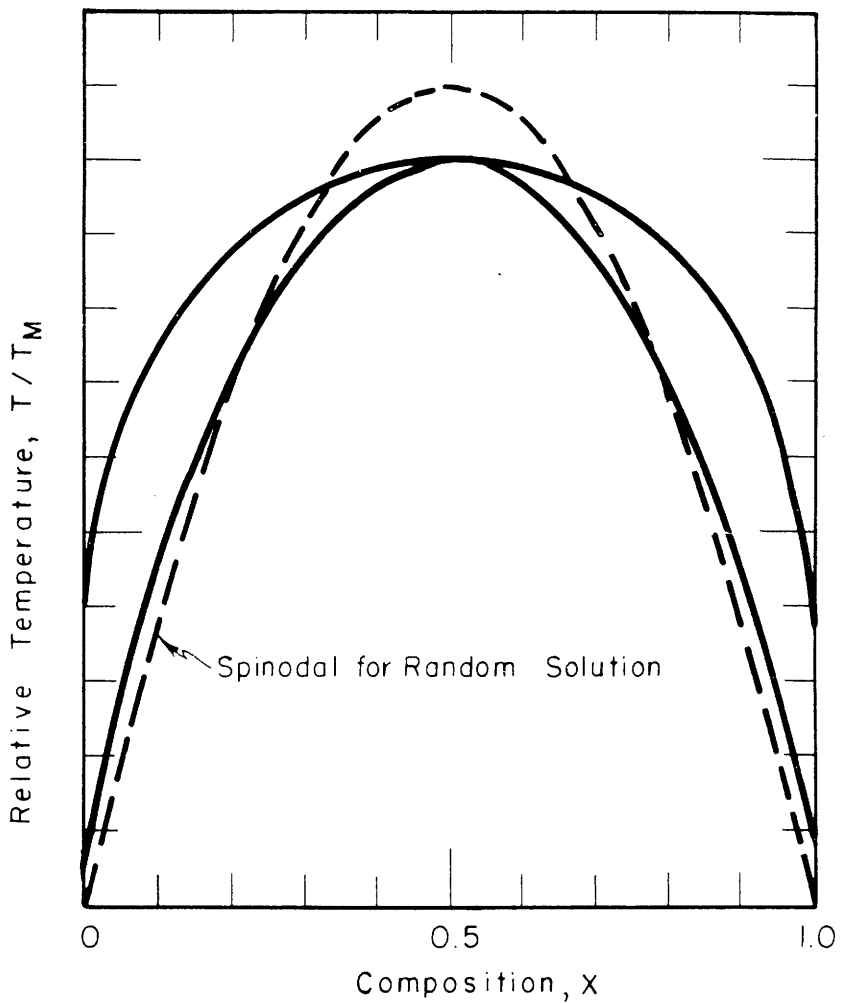


FIG. 30. MISCIBILITY GAP FOR FIRST APPROXIMATION WITH SPINODAL FOR RANDOM SOLUTION.

solution can apparently be decreased by an ordering of the atoms, which corresponds to negative  $\nu$  values. It can also be decreased by separation of the different kinds of atoms, which corresponds to positive  $\nu$  values. The interaction energy might thus be strongly dependent on the configuration and the value calculated from the shape of the miscibility gap may not be the right one for a calculation of the spinodal for a homogeneous solution. The Au-Ni system may illustrate this case. It has a miscibility gap but X-ray measurements<sup>(30)</sup> indicate that homogeneous solutions contain short-range order. There is consequently no true spinodal for homogeneous solutions inside the miscibility gap. It is not surprising that Au-Ni alloys do not transform by means of an exchange transformation. An alloy quenched inside the miscibility gap remains homogeneous until nuclei of new orientations form on grain boundaries and inclusions<sup>(24)</sup>.

It is quite possible that the main reason why Cu-Ni-Fe alloys show exchange transformation is the similarity of the atomic sizes. However, there is a definite difference in size and this may distort considerably the result of the theoretical calculation of the spinodal.

(3) The structure of the specimens have hitherto been treated as quite homogeneous. However, there are usually heterogeneities in real specimens, for instance, surfaces, grain and subgrain boundaries, dislocations, and impurities. The criterion for the spinodal,  $d^2F/dx^2 = 0$ , gives different alloy compositions at such heterogeneities. It is thus quite possible that the



nucleation in alloys outside the spinodal calculated for a homogeneous region can occur without any retardation. The nucleation must then be characterized as heterogeneous.

It was suggested by Hargreaves<sup>(45)</sup> that the transformation begins at particular points and spreads gradually through the specimen, and he presents photomicrographs in support of this suggestion. This should indicate that the nucleation actually is heterogeneous. However, Hargreaves mentioned that Daniel<sup>(51)</sup> concluded from microscopic observations that the transformation was homogeneous instead. In order to decide whose observations are correct, the present alloys were examined microscopically after different annealing treatments. The same structures were observed as those published by Hargreaves, but in the opinion of the present author they give no proof of heterogeneous nucleation. A saturated solution of  $K_2Cr_2O_7$  with 1% HCl and 1%  $H_2SO_4$  was used as etching agent. It had a staining effect on all the transformed specimens but not on the quenched specimens. For the early stages of the transformation the etching time necessary to develop the color was shorter the longer the annealing time, i.e. the more the transformation had proceeded. Each grain always showed a uniform color and this may indicate that the transformation proceeds uniformly in each grain. There was a difference in color between neighboring grains, probably due to the difference in orientation.

The above microscopic observations do not rule out the possibility of heterogeneous nucleation. However, if the trans-

formation starts at certain preferred sites and spreads gradually through the whole specimen, these sites must be exceedingly close to each other or the growth rate must be very high; otherwise it should have been possible to detect transformed regions in an untransformed matrix. It is possible that dislocations or impurities could furnish preferred sites for heterogeneous nucleation in such a large number that the transformation appears uniform.

#### 6. Discussion of Guinier's Model

It was mentioned in Section IV.1 that the satellites have a considerable width, whereas all the older models predict sharp satellites. Guinier<sup>(39)</sup> pointed out that such a width would be expected if each transformed region only contained one central lamella surrounded by two lamellae of the other kind. With the same model he also explained the continuous growth of the wave length (see Fig. (12)).

An alternative explanation of the width and the continuous growth is offered by the conclusion in Section III.9 that the nucleation process should give rise to a spectrum of wave lengths. In Section III.10, the continuous growth of the average wave length was explained from this standpoint.

These two explanations are in fact rather similar. The main difference is that Guinier suggests a specific kind of a zone as the carrier of the spectrum of wave lengths. His model has advantages as well as disadvantages. The main advantage is that it gives a specific prediction about the spectrum of wave lengths, i.e., the width of the satellites. Guinier

claimed that the predicted width is of the same order of magnitude as the observed width. In the present investigation these observations were confirmed for the first stages of the transformation. The width then corresponds to the value 1 of the quantity  $v$ , introduced in Section V.3. However, the satellites soon become sharper, the width corresponding to the  $v$  values 2 or 3 (see Fig. (14)). In terms of Guinier's model this could be explained by an interference between different zones as they grow closer to each other. In view of the theoretical treatment of the nucleation process developed in Chapters II and III, it is simply a consequence of the disappearance of the shortest wave lengths due to the higher degree of stability of the longer wave lengths. It should be noticed, however, that this treatment does not give any detailed picture of the different stages of the transformation. The reason is that it is mainly concerned with different kinds of equilibrium states.

A disadvantage of Guinier's model is that it assumes the matrix surrounding a zone will stay homogeneous until it is reached by the laterally growing zone. Instead, the whole matrix should start to transform spontaneously if the alloy is within the spinodal. Moreover, if the spontaneous transformation is prevented, for instance by the influence of strains as suggested in Section VI.5, the growth process should not proceed as Guinier suggested. He proposed that the two side strips of the zone receive material by downhill diffusion from the

surrounding matrix and that this material can be transferred to the center lamellae by uphill diffusion. However, if the alloy is within the spinodal, there should be uphill diffusion also between the side strips and the surrounding matrix. This would give rise to more lamellae outside the original zone. This growth process is demonstrated schematically in Fig. (31), where the sharp discontinuities in composition have also been eliminated in view of the results in Chapter III.

An attempt was made to compute quantitatively the growth process by means of the diffusion equation derived in Section III.6. Such a computation is theoretically possible, of course, but it was found too difficult to make it accurate enough to give any significant results.

For alloys outside the spinodal, on the other hand, there are no such objections to Guinier's model. In fact, it seems to give a very reasonable picture of the transformation process in such alloys. However, no discontinuity was observed at the spinodal, neither for the width, nor for any other quantity. This indicates that there is no main difference in the transformation process outside and inside the spinodal, and approximately the same model should be chosen for both cases. It is possible that the suggested change of Guinier's model inside the spinodal is not very significant and Guinier's model may consequently hold fairly well on both sides of the spinodal. The reason may be that the sidewise growth, which has been discussed here, is of minor importance compared with the edgewise growth of the zone.

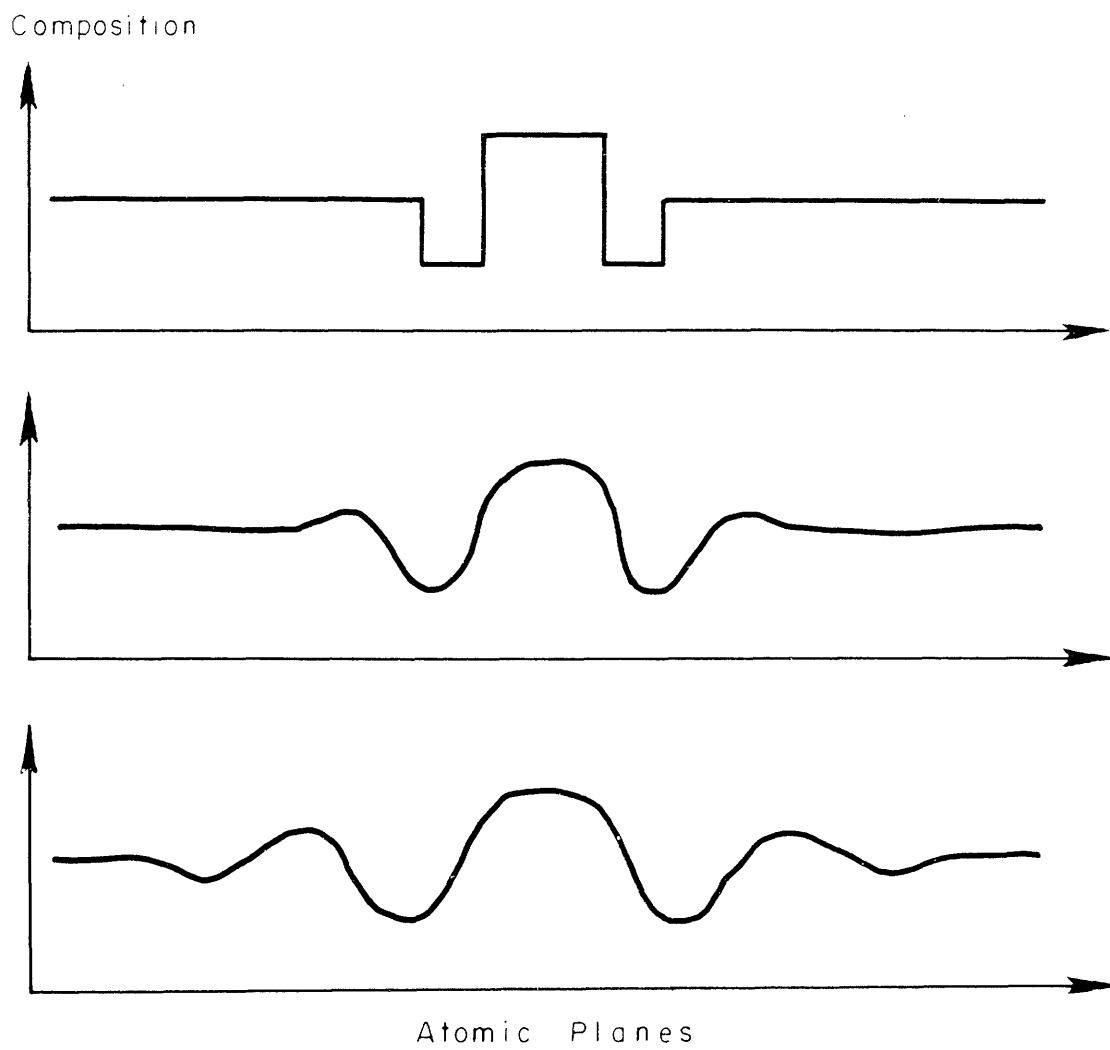


FIG. 31. SUGGESTED DEVELOPMENT OF GUINIER'S ZONE

### VIII. SUMMARY AND CONCLUSIONS

It has been shown how a nucleation theory can be developed for exchange transformations without using the concept of size for nuclei. Only compositional variations in one crystal-line direction are considered, however. The new nucleation theory predicts spontaneous nucleation inside the spinodal in agreement with Borelius' and Hobstetter's theories. The activation energy for nucleation outside the spinodal is much lower according to the new theory than given by Becker's and Hobstetter's theories.

Measurements on Cu-Ni-Fe alloys inside the miscibility gap were unable to prove the significance of the spinodal experimentally. The reason may be that the process of development of nuclei into detectable structures, and not the nucleation process itself, determines the apparent incubation time. Another explanation may be that the theoretical spinodal has no significance on the nucleation process in real systems with imperfections.

It is not possible to decide from the experiments whether the nucleation process in the Cu-Ni-Fe alloys is homogeneous or heterogeneous.

The new nucleation theory predicts that exchange transformations should lead to structures with a periodic variation of the composition. Such structures are found in Cu-Ni-Fe alloys and experimental measurements of the wave lengths show a

fair agreement with the predictions. This lends some support to the new nucleation theory. The picture of the transformation obtained from the new theory is compared with Guinier's model and it is found that they are rather similar. A slight change of Guinier's model is suggested.

Several previous X-ray treatments of periodic structures are brought together to a more general treatment, which can be applied to any physical model for the transformation. Equations are derived for the influence of the number of periods in each transformed region on the width of the satellites, and also for the asymmetry of the intensity of the satellites.

The validity of the interaction energy concept is discussed, and it is shown that the quasi-chemical theory can be derived without the usual assumption that the interaction energy is independent of temperature and composition. The derivation shows that the interaction energy should not be calculated from experimental  $H^M$  values, as is usually done, but from  $F^M$ .

Coherent grain boundaries and anti-phase domain boundaries are examined theoretically. It is found that they show a gradual change in composition and phase, and not an abrupt change as is usually assumed. The grain boundary energy is calculated for a coherent grain boundary and a value considerably lower than the one obtained by Becker is found.

A new diffusion equation is derived for crystalline structures, which takes into account the third derivative of the

concentration as well as the first derivative, i.e., the gradient itself.

#### IX. SUGGESTIONS FOR FUTURE WORK

1. The significance of the spinodal on the nucleation process should be tested on more exchange transformations, e.g. the one occurring inside the miscibility gap of the Al-Zn system.

2. The conditions for the formation of layered structures in exchange transformations should be examined. Such structures should be looked for in more systems, e.g. in the Fe-Cr and the Al-Zn systems.

3. The predictions of the wave length of the periodic structures should be tested again, if another system is discovered that gives layered structures.

4. A new attempt should be made to calculate quantitatively the development of a Guinier Zone by means of the revised diffusion equation. Perhaps an electronic computer could be successfully employed.



REFERENCES

1. C. Wagner, Thermodynamics of Alloys, Cambridge, Mass. (1952).
2. M. Volmer and A. Weber, Z. Phys. Chem. 119 (1926) 277.
3. R. Becker and W. Döring, Ann. Physik 24 (1935) 719.
4. S. Konobejewski, Z. Physikal Chem. A171 (1934) 25.
5. G. Borelius, Ann. Physik, 28 (1937) 507.
6. G. Borelius, Arkiv Mat. Astron. Fysik, 32A (1944) 1.
7. R. Becker, Z. Metallkunde, 29 (1937) 245.
8. U. Dehlinger, Chemische Physik der Metalle und Legierungen, (Leipzig 1939).
9. G. Borelius, Arkiv Mat. Astron. Fysik, 32A (1945) 1.
10. N. P. Allen and C. C. Earley, J. Iron Steel Inst., 166 (1950) 281.
11. J. H. Hollomon and D. Turnbull, Progress in Metal Physics, 4 (1953) 333.
12. D. Turnbull, Acta Met., 3 (1955) 55.
13. R. Becker, Ann. Physik, 32 (1938) 128.
14. J. N. Hobstetter, Trans. AIME, 180 (1949) 121.
15. E. Scheil, Z. Metallkunde, 43 (1952) 40.
16. W. L. Fink and D. W. Smith, Trans. AIME, 137 (1940) 95.
17. L. S. Darken, Trans. AIME, 175 (1948) 184.
18. C. G. Victorin, Studies in Gold-Platinum Alloys, Stockholm (1947).
19. G. Borelius, J. Metals, 3 (1951) 477.
20. C. H. Johansson and G. Hagsten, Ann. Physik, 28 (1937) 520.
21. G. Borelius, F. Larris and E. Ohlsson, Arkiv Mat. Astron. Fysik, 31 (1944) 1.

22. G. Borelius and L. E. Larsson, Arkiv Mat. Astron. Fysik, 35 (1948) 13.
23. E. Scheil and H. Stadelmaier, Z. Metallkunde, 43 (1952) 227.
24. E. Underwood, Sc.D. Thesis, M.I.T., 1954.
25. D. Turnbull and H. N. Treafis, Acta Met., 3 (1955) 43.
26. J. M. Cowley, Phys. Rev., 77 (1950) 669.✓
27. E. A. Guggenheim, Mixtures, Oxford (1952).✓
28. E. A. Guggenheim, Trans. Faraday Soc., 44 (1949) 1007.
29. Y. Takagi, Proc. Phys. Math. Soc., Japan, 23 (1941) 44.
30. B. L. Averbach, P. A. Flinn and M. Cohen, Acta Met., 2 (1954) 92.
31. R. A. Oriani, Acta Met., 4 (1956) 15.
32. E. S. Machlin, J. Metals, 6 (1954) 592.
33. M. Hillert, B. L. Averbach and M. Cohen, Acta Met., 4 (1956) 31.
34. H. K. Hardy, Acta Met., 1 (1953) 203.
35. E. Scheil and F. Wegener, Z. Metallkunde, 46 (1955) 659.
36. U. Dehlinger and H. Knapp, Z. Metallkunde, 43 (1952) 223.
37. U. Dehlinger, Defects in Crystalline Solids, Report of 1954 Conference, page 423.
38. H. K. Hardy and T. J. Heal, Progress in Metal Physics, 5 (1954) 143.
39. A. Guinier, Acta Met., 3 (1955) 510.
40. U. Dehlinger, Z. Kristallogr., 65 (1927) 615.
41. A. Kochendorfer, Z. Kristallogr., 101 (1939) 149.
42. V. Daniel and H. Lipson, Proc. Roy. Soc., 181 (1942) 368.
43. A. J. Bradley, W. F. Cox and H. J. Goldschmidt, J. Inst. Met., 67 (1941) 189.

44. V. Daniel and H. Lipson, Proc. Roy. Soc., 182 (1943) 378.
45. M. E. Hargreaves, Acta Cryst., 4 (1951) 301.
46. D. Balli and M. Zakharova, Doklady Akademii Nauk., SSSR, 96 (1954) 453.
47. D. Balli and M. Zakharova, Doklady Akademii Nauk., SSSR, 96 (1954) 737.
48. R. W. James, Optical Principles of the Diffraction of X-rays, London, (1954).
49. W. Köster and W. Dannöhl, Z. Metallkunde, 27 (1935) 220.
50. V. Daniel, Proc. Roy. Soc., 192 (1947) 575.
51. V. Daniel, Dissertation for Ph.D., Cambridge University, (1943).

BIOGRAPHICAL SKETCH

Mats Hilding Hillert was born in Göteborg, Sweden on November 28, 1924. In 1943 he entered Chalmers Institute of Technology and obtained the degree of Civilingenjör in Chemistry in 1947. After research work in the field of Metallurgy at the Swedish Institute for Metal Research he entered Massachusetts Institute of Technology and obtained the degree of S.M. in Metallurgy in 1954.

APPENDIX I

Derivation of Free Energy for Layered Structure

The free energy of mixing according to the zeroth approximation is

$$F^M = \nu NZx(1-x) + NkT [x \ln x + (1-x) \ln(1-x)]$$

and the partial free energy is obtained by

$$F_A^M = F^M - (1-x) \frac{\partial F^M}{\partial x} = \nu NZ(1-x)^2 + NkT \ln x$$

The change in free energy of an atomic plane containing  $m$  atoms, caused by a change of its composition from  $x^0$  to  $x^p$  by an exchange of atoms with a large reservoir of the composition  $x^0$ , is given by

$$F = \frac{m}{N} \left\{ x^p \left[ F_A^M(x^p) - F_A^M(x^0) \right] + (1-x^p) \left[ F_B^M(x^p) - F_B^M(x^0) \right] \right\} =$$

$$= -\nu mZ(x^p - x^0)^2 + m kT \left[ x^p \ln \frac{x^p}{x^0} + (1-x^p) \ln \frac{1-x^p}{1-x^0} \right]$$

where the interfacial energy has been neglected.

Becker<sup>(7)</sup> derived the interfacial energy between two planes of different compositions and obtained

$$F_s = \nu m \zeta (x^p - x^{p+1})^2$$

where  $\zeta$  is the number of nearest neighbors, for a given atom, which are situated in a neighboring plane.

The total change in free energy when a homogeneous specimen of composition  $x^0$  is transformed into a state where succeeding

have the compositions  $x^p$ ,  $x^{p+1}$ ,  $x^{p+2}$ , etc., is thus

$$F = - \nu_m \sum_p \left[ Z(x^p - x^0)^2 - \beta (x^p - x^{p+1})^2 \right] + \\ + m k T \sum_p \left[ x^p \ln \frac{x^p}{x^0} + (1 - x^p) \ln \frac{1 - x^p}{1 - x^0} \right]$$

APPENDIX II

Composition of Alloys

<u>Alloy</u>	<u>Atomic % Cu</u>	<u>Atomic % Ni</u>	<u>Atomic % Fe</u>
A	84.9	10.5	4.6
B	79.7	14.2	6.1
C	74.3	18.0	7.7
E	64.4	24.8	10.8
F	56.0	30.7	13.3
G	48.3	36.6	15.1
H	39.6	42.2	18.2
I	33.8	46.2	20.0
J	24.9	53.0	22.1

APPENDIX III

Wave-Lengths Q in Unit Cells for Different Alloys

Temp. °K	Time in min	A	B	C	E	F	G	H	I	J
1111	60					(520)				
1100	0*					48				
	0.17					56				
	0.5					61				
	2					75				
1080	0*					36				
	0.15					41				
	0.5					51				
	2					61				
1050	0*			57	39	31	27	27		
	0.2					37				
	0.5			68	50	41	36	44		
	2			87	59	52	50			
	16			(185)	128	90	70	72		
1003	0*			48	34	28	23	23	23	
	0.33				38	34				
	1.5			61	47	45	37	38	35	
	5		63	70	59	51	46	45	45	
	16		101	101	77	69	59	57	60	
	30			128	110	81	68	70	74	
	180					150	102	102	111	
895	0*		50	41	34	28	22	22	22	22
	15		58	51	43	38	32	34		
	60	68	73	61	54	50	44	41	43	41
	240	(110)	81	76	78	69	61	57	60	54
	720	(145)	121	121	93	84	74	72	74	72
800	0*	49	38	34	32	25	23	21	21	21
	240	60		41	39	31	30			
	480			44		34		30		
	960	63	52	47	44	43	35	34	36	37
	2880	68	62	59	53	47	42	44	44	42
	11880	119	78	81	76	64	61	60	60	60
720	0*					20				
	2880					28				
	11880					36				
662 18720										No satellites

\*Extrapolated values.